ROLES OF PALMITIC ACID ON THE KINASE PROTEINS

By

Hyunju Cho

A DISSERTATION

Submitted to
Michigan State University
in partial fulfillment of the requirements
for the degree of

Chemical Engineering - Doctor of Philosophy

2013

ABSTRACT

ROLES OF PALMITIC ACID ON THE KINASE PROTEINS

By

Hyunju Cho

The Endoplasmic Reticulum (ER) is a cellular compartment responsible for protein folding, lipid synthesis, and calcium storage. Physiological conditions such as elevated levels of free fatty acids (FFAs) and glucose, oxidative stress, and inflammatory cytokines are known to perturb ER homeostasis, leading to the accumulation of unfolded/misfolded proteins in the ER lumen. Especially, palmitic acid, a saturated FFA, is recognized to induce ER stress, in particular, with respect to two kinases proteins, PKR (cytosolic kinase) and IRE1α (Type-I transmembrane ER kinase), and to contribute to many diseases, e.g. cancer, diabetes, neurodegenerative and inflammatory diseases. However, the molecular mechanisms by which palmitate regulates the activities of the PKR and IRE1a proteins, the latter is a transmembrane (TM) protein, are not known. With the assistance of computational analysis, the biological and biochemical experiments showed that palmitic acid directly interacts with the kinase domains of both PKR and IRE1α. Palmitic acid bound to the αC-helix, an important structural feature for correct alignment of the catalytic residues, to regulate the enzymatic activity of these proteins. Furthermore, for a better understanding of the roles of palmitic acid on the IRE1α protein, the functional and structural roles of the TM domain were investigated. Mutational studies showed that Tryptophan (IRE1α-W457) serves as a driving force for the TM dimerization process and both the aromatic interaction and hydrogen bond formed by Trp457 are crucial for stabilizing the

oligomerization of the TM domain, and possibly contributing to the palmitate-induced activity. Therefore, the current study could shed light into the molecular mechanisms by which palmitic acid mediates ER-stress induced diseases and further could lead to novel drug therapies.

ACKNOWLEDGMENTS

First, I would like to thank my advisor Dr. Christina Chan and my dissertation committee members; Dr. Michael Feig, Dr. R. Mark Worden and Dr. David Weliky. I would like to thanks all my collaborators; Dr. S. Patrick Walton, Dr. Amadeu K. Sum, Dr. Liang Fang, Dr. Francesca Stanzione, Dr. Shayantani Mukherjee, Dr. Ming Wu, Dr. Linxia Zhang, Betul Bilgin, Ryan Thompson, Aritro Nath. I thank the current and former members from the Chan and Walton labs, especially thank Dr. Li Liu and all members under my projects; Pratheeba Palasuberniam, Ryan LaMarca, Lisa Pillow, Catherine Nezich, Chris Bush, Shruthy Suresh, Jason Portis, Sindura Yerneni, Amrita Oak for their great help. Additionally, I like to thank Lee Alexander for his kind help with several equipment and reagents. Finally, I am deeply grateful for the great support from my family and friends.

TABLE OF CONTENTS

LIST OF TABLES	viii
LIST OF FIGURES	ix
CHAPTER 1. INTRODUCTION	1
1.1. Free fatty acids (FFAs) and diseases	1
1.2. The ER stress and the Unfolded Protein Response (UPR)	
1.3. The UPR sensor proteins	2 3 5
1.4. Palmitate-induced UPR signaling pathways	5
1.5. Molecular mechanisms of the ER stress mediated by palmitate	7
1.6. Palmitate-binding proteins	8
1.7. Specific aims of the current study	11
CHAPTER 2. LATEST DEVELOPMENTS OF EXPERIMENTAL METHODS TO	
CHARACTERIZE PROTEIN-LIPID INTERACTIONS	13
2.1. Solution-based methods for studying protein-lipid interactions	14
2.2. Array-based methods for analysis of protein-lipid interactions	18
2.2.1. Immobilization techniques	18
2.2.2. Detection techniques	21
2.2.2.1. Label-based techniques	21
2.2.2.2. Label-free techniques	25
2.3. Development of the experimental methods for analysis of protein-palmitic acid	
interactions	27
CHAPTER 3. MOLECULAR MECHANISM BY WHICH PALMITATE INHIBITS P	KR
AUTOPHOSPHORYLATION	34
3.1. Abstract	34
3.2. Introduction	35
3.3. Materials and Methods	39
3.3.1. Materials	39
3.3.2. Protein expression and purification of PKR protein constructions	40
3.3.3. Bodipy-Palmitic acid binding assay	41
3.3.4. Competition assay and IC ₅₀ calculations	41
3.3.5. Palmitate treatment on HepG2 Cell and western blotting analysis	42
3.3.6. Statistical Analysis	43
3.4. Results	43
3.4.1. Palmitic acid binds to PKR proteins	43
3.4.2. Bodipy-C16 Binds to Other Kinases, Likely Due to the Conservation of the ATP-	-Binding
Site	47
3.4.3. Bodipy-C16 binds to residues surrounding the ATP-binding site and alphaC-helix	κ, thereby
preventing the autophosphorylation of PKR WT protein	49

3.5. Discussion and Conclusions	60
CHAPTER 4. ROLES OF TRYPTOPHAN ON THE OLIGOMERIZATION OF THE	
TRANSMEMBRANE DOMAIN OF IRE 1α	64
4.1. Abstract	64
4.2. Introduction	65
4.3. Materials and Methods	67
4.3.1. Peptide synthesis and purification	67
4.3.2. Circular dichroism (CD) spectroscopy	68
4.3.3. Förster resonance energy transfer (FRET) measurements	68
4.3.4. Sample Preparation for SDS micelles	69
4.3.5. Preparation of Liposome containing TM peptides	69
4.3.6. TOXCAT Chimera Constructions	70
4.3.7. TOXCAT assay	70
4.3.8. MalE Complementation Assay	70
4.4. Results	71
4.4.1. Prediction of IRE1α Transmembrane (TM) Segment from various prediction methods	
4.4.2. Oligomerization of the transmembrane domain of IRE1α in SDS micelles	71
4.4.3. Oligomerization of the transmembrane domain of IRE1α in POPC liposome	76
4.4.4. Trp457 mutations reduce the self-association of IRE1α-TM domain	79
4.5. Discussion and Conclusions	87
CHAPTER 5. ROLES OF PALMITIC ACID ON THE IRE1α PROTEIN	93
5.1. Introduction	93
5.2. Materials and Methods	95
5.2.1. Western blot analysis	95
5.2.2. RT-PCR	96
5.2.3. Protein expression and purification of the IRE1α protein constructions	96
5.2.4. <i>In-vitro</i> XBP1 cleavage assay	97
5.2.5. Protein expression in Drosophila Schneider 2 (S2) Cells	97
5.3. Results	98
5.3.1. Palmitic acid elevates the levels of both IRE1α phosphorylation and XBP1 splicing in	
HepG2 cells	98
5.3.2. Palmitic Acid binds to the cytosolic domain (CD) of IRE1α protein	98
5.3.3. Palmitic Acid binds to the alphaC helix on IRE1α protein	101
5.3.4. IRE1α-CD protein expressed in the E. coli cells retains weak RNase activity	108
5.4. Discussion and Future works	111
CHAPTER 6. CONCLUSIONS AND FUTURE DIRECTIONS	114
6.1. A potential for palmitate to interact with the PERK protein	114
6.2. Myristoylation of the kinase proteins	116
6.3. Palmitoylation of the kinase proteins	119
6.4. Human IRE1α vs. yeast Ire1	120
6.5. Roles of palmitate on the transmembrane domain of IRE1 α	121
6.6. FABPs-mediated transport mechanisms	121
6.7 Future works and conclusions	122

REFERENCES 124

LIST OF TABLES

Table 1. Palmitic acid binding proteins and their functions	9
Table 2. Solution-based techniques to detect PLI	15
Table 3. Prediction of IRE1α Transmembrane Segment from various prediction programs	72

LIST OF FIGURES

Figure 1. The signaling network of palmitate-induced apoptosis mediated by ER stress	6
Figure 2.1. Immobilization techniques	19
Figure 2.2. Detection techniques for lipid microarray systems	22
Figure 2.3. The structure of Bodipy-PA (Bodipy-C16)	29
Figure 2.4. Fluorescence polarization measurement of Bodipy-PA	30
Figure 2.5. Fluorescence polarization measurement of the Bodipy-PA and BSA interaction	31
Figure 2.6. Optimization of FP-based Bodipy-PA binding assay	32
Figure 3.1. Binding mode of AMP-PNP with PKR	37
Figure 3.2. Binding affinity of Bodipy-C16 to PKR wild-type proteins	44
Figure 3.3. Bodipy-C16 binding to kinases	48
Figure 3.4. PKR mutant sites	50
Figure 3.5. Inhibitory effects of PA on PKR phosphorylation	51
Figure 3.6. Fluorescence intensity measurement for the binding of Bodipy-PA and PKR proteins	54
Figure 3.7. ATP competition assays	55
Figure 3.8. Bodipy-PA binding to PKR-WT and mutant proteins	58
Figure 3.9. Inhibitory effects of Bodipy-PA on PKR-WT and PKR-R307A autophosphorylation	59
Figure 4.1. Secondary structure of IRE1 α TM model peptide determined by circular dichroisi spectroscopy	m 74
Figure 4.2. Oligomer formation of IRE1 α TM model peptide by SDS-PAGE	75
Figure 4.3. Oligomer formation of IRE1 α TM model peptide by FRET	77
Figure 4.4. CD spectrum of IRE1-TM peptide in POPC liposome	80

Figure 4.5. FRET analysis of IRE1α-TM interactions in POPC liposomes	81
Figure. 4.6. CD spectra of IRE1α-TM peptides in TFE	83
Figure 4.7. TOXCAT and SDS-PAGE analyses of IRE1α-TM oligomerization	84
Figure 4.8. TM Sequence comparison of IRE1 and PERK proteins	91
Figure 5.1. Cytosolic domain of human IRE1α	94
Figure 5.2. Effect of palmitate on the phosphorylation of IRE1α and XBP1 splicing	99
Figure 5.3. Purification of IRE1α-LD and IRE1α-CD proteins	100
Figure 5.4. Binding affinity of Bodipy-PA to the luminal domain (LD) and cytosolic domain (CD) of the IRE1 α protein	102
Figure 5.5. Potential residues identified from the MD simulation	103
Figure 5.6. Effects of the mutants on the palmitic acid binding to $IRE1\alpha$	104
Figure 5.7. Fluorescence polarization measurements of the IRE1α-KD protein	107
Figure 5.8. Fluorescence intensity-based XBP1 cleavage assay	109
Figure 5.9. Urea-PAGE of XBP1 mini-substrate cleavage by IRE1α-CD	110
Figure 5.10. Protein expression of IRE1α-CD in insect cells	113
Figure 6.1. Effects of palmitate on the PERK activity	115
Figure 6.2. Superimposition of the kinase domains of PERK and PKR	117
Figure 6.3. Superimposition of the kinase domains of four proteins	118

CHAPTER 1. INTRODUCTION

1.1. Free fatty acids (FFAs) and diseases

Free fatty acids (FFAs) are generated by three major sources, diet, endogenous synthesis, and release from adipose tissues. Upon entering the liver, FFAs can be metabolized by β -oxidation in the mitochondria, esterified/stored as triglycerides (TG) in lipid droplets or used for lipid synthesis for components of the cellular membrane [1]. Elevated influx of FFAs is associated with several diseases, such as non-alcoholic fatty liver diseases (NAFLD), diabetes, cancers, and cardiovascular diseases [2-7].

Of the diseases associated with elevated levels of FFAs, NAFLD is one of the best characterized and the most common form of liver disease, with ~ 30 % of the adult population in the United States having NAFLD [2, 3]. NAFLD refers to a spectrum of conditions, ranging from simple steatosis to nonalcoholic steatohepatitis (NASH) to cirrhosis to hepatocellular carcinoma. It is estimated that 10% of the patients with simple steatosis progresses to NASH [4]. According to traditional models, the progression from simple steatosis to NASH follows a "two-hit hypothesis". This theory suggests the "first hit" involves lipid accumulation in the hepatocytes, with a second hit coming from proinflamatory cytokines, mitochondrial dysfunction, or endoplasmic reticulum (ER) stress, to lead to the progression to NASH [8]. However, there is emerging evidence that excess amounts of nonesterified saturated FFAs that fail to convert to TG in liver cells directly enhance the risk of hepatocellular lipoapoptosis, a pathogenic feature observed in NASH [9]. The levels of saturated FFAs in the plasma of NASH vs. control individuals were found to be 0.316 mM and 0.200 mM, respectively [10]. Of the saturated FFAs,

palmitic acid is the most common saturated fatty acid (~50%) in the plasma serum and was found increased from 0.097mM to 0.155mM in NASH patients [10]. In addition, elevated levels of saturated FFAs are associated with other diseases, including diabetes and cardiovascular diseases. They impair insulin signaling pathways, promote expression of cytokines and induce lipotoxicity [4-7]. Thus it is thought that these diseases (NAFLD, diabetes, and cardiovascular diseases) are inter-connected as a consequence of the FFA-induced toxicity, however the mechanisms involved in the FFA-induced toxicity remain unresolved. Several recent studies suggest that hepatic lipoapoptosis arises predominantly from FFA-induced lipotoxic stress of intracellular organelles, in particular the endoplasmic reticulum (ER) and mitochondria [11, 12].

1.2. The ER stress and the Unfolded Protein Response (UPR)

The ER is one of the largest organelles in the cells, and is responsible for protein folding, lipid synthesis, and calcium storage. The protein folding process specially requires oxidizing enzymes, chaperones, and glycosylation enzymes that are localized in the ER lumen with its high Ca²⁺ levels (~5 mM) [13]. However, cellular perturbations such as alterations in calcium storage in the ER lumen or an imbalance in the luminal-oxidizing environment can lead to the accumulation of misfolded or unfolded proteins in the ER lumen, i.e. "ER stress".

In mammals, cellular adaptation to ER stress is achieved by the activation of the unfolded protein response (UPR), an integrated signal transduction pathway mediated by three ER stress sensor proteins, IRE1 α (Inositol-requiring enzyme 1 α), PERK (protein kinase R (PKR)-like ER kinase), and ATF6 α (activating transcription factor 6 α) [14]. UPR signaling pathways coordinate the cellular response by down-regulating protein translation, enhancing the expression of ER

chaperone proteins that promote protein refolding, and activating proteases involved in the degradation of misfolded proteins. When these adaptive processes are sufficient to attenuate the ER stress, the cells can re-establish ER homeostasis. However, certain pathophysiological conditions, i.e., hypoxia, elevated levels of FFAs, oxidative stress, glucose levels, and inflammatory cytokines, are known to induce chronic and prolonged ER stress whereby the UPR switches to a pro-apoptotic mode. This occurs with many ER stress-associated diseases such as cancer, diabetes, neurodegenerative and inflammatory diseases [15, 16].

1.3. The UPR sensor proteins

Among the sensor proteins, IRE1 α is expressed in most tissues and possesses the most conserved signaling pathway of the UPR proteins [17]. IRE1 α consists of an N-terminal luminal domain as an ER stress sensor and a C-terminal cytosolic domain carrying protein Ser/Thr kinase and endoribonuclease activities. Under ER stress, the luminal domain of IRE1 α triggers the self-association of the IRE1 α protein [18]. The subsequent face-to-face dimerization of the kinase domain facilitates trans-autophosphorylation, subsequently activating the RNase domain [19]. The active form of IRE1 α catalyzes the unconventional processing of the mRNA encoding the transcriptional factor X-Box binding protein-1 (XBP1), by splicing a 26-nucleotide intron from the XBP1 mRNA [20]. The spliced XBP1, as a transcription factor, controls the upregulation of UPR-target genes involved in enhancing ER protein-folding capacity and degrading unfolded or misfolded ER proteins [20, 21]. On the other hand, the active IRE1 α can also induce apoptosis by interacting with tumor necrosis factor-receptor-associated factor 2 (TRAF2), leading to

activation of c-JUN N-terminal kinase (JNK) through the apoptosis signal-regulating kinase 1 (ASK1) [22].

The luminal domain of PERK is known to have similar structural and functional features to the luminal domain of IRE1α [23]. Like the IRE1α protein, ER stress promotes the dimerization of the luminal domain of the PERK protein. Along with other kinase proteins (PKR (double-stranded RNA-activated protein kinase), GCN2 (general control nonrepressed 2), HRI (heme-regulated inhibitor)), PERK belongs to the eIF2α (Eukaryotic translation initiation factor 2α) kinase subfamily, containing a Ser/Thr kinase domain in the cytosol. Upon dimerization of the luminal domain, the cytosolic kinase domain undergoes trans-autophosphorylation. The active PERK phosphorylates eIF2\alpha at Ser 51 and the phosphorylated eIF2\alpha impedes global translation initiation to decrease the protein load in the ER [24]. However, activated eIF2a paradoxically favors an increase in the translation of the activating transcription factor-4 (ATF4) that activates downstream UPR target genes, including GADD34 (growth arrest and DNA damage inducible 34) and CHOP (C/EBP-homologous protein; also known as GADD153) [25-27]. GADD34 is involved in the dephosphorylation of eIF2a, providing a negative feed-back loop to reverse the translational attenuation mediated by PERK [28]. However under prolonged ER-stress, ATF4 activates CHOP, which in turn inhibits the expression of anti-apoptotic Bcl-2 (B cell lymphoma 2) protein [29, 30]. Concomitantly, CHOP forms a heteromeric complex with the phosphorylated c-Jun to bind the PUMA (p53-upregulated modulator of apoptosis) promoter which contributes to the upregulation of pro-apoptotic proteins [31].

While IRE1 α and PERK are a type I transmembrane protein carrying both a single α -helical transmembrane domain and a cytosolic kinase domain, ATF6 α is a type II transmembrane transcription factor containing several α -helical transmembrane domains and a DNA-binding

domain with a basic leucin zipper motif [32]. Upon ER stress, ATF6 α localizes into the Golgi apparatus and is cleaved by serine protease site-1 (S1P) and metalloprotease site-2 (S2P), subsequently releasing the active form of the transcription factor (pATF6 α (N)) [33]. pATF6 α (N) plays a major role in chaperone induction and can also transcriptionally induce XBP1s to synergistically contribute to the downstream pathways of IRE1 α [34].

1.4. Palmitate-induced UPR signaling pathways

Saturated long chain-FFAs, especially palmitic acid, have been implicated in ER stressinduced apoptosis in several types of cells [35, 36]. Most studies on the effect of palmitate have focused on the regulation of the downstream molecules, JNK and CHOP, of the major signaling pathway axes (IRE1α-JNK and PERK-eIF2α-ATF4-CHOP) involved in ER stress-induced apoptosis (See detail signaling pathways in Figure 1). In human hepatocarcinoma cell lines, such as HepG2 and Huh-7 cells, palmitate upregulates the phosphorylation of JNK which promotes lipoapoptosis by inducing the pro-apoptotic effector PUMA [37-39]. Similary, palmitate is known to induce ER stress by upregulating CHOP expression in human hepatocarcinoma cell lines [31, 39]. Our group and others have helped to elucidated the pamitated-mediated PERKeIF2α-ATF4-CHOP signaling pathway in HepG2 cells [40, 41]. Palmitate also induces ER stress in pancreatic β -cell to cause β -cell dysfunction and death, a central pathogenesis of type 2 diabetes, by mediating both IRE1α-JNK and PERK-eIF2α-ATF4-CHOP pathways [42]. In addition to the liver and pancreatic cells, palmitate participates in ER stress-mediated apoptosis in cardiomyocytes, neurons, mesenchymal stem cells and endothelial cells [43-45], consequently contributing to the development of ER stress-associated diseases.

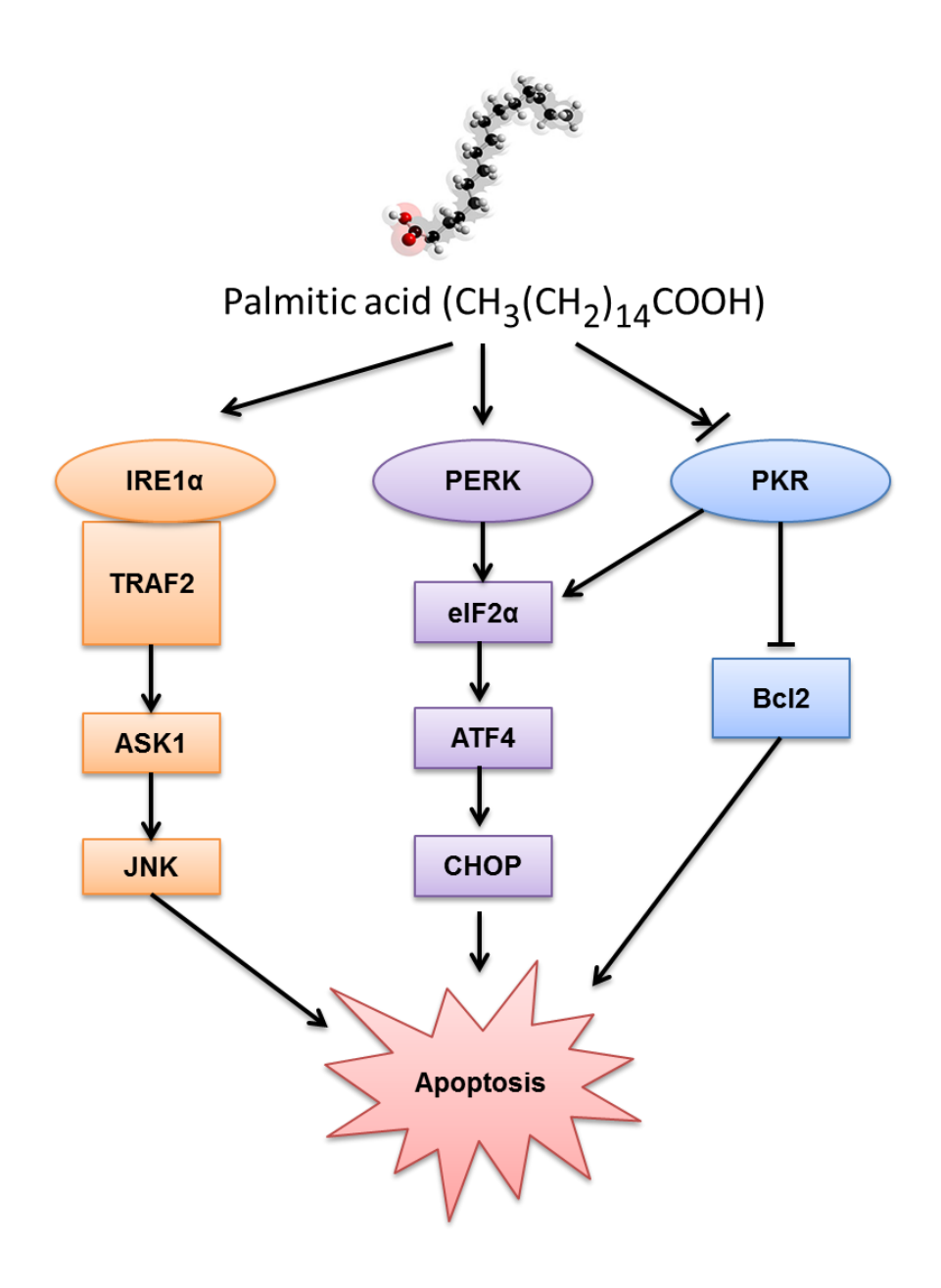


Figure 1. The signaling network of palmitate-induced apoptosis mediated by ER stress. The structure of palmitic acid is shown in balls and sticks. Major signaling components of IRE1α, PERK, PKR were shown in boxes. "For interpretation of the references to color in this and all other figures, the reader is referred to the electronic version of this dissertation."

Along with PERK (eIF2αk3), PKR (eIF2αk2) was also shown to be involved in ER stress-induced apoptosis by pharmacological ER inducers, thapsigargine and tunicamycin [46-48]. Our recent study showed that palmitate initiates the PKR-eIF2α-ATF4 pathway through PACT (PKR activating Protein)-PKR activation at an earlier time (3 hr) and PERK later helps to maintain the eIF2α phosphorylation [40]. In addition to this early response mediated by palmitate to inhibit global translation, long term exposure of HepG2 cells to palmitate reduces PKR phosphorylation and Bcl-2 protein levels, which in turn induce cellular apoptosis [49]. Thus the apoptosis induced by palmitate is mediated through three major kinase proteins, IRE1α, PERK, and PKR. These major signaling pathways are summarized in Figure 1.

1.5. Molecular mechanisms of the ER stress mediated by palmitate

Although increasing number of studies implicates an involvement of palmitate in ER stress, the molecular mechanisms by which palmitate activates the UPR signaling pathways (the IRE1α and PERK/PKR pathways) are unclear. One hypothesis is that palmitate increases calcium depletion in the ER, which regulates the functions of protein chaperones [50, 51]. However, other studies suggested that the effects of palmitic acid on the luminal Ca²⁺ do not always correlate well with ER stress [52, 53], indicating that multiple mechanisms could be involved in the palmitic acid-induced ER stress. Another potential mechanism by which palmitate mediates ER stress is by reducing ER-to-Golgi protein trafficking [54]. However, these previous studies do not explain how palmitic acid regulates IRE1α and PERK/PKR activities.

Interestingly, a recent study showed that IRE1 a and PERK lacking their luminal unfolded protein-stress sensing domain retained the ability to induce the palmitate-mediated ER stress [55].

In other words, the direct modulation of IRE1 α and PERK activities by palmitate is more likely independent of the luminal stress-induced activation. Nonetheless, it is still unclear whether the activation of these proteins by palmitate involves the transmembrane or the cytosolic domains.

1.6. Palmitate-binding proteins

Palmitate, the most common long-chain saturated fatty acid, has 16 carbon atoms (Figure 1). Due to its high hydrophobicity, palmitate is present at very low concentrations in the hydrophilic, cytosolic environment. In order to fulfill required cellular functions, palmitate overcomes its low solubility by interacting with proteins (Table 1). The most extensively studied palmitate-binding protein is serum albumin, which helps to transport FFAs to cells. Human serum albumin (HSA) contains three homologous α-helical domains and has seven palmitate-binding sites that share similar binding features: 1) A carboxyl group on palmitate that forms hydrogen bonds with basic amino acid side chains of HSA. 2) The carbon chain on palmitate fits readily into a hydrophobic cavity between the helices of HSA [56]. In contrast to serum albumin, fatty acid-binding proteins (FABPs) are mostly β -sheets and have very little helical structure. However, the binding modes of palmitate to FABPs are similar to HSA; namely, FABPs also contain one or two conserved basic amino acids, which interact with the carboxyl group of palmitate, as well as a hydrophobic binding pocket [57]. FABPs, as FFA carrier proteins, are involved in the transport of FFAs to specific compartments in the cells, to the ER for signaling, trafficking and membrane synthesis, to the mitochondria or peroxisome for oxidation, to the enzymes in the cytosol to modulate their activities [58]. Although HSA and FABPs have similar binding modes, palmitate's binding affinity for HSA is 5-10 nM, while for FABPs the k_D ranges from 50 to 500 nM [59-61].

Table 1. Palmitic acid binding proteins and their functions

Protein	Function
Serum albumin protein	Transport
Fatty acid binding proteins (FABPs)	Transport
Myelin P2 protein	Transport (potential)
	Regulation of transcription
Hepatic nuclear factor 4 (HNF4)	factors
Peroxisome proliferator-activated receptors	Regulation of transcription
(PPARs)	factors
Cytochrome P450	Enzyme reaction
α-dioxygenases (α-DOX)	Enzyme reaction
Phospholipase A	Enzyme reaction

In addition to serum albumin and FABPs, human myelin P2 protein is known to have a similar structure to the FABPs, suggesting potentially that palmitate could bind to human myelin P2 protein which might be involved in the transport of fatty acids to neuronal cells during development [62].

In addition, palmitate interacts with nuclear receptor proteins, hepatic nuclear factor 4 (HNF4) and peroxisome proliferator-activated receptors (PPARs), which regulate the transcription of a variety of genes involved in fatty acid oxidation and cell differentiation [61, 62]. HNF4 interacts with palmitate to form a hydrogen bond with an arginine in its hydrophobic cavity, which changes its conformation upon binding with palmitate to function as a constitutively active transcription factor. Furthuremore, palmitate serves as a ligand/substrate for diverse enzymatic reactions by interacting with enzymes, i.e., cytochrome P450, α-dioxygenases (α-DOX), and phospholipase A [63-65]. The carboxyl group on palmitate interacts with the Arg residue within the active sites of both cytochrome P450 and α-DOX, heme-containing enzymes that oxygenate a variety of fatty acids [63, 64]. In addition, palmitate locates in the active site (hydrophobic channel) of phopholipase A, inhibiting its enzyme activity and eventually ameliorating inflammation [65]. Due to the structural simplicity of palmitate, its ability to bind to various types of proteins is enhanced in the presence of a hydrophobic pocket that contains amino acids that can stabilize the carboxyl group of palmitate. This raises the question of whether palmitate could interact with kinases, involved in ER stress-induced apoptosis, to modulate their enzymatic activities.

Interestingly, several lipid binding domains have been identified on kinase proteins over the years. The first lipid binding domain was identified on a kinase protein, PKC (Protein Kinase C), which requires the amino phospholipid phosphatidylserine for optimal kinase activity [66]. Similarly, PKB (Protein Kinase B)/Akt, another kinase protein, has a pleckstrin homology (PH) lipid binding domain which interacts with lipids, i.e., phosphatidylinositol 3,4,5-trisphosphate. Thus lipids are known to regulate, either directly or indirectly, the activities of many proteins, including kinases involved in signal transduction [67]. Diskin R. et al. found a novel lipid binding site on the kinase C-terminal domain of p38α MAP kinase and showed that the binding site is able to accommodate a lipid (n-oxtyl-β-gluocopyranoside) as well as fatty acids (15(s)-hydroxyeicosatetraenoic acid and arachidonic acid). This is notable given that the structures of lipids and fatty acids are quite different; nevertheless they both can bind to the same site on the MAP kinase, suggesting that there may be other untested lipids or fatty acids that could also bind to this site [68]. Based on these evidences in the literature, we hypothesize that palmitate binds to kinase proteins to modulate their activities, and thereby suggesting potentially novel lipid-fatty acid binding sites.

1.7. Specific aims of the current study

Although palmitate is a strong inducer of ER stress-mediated apoptosis, the molecular mechanism by which palmitate activates UPR signaling is not well studied. As previously introduced, several lipids and fatty acids directly interacte with kinases to control the their enzymatic activities. Thus, here **we hyphothesize that palmitate binds to kinase proteins involved in ER-stress**. We have selected two model kinases, PKR (as a cytosolic protein) and IRE1 α (as a transmembrane protein), due to their structural similarity in the back to back conformation. The information we gain from these model kinases would provide a broader view of how palmitate could directly regulate kinases. Therefore, the hypothesis will be tested with the

following three aims. (1) Investigate the effects of palmitate on PKR activity. (2) Elucidate the role of the transmembrane (TM) domain in regulating the dimerization/oligomerization of the IRE1 α protein. Since the functional and structural information on the TM domain is currently not available, this study would be a framework to further investigate how palmitate is involved in regulating the dimerization/oligomerization of the IRE1 α -TM domain. (3) Investigate the effects of palmitate on IRE1 α activity.

CHAPTER 2. LATEST DEVELOPMENTS OF EXPERIMENTAL METHODS TO CHARACTERIZE PROTEIN-LIPID INTERACTIONS

Publications:

- (1) **Cho H**, Wu M, Bilgin B, Walton SP, Chan C. Latest developments in experimental and computational approaches to characterize protein-lipid interactions. Proteomics. (2012) 12(22):3273-85
- (2) **Cho H**, Mukherjee S, Palasuberniam P, Pillow L, Bilgin B, Nezich C, Walton SP, Feig M, Chan C. Molecular mechanism by which palmitate inhibits PKR autophosphorylation. Biochemistry (2011) 50(6):1110-9.

Lipids are one of the most abundant classes of cellular metabolites and there are data that show binding of proteins by lipids affects the functions of the proteins, nevertheless, the experimental methods to measure protein-lipid interactions (PLI) are underdeveloped. This is due both to technical difficulties in identifying each member of the diverse classes of cellular lipids and to the relative dearth of screening techniques for detecting global PLI. Nevertheless, advances in lipidomic research [69] have facilitated the recent development of novel approaches to characterize PLI. In this chapter, we first describe the main experimental approaches, namely solution-based and array-based approaches, for analyzing PLI. Second, more specifically, we introduce the development of an experimental method to characterize the protein-palmitic acid interactions and compare it with the current available methods.

2.1. Solution-based methods for studying protein-lipid interactions

Solution-based methods allow one to estimate the equilibrium binding and binding kinetics for protein-lipid interactions (PLI) in complex solutions that mimic biological environments. In this section, we discuss current experimental techniques to detect PLI in solution. The basic principles and recent applications of the methods are introduced. In addition, the merits and pitfalls of each method are compared (Table 2), providing a guide on which approaches might be of use in the study of PLI under different contexts.

The liposome sedimentation assay is most frequently employed for measuring PLI in solution. Similar to sedimentation velocity analytical ultracentrifugation used for studying protein-protein interactions (PPI) [70], the sedimentation efficiency of the liposomes depends, in this case, on their size. Typically, liposomes are mixed with a target protein and the lipid-protein complex is separated from the unbound proteins through high-speed centrifugation (> 20,000g). The proteinbound liposome (higher molecular size) is contained in the pellet while the unbound proteins (lower molecular size) remain in the supernatant. Thus, the fraction containing the proteinliposome complex can be separated from the unbound proteins. This method does not require the attachment of labels, and each protein fraction can be readily quantified by SDS-PAGE (sodium dodecyl sulfate polyacrylamide gel electrophoresis) and coomassie staining [71-73]. In some studies, labels (e.g., GST (Glutathione S-transferase), MBP (Maltose binding protein), radioactivity) are attached to the proteins to improve detection sensitivity [74-76]. Depending on the detection methods, liposome sedimentation can be used for protein concentrations in the range of 1 to 20 µM. Alone, this assay is qualitative, useful for determining whether a protein interacts with the lipids of the liposome. However, it was recently combined with proteomics

Table 2. Solution-based techniques to detect PLI

Methods	Advantages	Disadvantages
Liposome sedimentation assay	 applicable for proteomics analyses (<i>in-vitro</i> and <i>in-vivo</i>). available as both label-free and label-based methods. 	difficult to quantify the equilibrium constants.
Photoactivated crosslinking assay	 applicable for proteomics analyses (in-vitro and in- vivo). 	 low sensitivity (provides low yield of the cross-linked lipid-binding proteins).
Isothermal titration calorimetry (ITC)	provides thermodynamic parameters.is a label-free method.	 low sensitivity (requires higher protein concentrations)
Electron spin resonance (ESR) spectroscopy	 provides stoichiometry, selectivity, and geometric information of PLI. can be applied on opaque samples. 	 requires post-hoc molecular modification that limits the applicability of the approach in biological membranes.
Fluorescence- based assays	 higher sensitivity. 	 problems with light scattering and auto- fluorescence.

analysis, using nano-liquid chromatography-tandem MS (Nano-LC-MS/MS), to identify ~300 potential acidic phospholipid-binding proteins [77]. This novel combination provides a powerful tool to identify the variety of proteins that bind to a particular lipid.

Combined with the sedimentation assay, photoactivatable groups incorporated into lipids have been successfully used to study PLI [78, 79]. Upon UV activation, photoactivatable groups such as benzophenones, aryl azides, 3-trifluorophenyl diazirines, and alkyl diazirines yield highly reactive species that crosslink to form covalent bonds with proteins in contact with the activated site. The covalently labeled-protein can be subsequently separated from unbound proteins through high-speed centrifugation and then detected by SDS-PAGE or MS-based proteomic analyses. Protein interactions with cholesterol, sphingolipids, and phosphatidylcholine have been successfully identified using the photo-crosslinking approach and their applications of photo-crosslinking with lipids have been extensively reviewed [80, 81]. In addition, recent developments of click chemistry coupled with the use of photoactivatable groups have enabled proteome-wide detection of PLI in the mitochondria, contributing to the realization of high throughput PLI proteomics [81].

Isothermal titration calorimetry (ITC) is one of the popular label-free, solution-based tools for detecting PLI. In this case, ITC measures the heat generated (exothermic) or absorbed (endothermic) during formation of protein-lipid complexes [82]. From ITC data, thermodynamic parameters of the interaction (i.e., binding enthalpy, Gibbs free energy, dissociation constant) can be determined. Although this method requires relatively higher protein concentrations than the sedimentation assay, ranging from tens of micromolar to several millimolar, it is increasingly being applied in conjunction with structure-based techniques, such as NMR (nuclear magnetic

resonance), FTIR (Fourier transform infrared), and CD (circular dichroism) [83-86], to provide structural details of the PLI coupled with thermodynamic information.

Another widely used and label-based biophysical methodology for PLI is ESR (electronic spin resonance) spectroscopy, which discriminates between immobilized lipids (near the protein interface) and free lipids in solution [87]. By attaching the spin-label nitroxyl ring to the lipid hydrocarbon chain, ESR is able to determine both the stoichiometry of the PLI and the selectivity of the protein for different lipid species [88]. Spin—spin interactions can also be observed between different lipid species or between lipids and spin-labeled proteins. In addition, by changing the location of the spin-label on the lipids, ESR can provide geometrical information on the PLI, i.e., the depth to which the membrane protein penetrates the lipid bilayer [89, 90].

Fluorescence-based methods, such as FRET (fluorescence resonance energy transfer) and fluorescence anisotropy (see reference [91] for a detail review of the theory), can also be applied to the characterization of PLI. Each of these methods is based on the sensitivity of fluorophores to their local environment. For FRET, once a protein containing a donor fluorophore and a lipid labeled with an acceptor fluorophore are in close proximity (typically 10-100 Å), acceptor fluorescence signals will increase [92-94]. In cases where sensitivity is not an issue, the use of tryptophan, with intrinsic fluorescence, as a donor bypasses the need for post-hoc labeling of the protein. Several paired acceptors for the tryptophan donor (e.g., dansyl [95], pyrene [96], and NBD (nitrobenzoxadiazole) [97]) have been employed to characterize PLI. Unfortunately, light scattering and autofluorescence can be challenges when using conventional FRET. Therefore, time-resolved FRET (TR-FRET) can overcome this issue by employing europium, which has a long fluorescence lifetime, in the range of milliseconds [98, 99]. TR-FRET has been applied

successfully, due to its high signal-to-noise ratio [100], in 96-well plates for screening purposes [98].

In contrast to FRET, fluorescence anisotropy is determined by measuring the emission intensities parallel and perpendicular to the excitation plane. When a small molecule interacts with a larger one, the hydrodynamic volume of the complex increases, resulting in higher fluorescence anisotropy values. The fluorophore can be labeled either on the protein [101, 102] or lipid [103, 104]. Intrinsic tryptophan fluorescence has also been used in anisotropy measurements for quantifying the binding affinity of a PLI [105]. In addition to FRET and fluorescence anisotropy, other fluorescence-based methods employed to quantify the interactions between proteins and lipids include two-photon microscopy [106], fluorescence correlation spectroscopy [107], and flow cytometry [108]. As with the sedimentation assay and ITC, fluorescence-based methods have also been combined with structural-based methods for improved characterization of the protein-lipid complexes.

2.2. Array-based methods for analysis of protein-lipid interactions

2.2.1. Immobilization techniques

High-throughput screening of PLI have been performed using both protein [109] and lipid [110] microarrays. Here, we will focus on the application of lipid microarrays to probe PLI, with particular emphasis on the most recent developments in this technology. Lipid microarrays typically require the lipid molecules to be immobilized onto a planar surface. Several types of lipid systems can be immobilized onto surfaces (Figure 2.1), including single lipids, liposomes, and supported lipid bilayers. In addition to these lipid systems, nanodiscs consisting of a

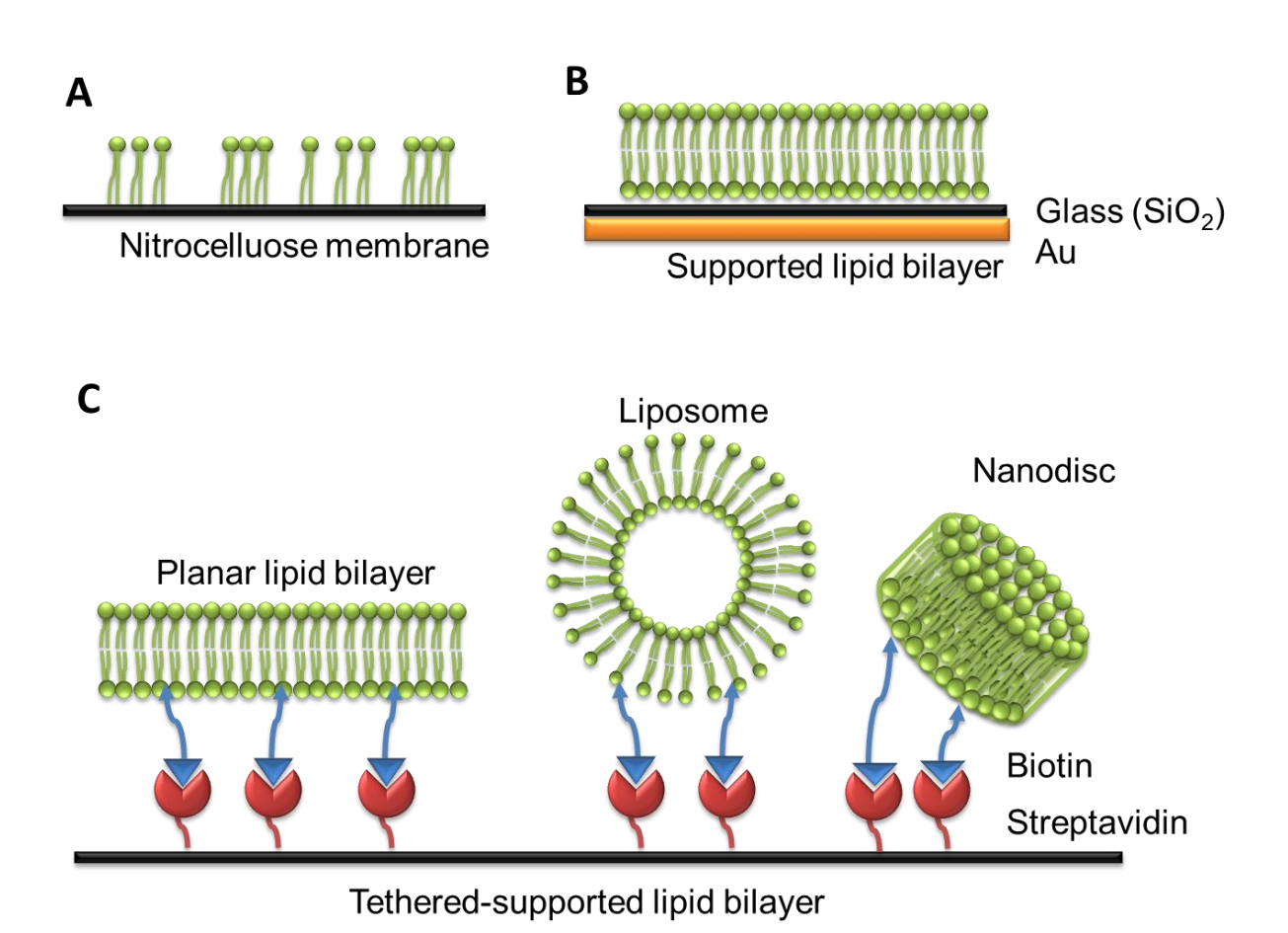


Figure 2.1. Immobilization techniques. (A) Protein lipid overlay assay. Lipids can be non-covalently spotted on hydrophobic surfaces such as nitrocellulose membrane. (B) Supported lipid bilayer. The lipid bilayers can be generated from lipid vesicle fusion on silica surface supported by gold. (C) Tethered-supported lipid bilayer. Planar lipid bilayers and liposomes and nanodiscs containing biotinylated lipids can be anchored onto streptavidin-coated surface.

discoidal lipid bilayer enclosed within an amphipathic protein belt were recently used to immobilize lipid bilayers on sensor chips for PLI studies [111]. Although the nanodisc approach requires additional steps to incorporate the lipids within the supporting protein, they provide a more soluble, uniform, and stable environment than the single lipid, liposome, and supported lipid bilayer approaches.

Techniques for immobilizing liposomes and supported lipid bilayers have been recently reviewed in [112, 113]. The most common and conventional method used for PLI studies is to spot the lipids on nitrocellulose membranes (Figure 2.1A), which has been employed in proteinlipid overlay assays [114, 115]. This method is the simplest one in that it does not require any chemical modification of the lipids or fabrication steps on the surfaces. Immobilization techniques are well developed, and have been adapted into commercial products for screening. These immobilization methods are incorporated in commercial lipid arrays, such as PIP Strips TM, PIP MicroStripsTM, SphingoStripsTM and PIP ArrayTM. In addition, these membrane surfaces are typically fragile, making them infeasible for high-throughput screening systems for detecting PLI. However, recent studies used the nitrocellulose or PVDF (polyvinylidene difluoride) membranes attached onto glass slides for automated spotting systems [116, 117]. To obtain more uniform lipid bilayer structures, supported lipid bilayers can be generated from lipid vesicle fused onto hydrated surfaces made of silica or polydimethylsiloxane (PDMS) (Figure 2.1B). By applying a thin silicate layer to the gold substrate, without any surface chemistry modifications, the lipid vesicles fused onto the silicate surface to produce a single lipid bilayer [118, 119]. In addition, PDMS is an ideal alternative for hydrophilic surfaces to generate supported lipid bilayers [120]. However, it is known that the planar supported lipid bilayers have stability issues, by causing vesicle deformation which induces stress into the lipid bilayer [113]. There are two ways to

improve the stability of the supported lipid bilayers. One approach is to introduce poly(ethylene glycol) (PEG)-derivative-lipids (PEG-brush configuration), which helps to retain a functional air-stable bilayer membrane [121, 122]. Alternatively, to achieve gentler immobilization, the irreversible interaction between biotin-streptavidin can be capitalized to generate tethered-supported lipid bilayers [123] (Figure 2.1C). In addition, liposomes and nanodiscs also have been immobilized using biotin-streptavidin interactions in the tethered lipid systems [111, 124].

2.2.2. Detection techniques

While techniques for immobilization have been extensively studied, methods to detect PLI are not well developed. Similar to protein microarray [125, 126], detection techniques employed in lipid microarray analyses can be categorized into two classes: label-based and label-free methods (Figure 2.2). Label-based detection methods require labeling of the target proteins with fluorescent dyes, epitope tags, radioisotopes, or signal-generating enzymes (e.g., horseradish peroxidase (HRP)). Label-free methods (e.g., surface plasmon resonance (SPR), MS, atomic force microscopy (AFM), and interferometry) measure the inherent physical properties of the target proteins such as mass or dielectric properties. Label-based methods are more widely used, because the associated instruments are readily available. However, they are more laborious, requiring the attachment of tags on the proteins which could interfere with protein function. Although label-free techniques avoid these issues, they are typically less sensitive than the label-based approaches. However, the sensitivity of label-free techniques (especially SPR) has dramatically increased in recent years using approaches that can amplify the signals.

2.2.2.1. Label-based techniques

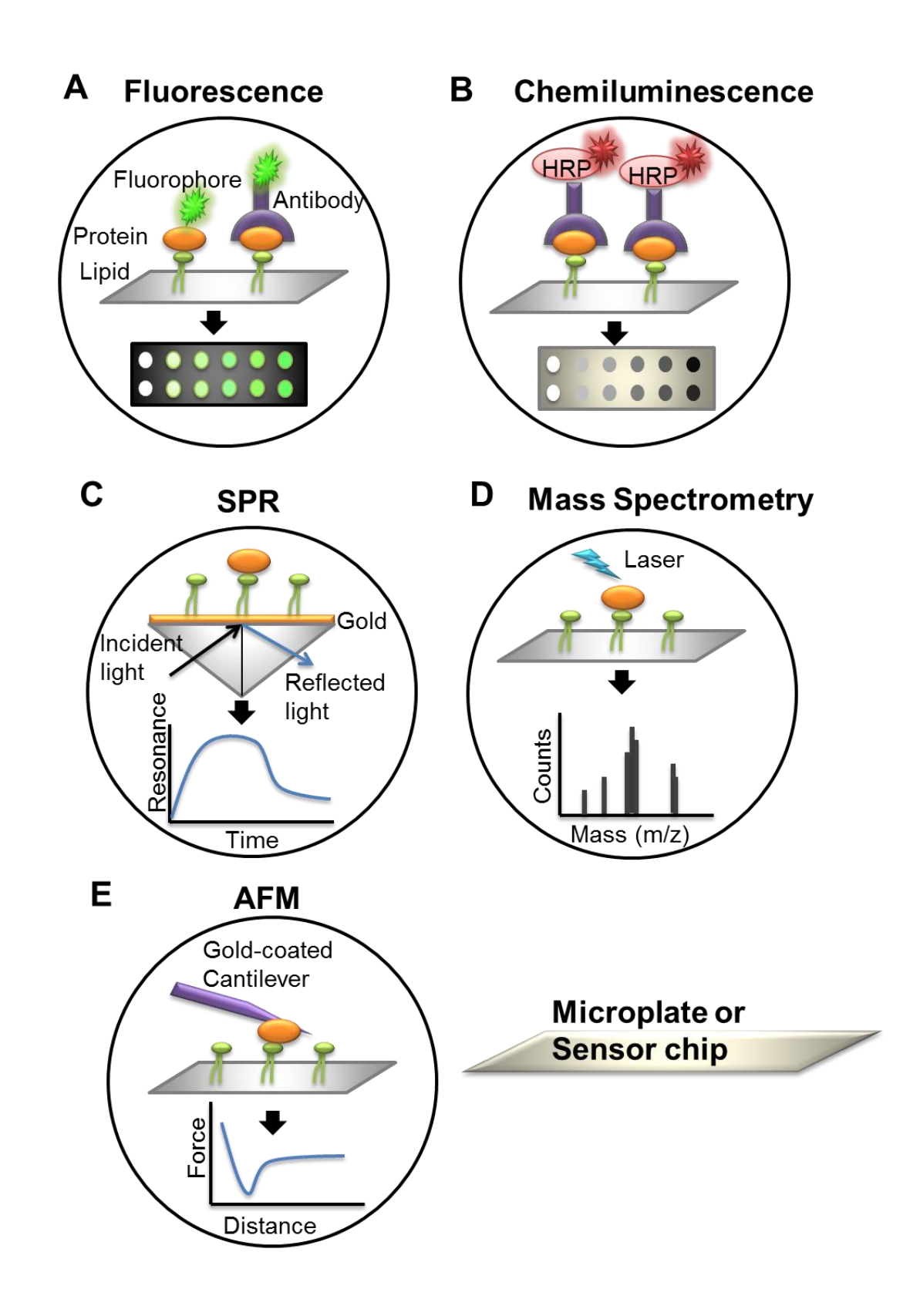


Figure 2.2. Detection techniques for lipid microarray systems.

(Figure 2.2 cont'd) detection uses either fluorophore-tagged proteins or fluorophore-tagged antibodies against target proteins to detect protein-lipid interactions. (B) Chemiluminescence generates signals from HRP-conjugated antibody targeted for lipid-bound proteins. (C) SPR measures changes in the refractive index near a sensor surface. The interaction between the surface immobilized lipid bilayer and the proteins results in a change in the refractive index. (D) TOF-MS method uses laser energy to generate ions, displaying the mass-to-charge values and signal intensities of the proteins that interact with the lipids. (E) AFM equipped with a gold-coated cantilever sensor measures changes in the forces when the proteins interact with the lipids.

As with the solution phase analyses discussed above, fluorescent labels are commonly applied in label-based methods (Figure 2.2A). Fluorophore-tagged proteins can be detected on lipid-coated surfaces using fluorescence microscopy. Often, these studies are piloted using the model Cholera toxin protein, which binds to GM1 gangliosides and is clinically relevant. In such studies, GM1 lipids are incorporated into phospholipid bilayers immobilized onto a surface, and the Cholera toxin protein is labeled with either FITC [122, 123] or Alexa dyes [127-129]. It was demonstrated that the tethered supported bilayer system has relatively high sensitivity and can detect protein at nanomolar concentrations [123]. In addition, total internal reflection fluorescence microscopy (TIRFM), one of the preferred techniques used to observe single molecules attached to planar surfaces, has been employed to measure the Cholera toxin-GM1 interaction [127]. In TIRFM, since only the membrane-bound proteins can be excited by the evanescent wave of an internally reflected laser beam, the binding kinetics between the proteins and lipids can be quantified. Thus, TIRFM was able to detect the binding of GM1 in planar supported bilayers to Alexa 595 labeled-Cholera toxin protein at concentrations as low as 100 pM [127]. The fluorescence method has also been coupled with antibodies to detect PLI through an ELISA-like approach [120, 130]. Thus the fluorescence-based immunodetection method provides a fast, simple, and sensitive detect for high-throughput screening of PLI.

Chemiluminescence detection also can be used with label-based detection methods (Figure 2.2B). Protein-lipid overlay assay has adapted the chemiluminescence detection method for semi-quantitative measurements of PLI. Typically, nitrocellulose membranes immobilized with lipids are incubated with a protein possessing an epitope tag [115, 117, 131]. The lipid-bound protein is then detected by immonoblotting with an HRP-conjugated antibody against the epitope tag. The protein lipid overlay assay has been successfully applied to screen PLI in yeast

[117]. In addition, chemiluminescence has been used as a readout for a microplate-based approach to characterize PLI [130, 132]. Chemiluminescence methods typically have a detection limit in the range of 1 nM protein, roughly 10-fold lower than fluorescence-based methods.

2.2.2.2. Label-free techniques

SPR is an optical technique that measures changes in refractive index at a metal-coated surface, and is a powerful analytical method for studying biomolecular interactions. SPR allows for rapid, label-free characterization of PLI, with direct measurement (Figure 2.2C) and sensitivities of ~3 nM protein having been achieved [133]. Using an amplification approach involving functionalized gold nanoparticles in combination with an *in situ* atom transfer radical polymerization reaction, the detection limit was lowered to 160 aM $(1.6\times10^{-16} \text{ M})$ [134], achieving a higher sensitivity than previously reported detection methods. A recent study integrated SPR with neutron reflectivity and electrical impedance spectroscopy to investigate different aspects of a PLI, providing information about the lipid composition as well as the structural properties of β -lactoglobulin regulated by the PLI [135].

Single sample detection of PLI by SPR was successfully measured over a decade ago [136]. Recent publications have focused on using SPR as a screening tool for real-time analyses of multiple samples [111, 118, 133-135, 137, 138]. Further, SPRi (SPR imaging), an advanced format of SPR in which an image of the light reflected from the SPR substrate can be obtained, allows visualization of a whole array in real-time. SPRi was used to detect PLI, using both microfluidic and etched glass array formats [119, 121, 139, 140]. Current efforts are focused on achieving sensitivities with SPRi for parallel measurements that match those of fluorescence-based approaches.

MS technology has recently become one of the most popular methods to detect PLI in parallel, due to its capacity to identify the variety of lipids present in biological samples [141]. Many studies have focused on the identification of phosphoinositide (PI)-protein interactions using the lipid affinity capture method combined with MS [142]. In this approach, either proteins or lipids are immobilized on the affinity matrices. The immobilized molecules then capture their binding partners from cell extracts. The interactions are then detected by LC-MS/MS. Thus far, MS has rarely been applied on lipid microarray to detect PLI. Two types of time of flight MS (TOF-MS), which display mass-to-charge values and signal intensities of individual proteins, have been adapted to measure PLI [129, 143] (Figure 2.2D). MALDI-TOF (matrix-assisted laser desorption/ionization time of flight MS) and SELDI-TOF (surface enhanced laser desorption/ionisation-time of flight MS) have been applied to single PLI [129] and array-based measurements [143], respectively. Both MS applications were able to identify oligomeric lipid-binding proteins [129, 143].

Other techniques such as AFM, and interferometry are less frequently used to detect PLI. AFM has been used to probe PLI (AFM probing) or generate surface images (AFM imaging) of protein-lipid complexes [143, 144] (Figure 2.2E). The interaction force between phospholipids immobilized on a sensor chip and proteins conjugated on a gold coated cantilever was measured using AFM probing to show that lipids can interact with the C2A domain of synaptotagmin I [144]. AFM imaging showed that the α-synuclein protein penetrated a lipid monolayer and that the dimer form of the protein had higher affinity for the lipid bilayer relative to the monomer [143]. In addition, backscattering interferometry (BSI) was used to measure changes in refractive index on microfluidic chips that result from intermolecular associations, which provides the binding affinity between the proteins and lipids [145].

2.3. Development of the experimental methods for analysis of protein-palmitic acid interactions

Although saturated fatty acids are classified under lipids, due to their structural simplicity (a carboxyl group and a hydrocarbon chain), chemical modifications on the fatty acids for the label-based detection methods described in section 2.2.2 could be limited. Thus, two commonly available methods are the lipidex assay and the ADIFAB (an acrylodan labeled intestinal fatty acid binding protein) assay. The lipidex assay uses "Lipidex 1000", a 10% substituted hydroxyalkoxypropyl derivative of Sephadex G-25 (one type of cross-linked dextran gels), which has affinity for hydrophobic materials in a temperature dependent manner [146]. This assay requires radioactive labeled FFAs for the purpose of detection. The proteins and fatty acids are mixed at room temperature and then the FFA-bound proteins are attached onto the lipidex column while the unbound proteins are washed away at 4 °C due to the temperature-dependent physical property of Lipidex 100. Since this assay requires extensive washing to remove the unbound proteins and also the binding reaction is performed at 4 °C, the binding equilibrium in solution could be different from the one obtained from the lipidex assay. The ADIFAB assay uses a fluorescently labeled fatty acid binding protein (ADIFAB) that enables one to indirectly measure the fatty acid binding affinity in solution [59]. Fatty acids and proteins are mixed in solution and then ADIFAB is added in the mixture to detect the amount of FFAs. The affinity of the fatty acids for the target protein can be calculated by subtracting the ADIFAB bound FFAs from the total FFAs. Since co-incubation of ADIFAB and proteins could have the nonspecific interactions between two proteins, the ADIFAB assay would not reflect the real binding affinity of the fatty acids.

More recently, a fluorescently labeled palmitate molecule, Bodipy-PA (Bodipy-C16) (Figure 2.3), has been used for quantifying palmitate binding affinity to FABP proteins [147]. At high concentration (500 nM), Bodipy-PA molecules self-associate and quench the green fluorescence. Once the FABP protein is mixed with Bodipy-PA, the fluorescence is recovered, enabling calculation of the palmitate binding affinity to the protein. Free fatty acids (FFAs) in the plasma are transported by plasma proteins, i.e. albumin, leaving approximately 10 nmol/L of FFA unbound [148]. Thus, this fluorescence intensity-based assay does not reflect the physiological levels of unbound FFA (10 nM). Here we developed a fluorescence polarization (FP)-based palmitate interaction assay using 10 nM of Bodipy-PA. We first measured the FP values of Bodipy-PA, in the absence of any protein. Figure 2.4 shows there is no significant increase in the FP values. Next we assessed whether the FP-based assay is able to determine the binding constant of bovine serum albumin (BSA), which served as a positive control protein. As shown in Figure 2.5, the FP values of Bodipy-PA increased gradually with increasing concentrations of BSA and eventually approached a plateau. In contrast, lysozyme did not show any significant increase, suggesting that the assay is specific to palmitic acid-binding proteins. The binding constant (K_D) of BSA was determined using nonlinear regression analysis. The K_D value (29.21±1.85 nM) observed is similar to the value (22 nM) reported by Burczynski's group [149]. Thus, the FP-based palmitate interaction assay is well suited for quantifying the interaction between Bodipy-PA and palmitic acid-binding proteins. Since the fluorescence intensity influences the calculation of the FP values, we further tested whether the florescence intensity values of Bodipy-PA change upon adding BSA proteins. As shown in Figure 2.6A, there is no significant increase in the fluorescence intensity with 10 and 30 nM of Bodipy-PA with increasing BSA protein, unlike 50 nM of Bodipy-PA, which induced a change in the

Bodipy-C16 (Palmitic acid)

Figure 2.3. The structure of Bodipy-PA (Bodipy-C16) (4,4-difluoro-5,7-dimethyl-4-bora-3a,4a-diaza-s-indacene-3-hexadecanoic acid).

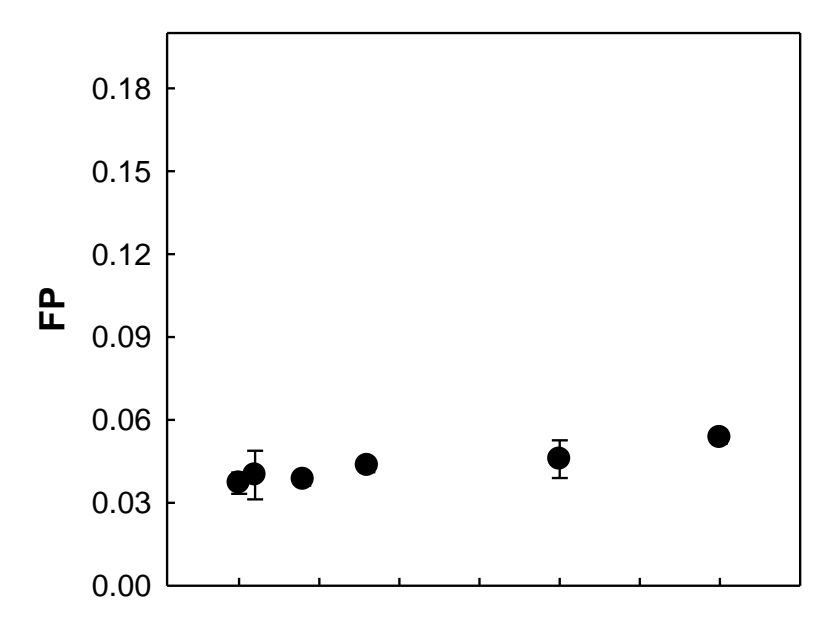


Figure 2.4. Fluorescence polarization measurement of Bodipy-PA. 10 nM of Bodipy-PA (4,4-difluoro-5,7-dimethyl-4-bora-3a,4a-diaza-s-indacene-3-hexadecanoic acid) was added to PBS buffer without any protein. After 5 min of incubation, the fluorescence polarization was measured at an excitation wavelength of 488 nm and an emission wavelength of 520 nm with a spectrofluorometer.

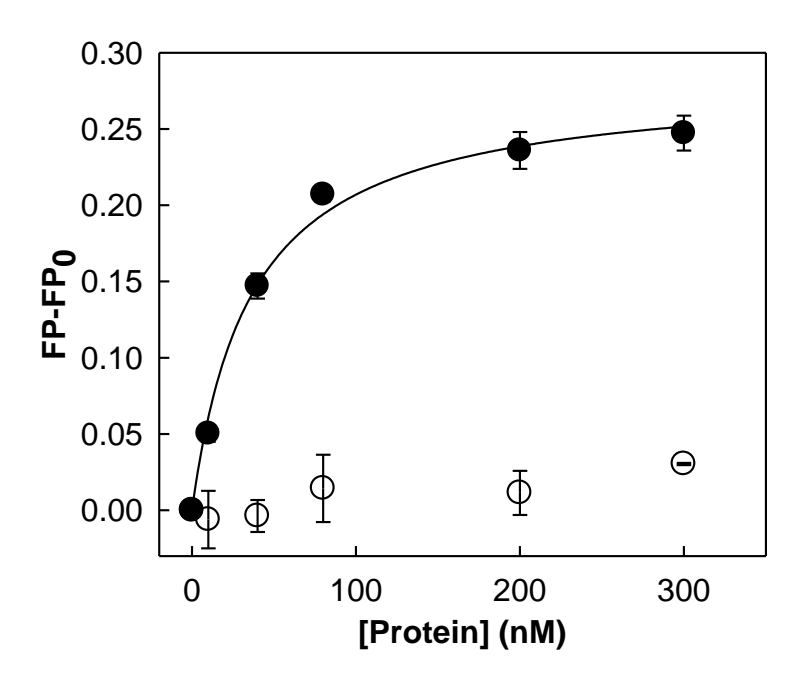


Figure 2.5. Fluorescence polarization measurement of the Bodipy-PA and BSA interaction.

10 nM of Bodipy-PA was added to PBS buffer with increasing concentrations of Lysozyme (open circles) or BSA (closed circles). After 5 min of incubation, the fluorescence polarization was measured at an excitation wavelength of 488 nm and an emission wavelength of 520 nm using a spectrofluorometer. The solid lines represent fitting of the data to the quadratic binding equation [150].

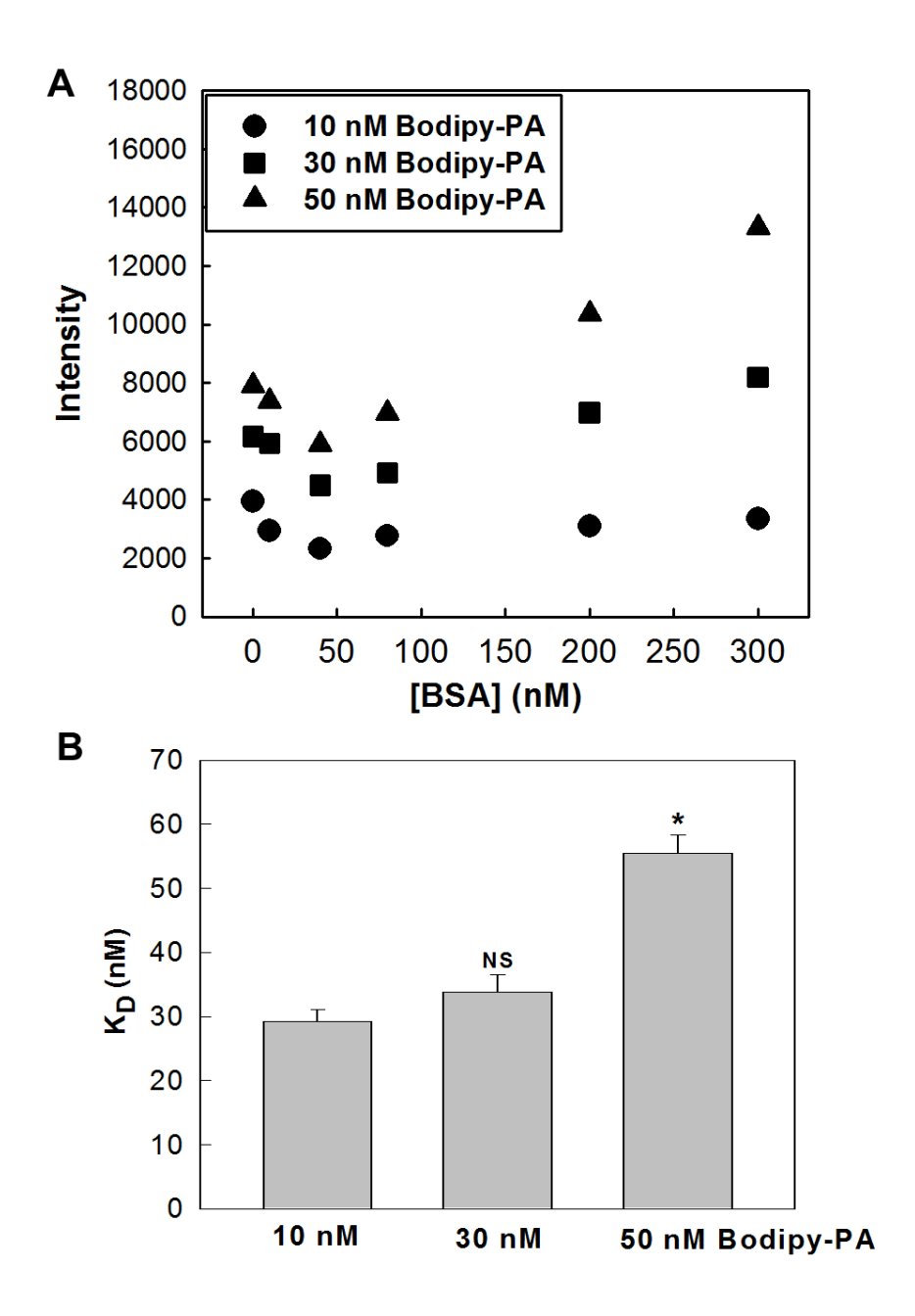


Figure 2.6. Optimization of FP-based Bodipy-PA binding assay. (A) 10, 30, and 50 nM of Bodipy-PA was added to PBS buffer with increasing concentrations of BSA protein. After 5 min of incubation, the fluorescence intensity was measured at an excitation wavelength of 488 nm and an emission wavelength of 520 nm using a spectrofluorometer. (B) K_D values were estimated by fitting the FP data using the Kaleida-Graph software. 50 nM is statistically different from 10 nM Bodipy-PA, * (p<0.001). There is no significant difference between 10 nM and 30 nM, indicated by NS.

fluorescence intensity with increasing BSA concentration. Further, we estimated the K_D values for 10, 30, 50 nM Bodipy-PA. As expected, there was no significant difference between 10 and 30 nM Bodipy-PA (p-value < 0.001), but the K_D value for 50 nM Bodipy-PA and BSA increased significantly (Figure 2.6B). These experiments suggest that at 10 nM Bodipy-PA, the Bodipy-PA likely exists as monomers in PBS (phosphate buffered saline) solution. In contrast, at 50 nM Bodipy-PA, the Bodipy-PA may begin to form a layered structure, thereby increasing the fluorescence intensity when the Bodipy-PA molecule disassociates from the layer to bind to the BSA protein. Thus at the physiological concentration of free palmitate (10 nM), the FP-based binding assay provides a reliable method for detecting palmitate binding in solution, without the washing steps or other helper molecules. We expect that the developed assay would facilitate screening of potential palmitic acid binding proteins using high-throughput techniques.

CHAPTER 3. MOLECULAR MECHANISM BY WHICH PALMITATE INHIBITS PKR AUTOPHOSPHORYLATION.

Publications:

- (1) **Cho H**, Mukherjee S, Palasuberniam P, Pillow L, Bilgin B, Nezich C, Walton SP, Feig M, Chan C. Molecular mechanism by which palmitate inhibits PKR autophosphorylation. Biochemistry (2011) 50(6):1110-9.
- (2) Fang L, **Cho H**, Chan C, Feig M. Palmitate Binding on the αC-helix Regulates PKR Autophosphorylation. (2013) (in review).

3.1. Abstract

PKR (double-stranded RNA-activated protein kinase) is an important component of the innate immunity, antiviral, and apoptotic pathways. Our group previously found that palmitate, a saturated fatty acid, is involved in apoptosis by reducing the autophosphorylation of PKR at the Thr451 residue; however, the molecular mechanism by which palmitate reduces PKR autophosphorylation is not known. Thus, we investigated how palmitate affects the phosphorylation of the PKR protein at the molecular and biophysical levels. Biochemical and computational studies show that palmitate binds to PKR, near the ATP-binding site and α C-Helix, thereby inhibiting its autophosphorylation at Thr451 and Thr446. Mutation studies suggest that either the ATP-binding site (Lys296 and Asp432) or the α C-Helix (R307) on the PKR protein are important for palmitate binding. We further confirmed that palmitate also interacts with other kinases, due to the conserved ATP-binding site. A better understanding of how palmitate interacts with the PKR protein, as well as other kinases, could shed light onto

possible mechanisms by which palmitate mediates kinase signaling pathways that could have implications on the efficacy of current drug therapies that target kinases.

3.2. Introduction

The double-stranded (ds) RNA-activated protein kinase (PKR) is a ubiquitously expressed serine/threonine kinase that is up-regulated upon interferon (IFN) production during mammalian innate immune response [151]. The enzyme is normally in its latent form, and is activated upon binding of double-stranded RNA (dsRNA), triggering dimerization and autophosphorylation [152]. Activated PKR can phosphorylate the α-subunit of eukaryotic translation initiation factor (eIF2α) at Ser 51, thereby decreasing the initiation of viral translation by inhibiting the guanidine nucleotide exchange activity of the eIF1 heterotrimeric complex [153]. PKR can also phosphorylate the regulatory subunit B56α on protein phosphatase 2A (PP2A) and thereby enhance the enzymatic activity of the PP2A-B56α trimeric complex, which can lead to dephosphorylation of eIF-4E and translational arrest [154]. In addition, PKR is broadly involved in diverse cellular processes, such as cellular differentiation, apoptosis, cell growth, and oncogenic transformation [155].

PKR is a 551-amino acid enzyme consisting of a N-terminal double-stranded RNA binding domain (dsRBD) and a C-terminal kinase domain connected by an 80 residue unstructured linker. The dsRBD contains two conserved dsRBD motifs responsible for dsRNA recognition. The NMR structure of the dsRBD revealed two motifs that adopt the canonical $\alpha\beta\beta\beta\alpha$ fold linked by a ~20 amino acid sequence or linker, however dsRBM1 (double-stranded

RNA-binding motif 1) has higher RNA binding activity than dsRBM2 [156, 157]. The X-ray crystal structure of the kinase domain of PKR complexed with eIF2α was previously resolved [158]. The kinase domain adopts a bilobal structure typical of protein kinases, with a smaller N lobe and a larger C lobe. The N lobe is involved in the back-to-back dimerization of the PKR kinase domain and the C lobe is responsible for substrate recognition. ATP binds the cleft between the two lobes and the binding mode required to mediate phosphoryl transfer is highly conserved across kinases [159, 160]. The two phosphorylation sites in the activation loop of the C lobe (Thr446 and Thr451) are critical for full catalytic activation of PKR as well as substrate binding [152, 158, 161].

In the kinase domain of the PKR protein, there are several regions that play important roles in the binding and hydrolysis of ATP (See Figure 3.1). One of them is the Mg^{2+} binding loop that contains the conserved motif DFG, the aspartic acid residue (Asp432) being important in binding and stabilizing the ATP- Mg^{2+} complex. The catalytic loop containing conserved residues, such as Asp414 and Asn419, is involved in the catalytic reaction of the nucleotide γ -phosphate. The activation loop contains the threonine residues (Thr446, Thr451) that undergo phosphorylation during activation of the kinase domain. Finally, Lys296 interacting with the α C helix orients the α and β phosphates of the ATP and the α C helix present in the N-lobe acts as an important conformational switch, changing its orientation along with the activation loop, during the inactivation-activation cycle [162]. It is observed that the nucleotide binding cavity is sandwiched between the β -sheet bundle of the N-lobe, the Mg^{2+} binding loop, the catalytic loop and the α C helix, while the mouth of the cavity is lined by parts of the activation loop.

A large body of biochemical and biological evidence revealed that PKR has both pro- and

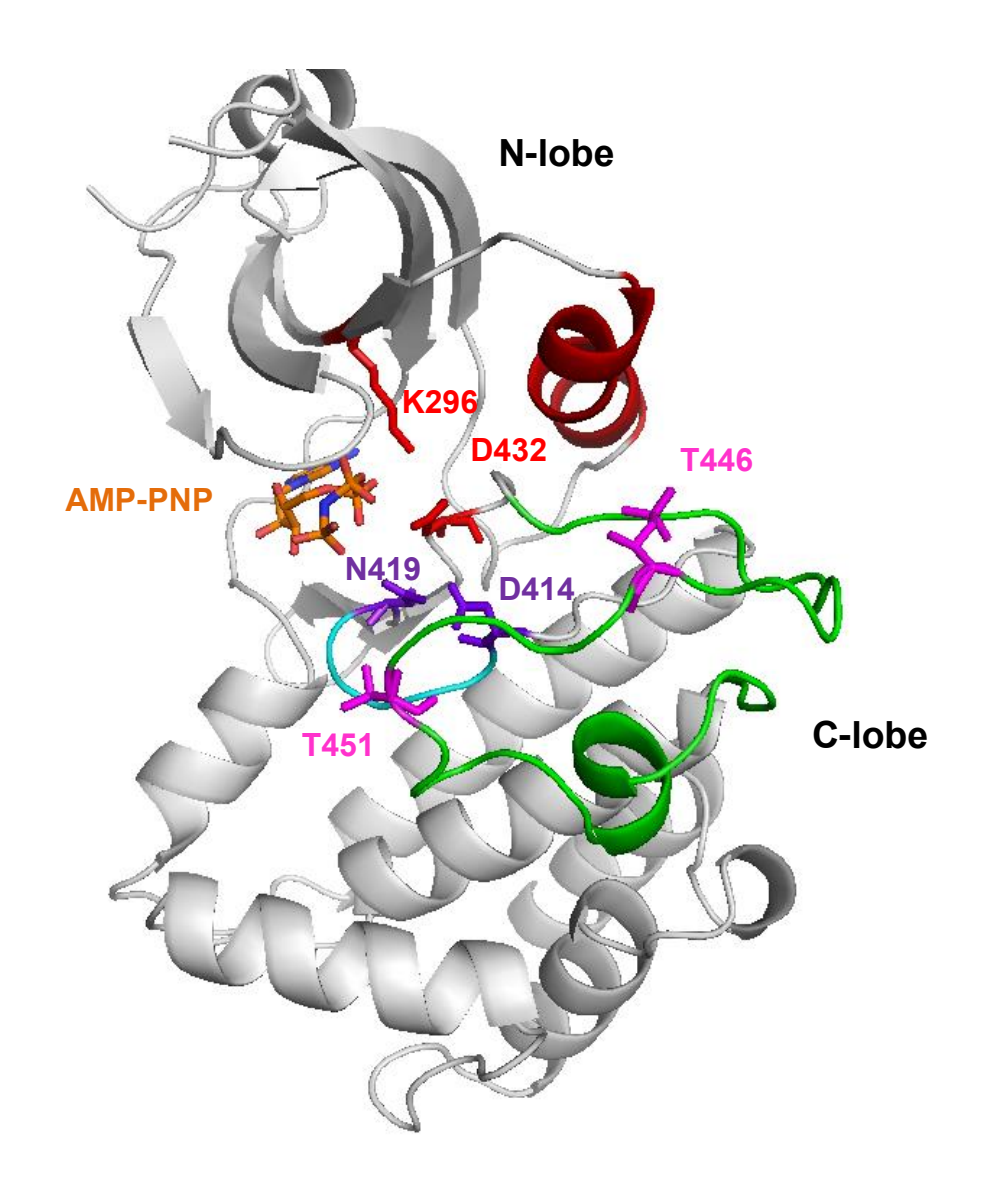


Figure 3.1. Binding mode of AMP-PNP with PKR. Kinase domain of PKR is shown in gray, catalytic loop in cyan, activation loop in green, and α C helix in red. Important residues in the nucleotide binding cavity are shown in sticks, and the bound ATP analogue adenylyl imidodiphosphate (AMP-PNP) is colored in orange for the carbon atoms. The figure was generated using the following structures: PKR:AMP-PNP:eIF2 α (PDB ID 2A19).

anti-apoptotic roles. The first evidence of a pro-apoptotic role of PKR was performed in PKRoverexpressed HeLa cells using a recombinant vector [163]. It was further demonstrated that PKR, triggered by viruses, induces apoptosis [164-166]. In the absence of viral infection, PKR has been generally recognized as a pro-apototic factor that phosphorylates eIF2 α , resulting in the inhibition of protein synthesis. Transcription factors, such as nuclear factor kappa-B (NF-κB), activating transcription factor 3 (ATF-3), and p53 also have been implicated in mediating PKRinduced apoptosis [167]. In contrast, other studies have shown that PKR plays anti-apoptotic roles in regulating tumor development and tumor-cell apoptosis [168-171]. A recent study suggests that PKR may act as a tumor suppressor, preventing apoptosis mediated by the transcription factor NF-κB [171]. Results from our lab support an anti-apoptotic role of PKR in human hepatocellular carcinoma cells (HepG2), by regulating the protein expression and phosphorylation levels of Bcl-2 (B-cell leukemia/lymphoma 2) [172, 173]. We found the autophosphorylation of PKR is attenuated by a saturated free fatty acid (FFA), palmitate. However, the molecular mechanism by which palmitate inhibits PKR autophosphorylation is not known.

Palmitate has low aqueous solubility and is present at very low concentrations in the hydrophilic, intracellular environment. In order to fulfill required cellular functions, palmitate overcomes its low solubility by interacting with proteins. As described in the introduction (Chapter 1.5), several proteins are known to interact with palmitate and some of kinase proteins have lipid binding domains which could regulate the protein kinase activities. This raises the question of whether a hydrophobic pocket exists within the PKR protein to which palmitate may bind to modulate its kinase activity.

Here we report a novel molecular mechanism by which palmitate modulates PKR activity, and thereby possibly regulates cellular functions. Using fluorescence techniques, we investigated the binding affinity between palmitate and the PKR protein. With the assistance of the computational simulation methods, biochemical and biophysical experiments were performed to further demonstrate that palmitate binds to the kinase domain of PKR, and reduces the autophosphorylation of PKR. Finally, we evaluated the ability of palmitate to interact with several kinases. The implications of this work, i.e. the role of palmitate on PKR signaling, and broadly on other kinases, are discussed.

3.3. Materials and Methods

3.3.1. Materials

4,4-difluoro-5,7-dimethyl-4-bora-3a,4a-diaza-s-indacene-3-hexadecanoic acid (BODIPY -FL C16), herein denoted as Bodipy-C16 or Bodipy-PA, 4,4-Difluoro-5-(2-Thienyl)-4-Bora-3a,4a-Diaza-s-Indacene-3-Dodecanoic Acid (Bodipy-C12), and 4,4-difluoro-5,7-dimethyl-4-bora-3a,4a-diaza-s-indacene-3-propionic acid (Bodipy-C3) were obtained from Invitrogen. γ
³³P-ATP was purchased from Perkin Elmer. Anti-PKR, anti-PKR-pThr451, and anti-PKR-pThr446 were purchased from Abcam, Sigma-Aldrich, and Novus Biologicals, respectively. Recombinant kinase proteins, Akt1 (Protein kinase B 1), MAP kinase-activated protein kinase 3 (MAPKAPK3), and Cyclin-dependent kinase 4 (CDK4), were obtained from GenWay Biotech, Inc. All other reagents used were reagent grade.

3.3.2. Protein expression and purification of PKR protein constructions

DNA recombinant plasmids, pET28a-pWT [174] and pET11a-WT [175] containing the full length of human PKR wild-type protein were kindly provided by Dr. Philip C. Bevilacqua's and Dr. James L. Cole's groups, respectively. As previously reported, wild-type PKR expressed in E. coli is phosphorylated, thus unphosphorylated protein was obtained by coexpressing PKR with phosphatases [176, 177]: Phosphorylated PKR and unphosphorylated PKR are herein denoted as PKR-pWT and PKR-WT, respectively.

The plasmids were transformed into E. coli BL21(DE3) pLysS (Invitrogen) or RosettaTM 2(DE3) pLysS cells (Novagen). Cells were grown in LB media at 37 °C until the OD at 600 nm reaches 0.6 and then protein expression was induced with 1 mM IPTG for three hours at 30 °C. The cells were collected by centrifugation at 4,000 rpm for 10 min and re-suspended in sonication buffer (50 mM HEPES, 500 mM NaCl, 5 % glycerol (pH 7.0), and 7 mM βmercaptoethanol) containing protease inhibitor cocktail and phenylmethanesulfonyl fluoride (PMSF). For PKR-WT protein, the sonication buffer without NaCl was used to re-suspend the cells. The suspension solution was lysed with 100 mM lysozyme and sonicated. The lysate was centrifuged at 12,000 rpm for 25 min and the supernatant was filtered by Millex-HV filter (Millipore). Two affinity chromatography techniques using HiTrapTM Chelating HP and HiTrap TM Heparin HP columns were separately employed for purification of PKR proteins (GE Healthcare). The supernatant was loaded onto the columns and the PKR proteins were eluted with an imidazole gradient or a NaCl gradient using ÄKTATM FPLC system (GE Healthcare). High salt contents in the fractions were removed using HiTrapTM Desalting column (GE Healthcare) and if necessary, size exclusion chromatography were performed using a Superdex

75 column (GE Healthcare) to improve purity. All purified PKR proteins were confirmed by SDS-PAGE and Western blotting analysis.

3.3.3. Bodipy-Palmitic acid binding assay

10 nM of Bodipy-C16 was mixed with PKR proteins in PBS buffer (pH 7.4) at room temperature. After 5 min of incubation, fluorescence polarization measurements were performed at 488nm/520nm using FluoroMax-4 (Horiba). The K_D values were determined by fitting the data to the one-site quadratic binding equation using the Kaleida-Graph software;

$$FP = FP_0 + \frac{1}{2} \frac{(FP_{max} - FP_0)}{[B - PA]_0} \{ (PKR_0 + [B - PA]_0 + K_D) - \sqrt{([PKR]_0 + [B - PA]_0 + K_D)^2 - 4[PKR]_0 \times [B - PA]_0} \}$$

Where FP is the fluorescence polarization value when the complex between [PKR] and [B-PA] (Bodipy-C16) is formed, FP_{max} is the fluorescence polarization value when the B-PA completely binds to the PKR, FP₀ is the fluorescence polarization value when the PKR is free, and [B-PA]₀ and [PKR]₀ are the initial concentrations of Bodipy-C16 and PKR, respectively.

3.3.4. Competition assay and IC₅₀ calculations

In the absence and presence of Bodipy-C16, the PKR proteins were incubated with phosphorylation buffer (20 mM HEPES (pH 7.5), 20 mM KCl, 2 mM MgCl₂, 0.04 mM EDTA, and 0.4 mM β-mercaptoethanol) for 20 min. The kinase reaction was performed by adding 100

μM ATP at room temperature for 30 min. The autophosphorylation reaction was stopped by heating to 95 °C for 5 min. The samples were loaded onto 9% Tris/Glycine SDS-PAGE gel and the phosphorylation level of T446 was quantified by Western blotting analysis. The phosphorylation level was normalized to the sample without Bodipy-C16. The concentration of Bodipy-C16 required for 50% inhibition (IC₅₀) was estimated using a sigmoidal dose-response model and the regression was performed by KaleidaGraph software:

$$Y = Y_{min} + \frac{(Y_{max} - Y_{min})}{1 + 10^{\{(X - logIC_{50}) \times (HillCoefficient)\}}}$$

where X and Y denote log (Bodipy-C16 concentration) and the phosphorylated T446 level is quantified from Western blotting analyses, respectively. Y_{min} and Y_{max} are the levels of phosphorylated T446 when the concentration of Bodipy-PA is infinite, respectively.

3.3.5. Palmitate treatment on HepG2 Cell and western blotting analysis

Human hepatocellular carcinoma cells were cultured in Dulbecco's modified eagle medium (DMEM) with 10% fetal bovine serum and penicillin-streptomycin (penicillin: 10 000 U/ml, streptomycin: 10 000 μg/ml). All detailed processes were described in the reference [173]. Palmitate (0.7 mM) were complexed to 2 % BSA (fatty acid free) dissolved in the DMEM medium. Palmitate treatment were performed for 24 hr and 2% BSA was used as a negative control. The HepG2 cells were washed twice with cold PBS and treated with CelLytic M cell lysis buffer (Sigma-Aldrich) supplemented with protease inhibitor cocktail (Sigma-Aldrich) for 10 min on ice. The cell lysate was clarified by centrifugation at 13000 rpm for 10 min, and the

supernatant was collected. Total protein levels were quantified by Bradford assay (Bio-Rad). 40 µg of total protein was loaded to 9 % SDS-PAGE gel, transferred to nitrocellulosemembranes, and probed with primary (anti-pThr446) and secondary antibodies. The image was analyzed using the Molecular Imager ChemiDoc XRS System from Bio-Rad.

3.3.6. Statistical Analysis

All experiments were independently performed at least three times, and representative results are shown. The statistical analysis was performed using a Student t-test on the SigmaPlot software.

3.4. Results

3.4.1. Palmitic acid binds to PKR proteins

We first used the FP-based assay to evaluate whether Bodipy-C16 interacts with the PKR proteins. Two recombinant PKR wild-type proteins, unphosphorylated PKR (PKR-WT) and phosphorylated PKR (PKR-pWT), were prepared for this assay. Prior to the binding assay, the phosphorylation status was assessed by immunoblot analysis against anti-PKR-pThr451 and anti-PKR-pThr446. PKR-pWT but not PKR-WT showed a phosphorylation fraction on the immunoblot (data not shown). The Bodipy-C16 binding assay was performed at 10 nM Bodipy-C16 with increasing concentrations of the PKR proteins. As shown in Figure 3.2A, the FP values for both PKR-WT and PKR-pWT proteins increased significantly. Assuming a 1:1 binding stoichiometry, PKR-WT and PKR-pWT have KD values of 23.22 ± 1.28 and 24.90 ± 1.00 nM, respectively, suggesting that both have similar binding affinities to Bodipy-C16.

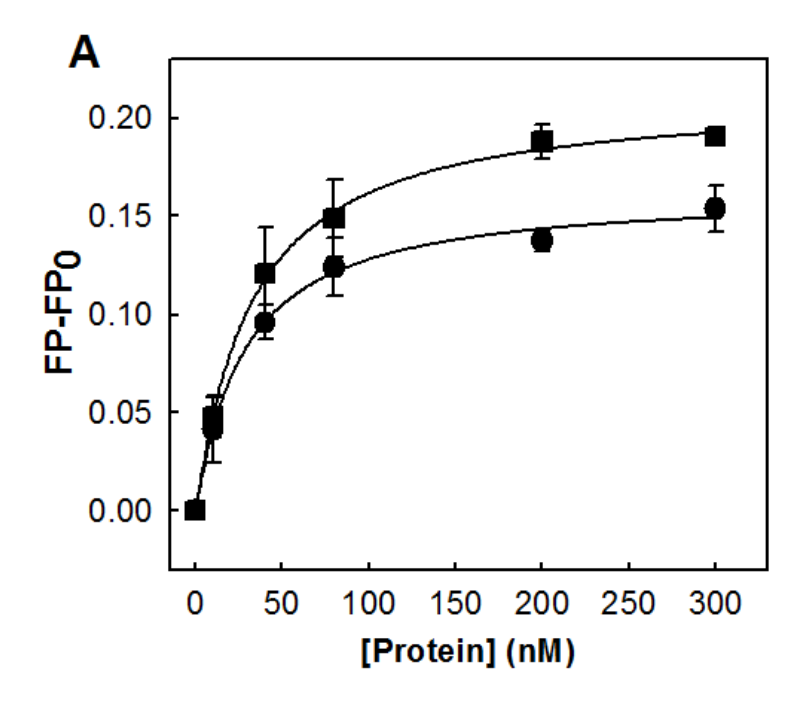
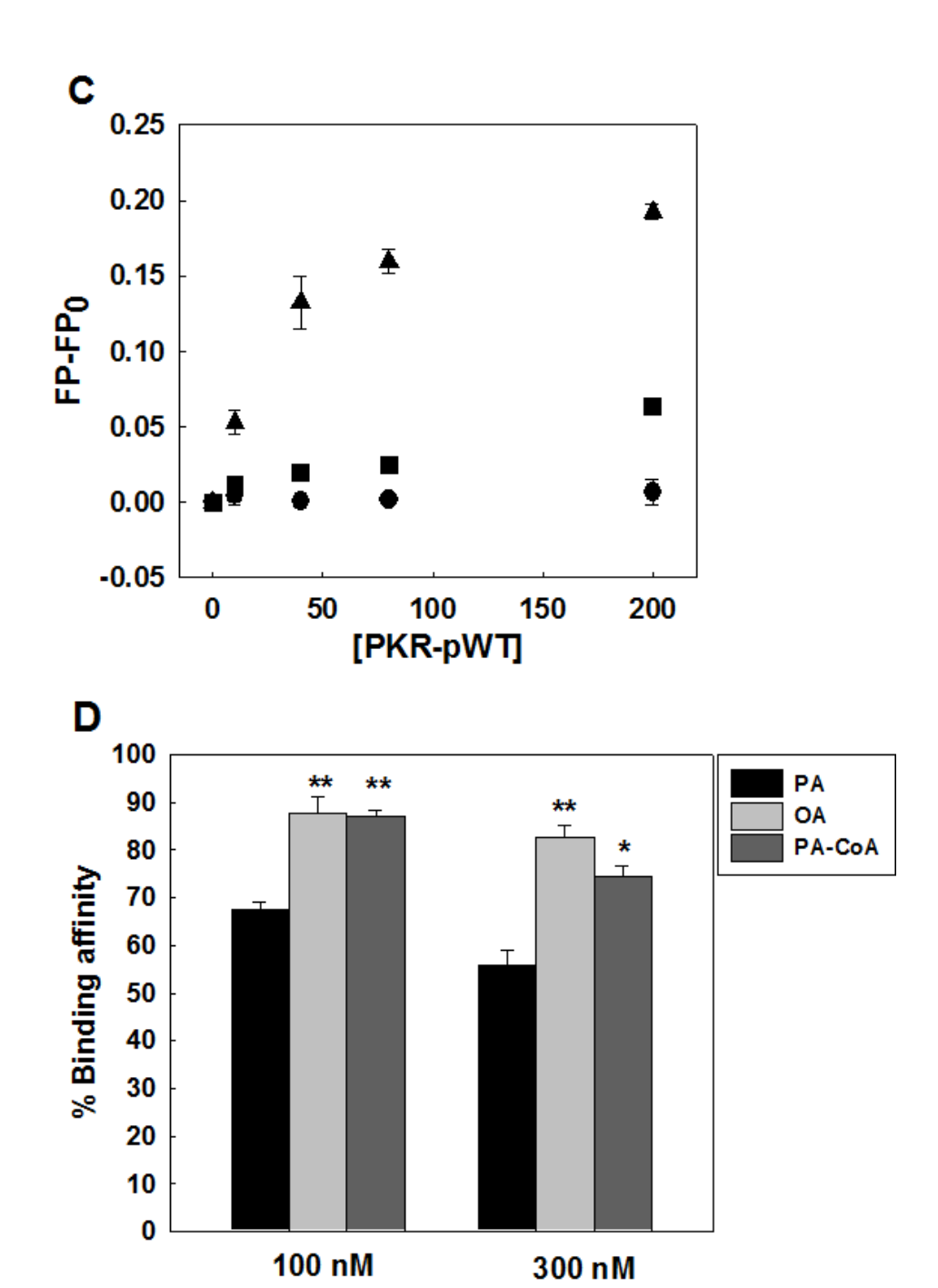


Figure 3.2. Binding affinity of Bodipy-C16 to PKR wild-type proteins.

Figure 3.2 (cont'd)



(A) 10 nM of Bodipy-C16 was added to PBS buffer with increasing concentrations of PKR-WT (circles) or PKR-pWT (squares). After 5 min of incubation, the fluorescence polarization was measured at 488/520 nm using a spectrofluorometer. The solid lines represent fitting of the data to the quadratic binding equation described in Materials and Methods. Each error bar represents

(Figure 3.2 cont'd) the mean of triplicates ± SD. (B) Structure comparison of Bodipy-C3, Bodipy-C12 and Bodipy-C16. (C) Binding affinity of 10 nM Bodipy-C3 (circles), Bodipy-C12 (squares), and Bodipy-C16 (triangles) with increasing concentrations of PKR-pWT in PBS buffer. After 5 min of incubation, the fluorescence polarization was measured at 488/520 nm with a spectrofluorometer. Representative data points shown are of average of three measurements and the error bars indicate the standard deviations. All data points of Bodipy-C16 were significantly different from both Bodipy-C3 and Bodipy-C12 (p<0.001). (D) Competition binding assay of fatty acids and lipid. At a constant concentration of PKR-pWT (20 nM), 5 nM of Bodipy-C16 was added to Tris buffer (20 mM Tris (pH 8.0), 100 mM NaCl) in the presence of 100 or 300 nM of palmitic acid (PA), oleic acid (OA), and palmitoyl CoA (PA-CoA). After 15 min of incubation, the fluorescence polarization was measured at an excitation wavelength of 488 nm and an emission wavelength of 520 nm with a spectrofluorometer. The percentage of binding is calculated based on the following equation: % Binding = (FP-FPnegative control)/(FPpositive control-FPnegative control)*100. * (p<0.05) and ** (p<0.001) indicate statistically different to PA.

We further addressed whether palmitic acid is a specific ligand to the PKR protein. In addition to Bodipy-C16, two more Bodipy-labeled saturated fatty acids, Bodipy-propanoic acid (Bodipy-C3) and Bodipy-lauric acid (Bodipy-C12), were evaluated for their binding affinity to PKR. Their structures are compared with Bodipy-C16 in Figure 3.2B. The structural difference is in the length of the methylene chain. As shown in Figure 3.2C, no significant change in FP values is observed for Bodipy-C3 (up to 200 nM) and Bodipy-C12 (up to 80 nM) with PKRpWT, and the FP values for both Bodipy-C3 and Bodipy-C12 are markedly different from Bodipy-C16. These results suggest that the PKR protein has a higher binding specificity to the long-chain saturated fatty acid, palmitic acid (C16). Additionally, using a competition assay with Bodipy-C16, we tested whether other long-chain unsaturated fatty acids or lipids are able to bind to the PKR protein. Palmitic acid (100 and 300 nM) (a saturated fatty acid), oleic acid (an unsaturated fatty acid), and pamitoyl-CoA (a lipid) were competed with 5 nM Bodipy-C16. We found that palmitic acid more readily displaced the Bodipy-C16 from PKR-pWT than either oleic acid or pamitoyl-CoA (Figure 3.2D), supporting that the PKR protein more likely interacts with a long-chain saturated fatty acid, palmitic acid.

3.4.2. Bodipy-C16 Binds to Other Kinases, Likely Due to the Conservation of the ATP-Binding Site

The results of the docking experiments (Dr. Feig's group at Michigan State University) indicate that palmitate positions near the ATP-binding site of the three other kinases, Akt1, CDK4, and MAPKAPK3, are similar to the PKR protein. Therefore, we also evaluated whether Bodipy-C16 can bind to these three kinases using the FP-based palmitate interaction assay. As shown in Figure 3.3, at 40 and 80 nM kinases, the FP values of all four kinases were

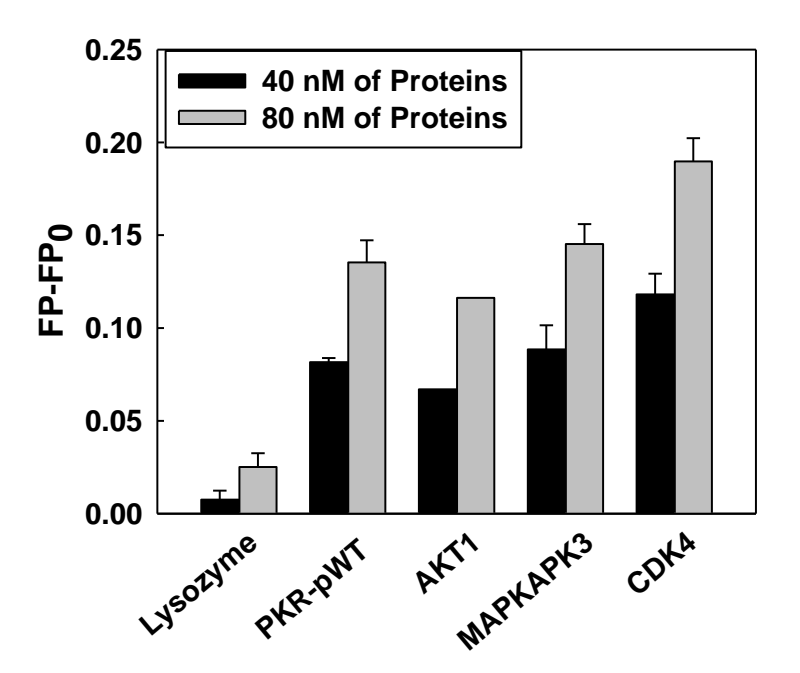


Figure 3.3. Bodipy-C16 binding to kinases. 10 nM of Bodipy-C16 was added to PBS buffer in the absence of kinase and in the presence of 40 nM and 80 nM of kinases, PKR-pWT, Akt1, MAPKAPK3, and CDK4. Lysozyme was used as a negative control under the same condition. After 5 min of incubation, the fluorescence polarization was measured at 488/520 nm using a spectrofluorometer. Representative data point shown is for the average of three measurements and the error bars indicate the standard deviations.

significantly different from the control protein (lysozyme). These results suggest palmitate binds to these kinases, likely near the conserved ATP-binding site (Figure 3.3).

3.4.3. Bodipy-C16 binds to residues surrounding the ATP-binding site and alphaChelix, thereby preventing the autophosphorylation of PKR WT protein

The computational docking experiments suggest that the most favorable palmitate binding residues on the ATP-binding site are Lys296 and Asp432 (See the Figure 3.4). Both residues are important for stabilizing the interactions with the nucleotide and magnesium ions. To examine whether Bodipy-C16 can be located in the ATP-binding site, we performed Alanine mutation on Lys296 and Asp432 on the PKR protein and performed the Bodipy-C16 binding assay. At protein concentrations of 40 and 80 nM, the binding affinities of the mutant K296A and D432A proteins decreased significantly as compare to the wild-type proteins (Figure 3.5A). However, since the mutant proteins are not able to completely block the Bodipy-C16 binding, it suggests that the palmitic acid may not binding exactly at these residues, but near it to interfere with ATP binding to PKR.

We further investigated whether inhibiting ATP binding by palmitate blocks the autophosphorylation reaction. Previously it was demonstrated that PKR-WT protein can be autophosphorylated in the absence of double-stranded RNA and ATP is sufficient for its autophosphorylation [175]. We performed another competition assay with Bodipy-C3 (negative control) or Bodipy-C16, at constant ATP and PKR-WT concentrations. With increasing Bodipy-C16 concentration, the phosphorylation of Thr451 and Thr446, the two major autophosphorylation sites on PKR, decreased significantly, whereas Bodipy-C3 had no impact on the autophosphorylation of PKR (Figure 3.5B). Upon binding of palmitate to PKR the

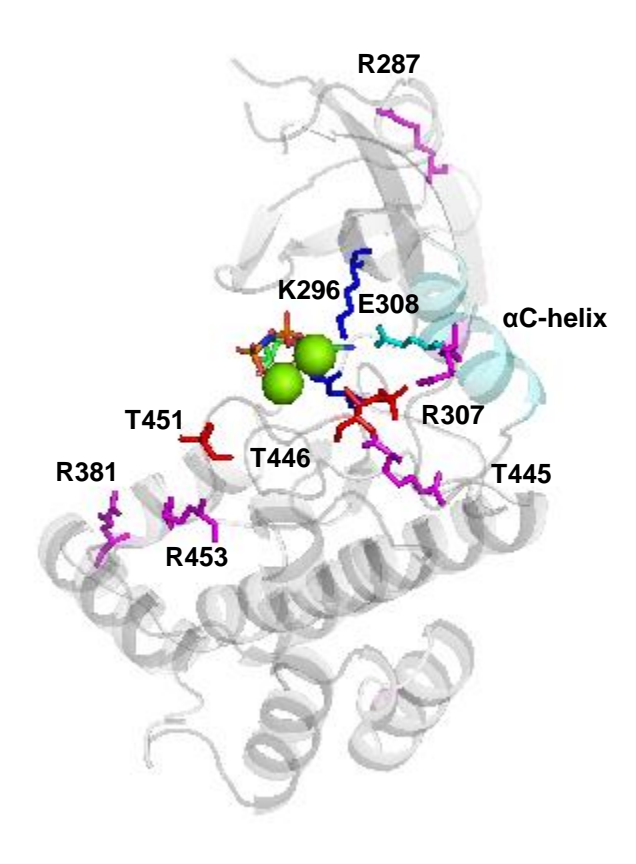
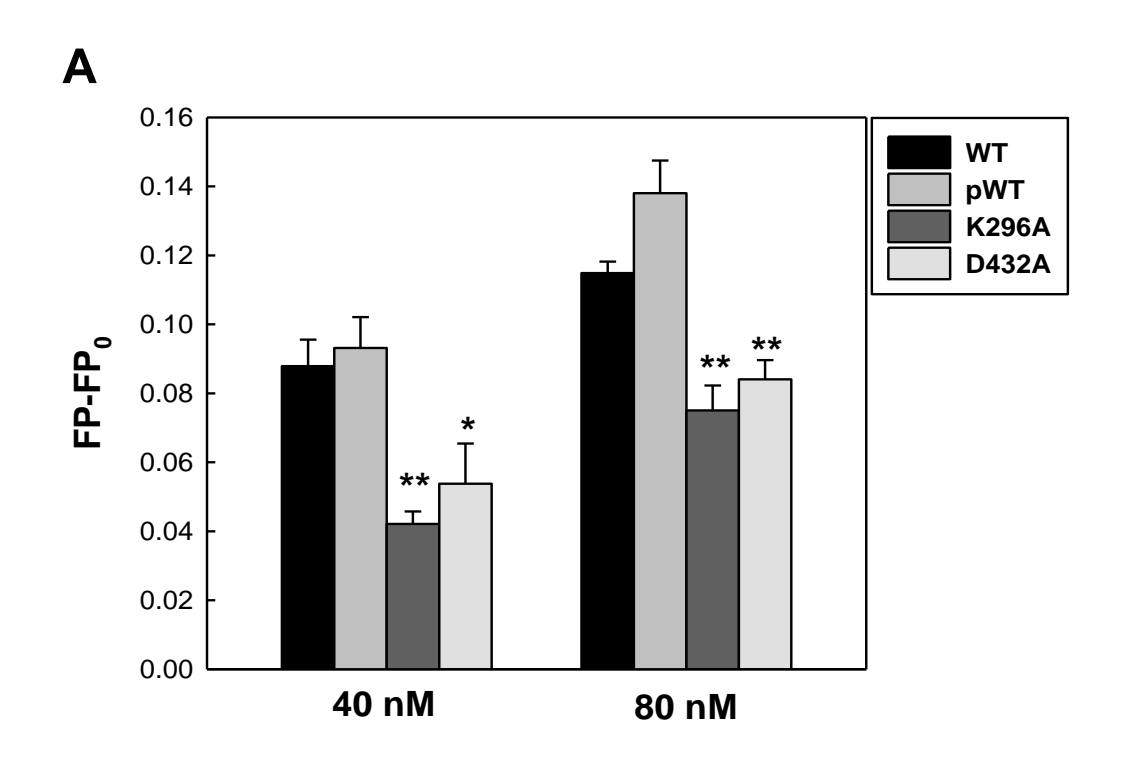
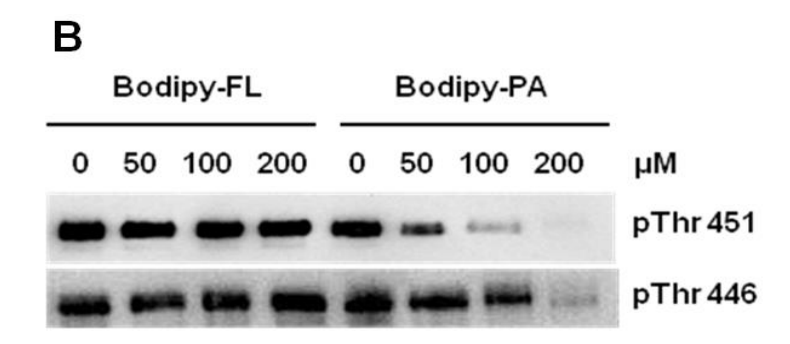


Figure 3.4. PKR mutant sites. Kinase domain of PKR is showed in gray and α C helix in cyan. Important residues (K296, D432, E308) in the nucleotide binding cavity are shown in sticks and bound the ATP analog adenylyl imidodiphosphate (AMP-PNP) and two Mg²⁺ ions (green balls). The figure was generated using the following structures: PKR:AMP-PNP:eIF2a (PDB id = 2A19).





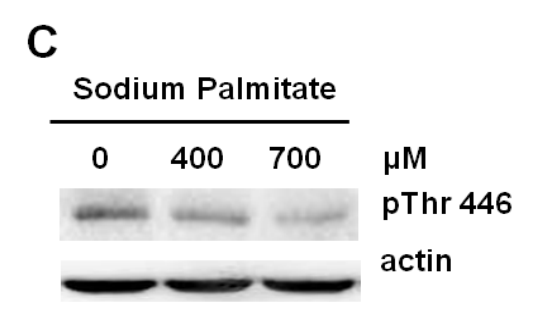


Figure 3.5. Inhibitory effects of PA on PKR phosphorylation. (A) Fluorescence polarization measurement of PKR mutants. 10 nM of Bodipy-PA was added to 40 and 80 nM of wild-type

(Figure 3.5 cont'd) PKR proteins (phosphorylated and unphosphorylated) and PKR mutants in PBS buffer. After 5 min of incubation, the fluorescence polarization was measured at an excitation wavelength of 488 nm and an emission wavelength of 520 nm using a spectrofluorometer. * (p<0.05) and ** (p<0.001) indicate statistically different to wild-type proteins. (B) Competition assay with Western blot analysis. 2 µM of PKR-WT was incubated with Bodipy-C3 or Bodipy-C16 at the indicated concentrations in phosphorylation buffer (10 mM HEPES (pH 7.5), 50 mM KCl, 5 mM MgCl₂, 0.1 mM EDTA, and 1mM DTT) for 20 min. Autophosphorylation of WT PKR was performed by adding 100 µM of ATP at room temperature for 30 min. To stop the autophosphorylation reaction, 5X SDS-PAGE sample buffer was added to the reactions, followed by heating at 95 °C for 5 min. The reactions were loaded onto 10 % Tris/glycine SDS-polyacrylamide gel and detected for PKR phosphorylation at Thr451 and Thr446 by Western blot analysis. (C) Effect of palmitate on the phosphorylated Thr446. HepG2 cells were cultured in regular medium until reaching 90% confluency and then exposed to 400 and 700 µM palmitate for 24 hr. 2% BSA was used as a negative control. After treatment, the cells were harvested and western blot analysis was performed to detect the level of phosphorylated PKR.

autophosphorylation is down-regulated, suggesting that palmitate could act as an ATP-binding site-directed inhibitor. These *in vitro* results are consistent with our computational docking results as well as our earlier results that showed palmitate decreases the cellular level of pThr451 [173]. Previously we did not evaluate the effect of palmitate on pThr446 in HepG2 cells. Thus we treated HepG2 cells with BSA or BSA complexed to palmitate at varying concentrations (400 and 700 μM) and found palmitate significantly decreased the level of pThr446 (Figure 3.5C).

To further evaluate whether Bodipy-C16 can be displaced by ATP, we performed two types of competition assays. Since the ATP binding affinity (34 µM) to PKR is much weaker [178] than Bodipy-C16 (28 nM) and high concentrations of ATP interfered with the FP-based palmitate interaction assay (data not shown), we adapted an intensity-based palmitate binding assay from a previous study that investigated the binding affinity of palmitate to FABPs [147]. The fluorescence intensity method required a much higher Bodipy-PA concentration (500 nM) and the fluorescence intensity increases upon binding of Bodipy-C16 to the FABPs. We found the fluorescence intensity-based palmitate binding assay can be used to evaluate the binding affinity of palmitate to the PKR proteins (Figure 3.6). For our studies, we used 600 nM as the PKR concentration for the competition assay, where PKR is unable to significantly autophosphorylate in the absence of dsRNA [175]. In the range of the ATP concentrations evaluated, the fluorescence intensity decreased significantly as the ATP concentration increased, suggesting that Bodipy-PA binds competitively to the PKR wild-type proteins to inhibit ATP binding (Figure 3.7A). To confirm that the Bodipy group was not altering the binding or competition, we evaluated whether radiolabeled ATP (hot ATP) bound to PKR could be displaced by unlabeled palmitate. In the absence or presence of palmitate, hot ATP was incubated with PKR-pWT. The mixture was loaded onto a ZipTip-C4 column to separate unbound ATP from the ATP-PKR complex (bound ATP). In the absence of palmitate, 16.61% of

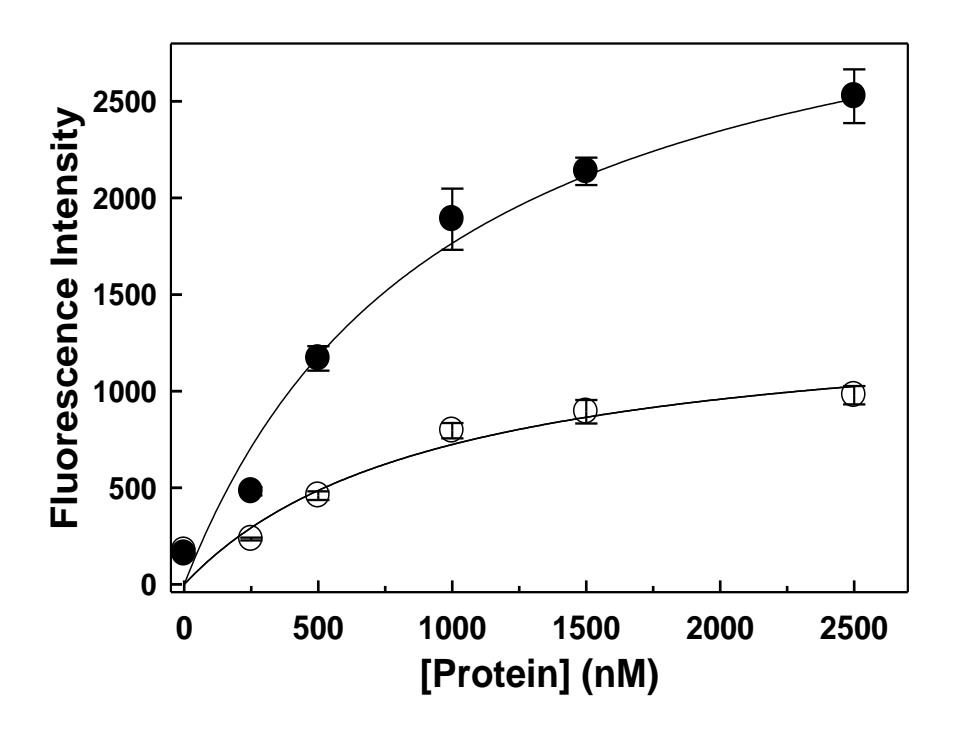
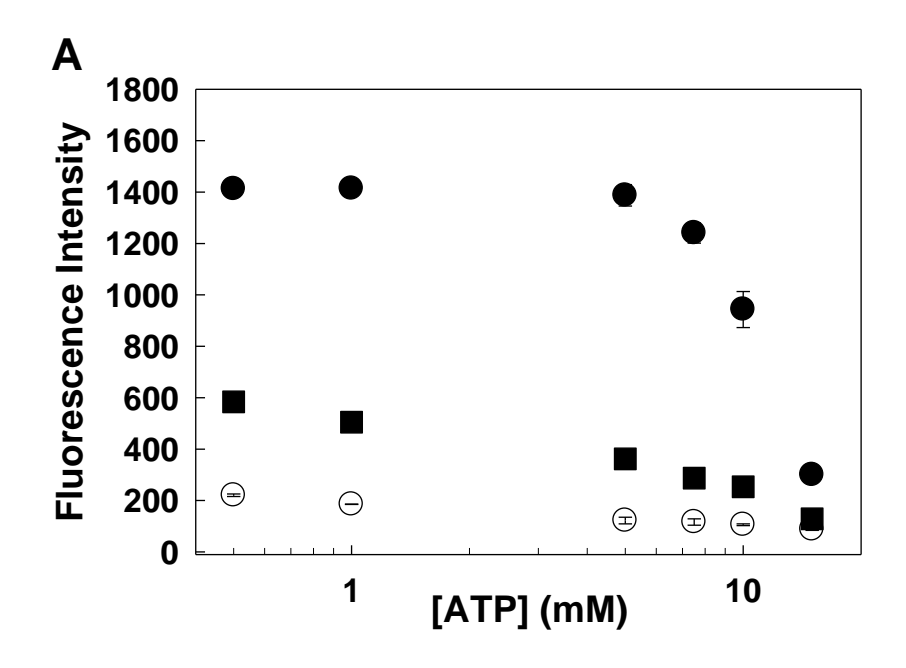


Figure 3.6. Fluorescence intensity measurement for the binding of Bodipy-PA and PKR proteins. 500 nM of Bodipy-PA was added to PBS buffer with increasing concentrations of PKR-WT (open circles) or PKR-pWT (closed circles). After 20 min of incubation, the fluorescence intensity was measured at an excitation wavelength of 488 nm and an emission wavelength of 520 nm with a microplate spectrofluorometer. The experiments were performed in duplicates, at least three independent times. Representative data points are shown.



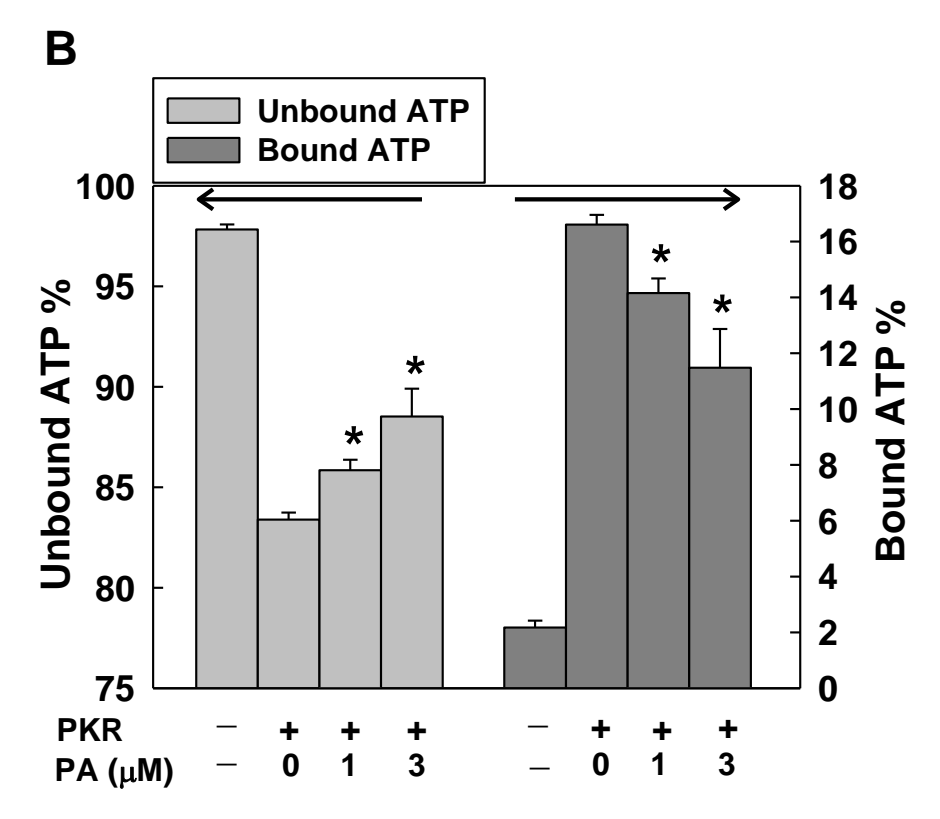


Figure 3.7. ATP competition assays. (A) ATP competition binding assay with Bodipy-PA. In the absence of PKR proteins (open circles) or in the presence of PKR-WT (closed squares) or

(Figure 3.7 cont'd) PKR-pWT (closed circles) proteins, increasing concentrations of ATP were incubated in PBS buffer containing 5 mM MgCl₂ and 0.1 mM EDTA for 10 min. 500 nM Bodipy-PA and 600 nM PKR proteins were added to the samples and incubated for 20 min. The fluorescence intensity was measured at an excitation wavelength of 488 nm and an emission wavelength of 520 nm using a microplate spectrofluorometer. Each data point represents the average of two measurements and the error bars show the differences between two measurements. (B) ATP competition binding assay with γ -³³P-ATP. In the absence and presence of sodium palmitate, 0.33 nM of γ -³³P-ATP was added to 1 μM PKR-pWT in the ATP-binding buffer, 20 mM HEPES (pH 7.5) containing 5 mM KCl, 0.5 mM MgCl₂, 0.01 mM EDTA, and 0.1 mM β-mercaptoethanol. After 30 min incubation, the samples were loaded into ZipTipC4 (Millipore) and pipetted 20 times with unbound sample collected for further analysis. 10 % acetonitrile was loaded to remove the unbound γ -³³P-ATP and the wash fractions were collected. The bound γ -³⁴P-ATP to PKR was eluted with 100 % acetonitrile. All sample fractions were analyzed using a scintillation counter (Perkin Elmer). As a negative control, only hot ATP was loaded and the same process was repeated. * indicates p< 0.01 as compared to 0 μM PA.

the hot ATP was bound to the PKR-pWT protein. With increasing palmitate concentration, ATP was dose-dependently displaced from binding to PKR. These results demonstrate that palmitate and ATP bind competitively to PKR. It should be noted that, in the absence of PKR, ATP did not bind to the column either in the presence or absence of palmitate (Figure 3.7B), demonstrating that ATP and palmitate do not bind to each other at these concentrations. This is further confirmation that ATP and PA competes for the kinase domain on PKR.

Our collaborator (Dr. Feig's group) further performed the molecular dynamics (MD) simulations (more extensive simulation than the molecular docking simulations) and identified five potential palmitic acid-binding residues (Arg287, Arg307, Arg381, Arg445, Arg453; see the Figure 3.4) on the PKR-WT (unphosphorylated) protein. To experimentally confirm the computational results and further test the autophosphorylation of the PKR protein, we performed Alanine mutations on the PKR-WT DNA plasmid. All five residues of the PKR protein were separately mutated to Alanine using site-directed mutagenesis and the mutant PKR proteins were expressed in *E.coli cells*, followed by affinity chromatography. To test the impact of the alanine mutations on palmitic acid-binding affinity, we used a fluorescence polarization (FP)-based assay. At constant concentrations of Bodipy-PA and PKR proteins, the binding affinity was compared to that of the PKR-WT protein. As shown in Figure 3.8, only R307A mutant protein significantly decreased the palmitic acid binding affinity, suggesting that palmitic acid interacts with the R307 residue located on the αC-helix.

To further assess whether the R307A mutation alters the kinase activity of the PKR protein in the presence of Bodipy-PA, we performed an in-vitro competition assay. The binding of Bodipy-PA results in a dose-dependent decrease on the autophosphorylation of both the WT and R307 mutant proteins (Figure 3.9A). However, as shown in Figure 3.9B, a reduction in

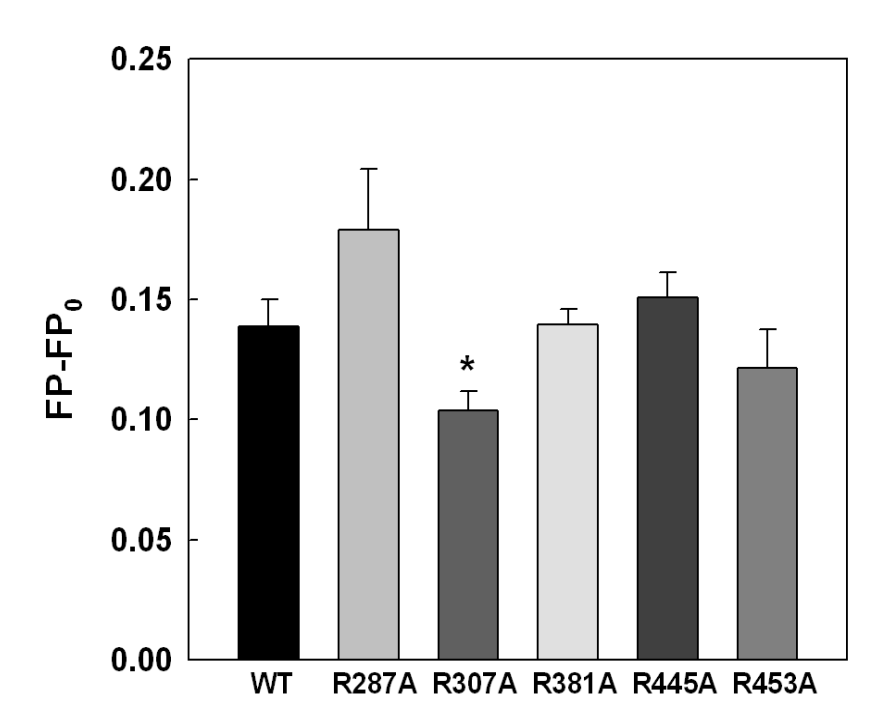
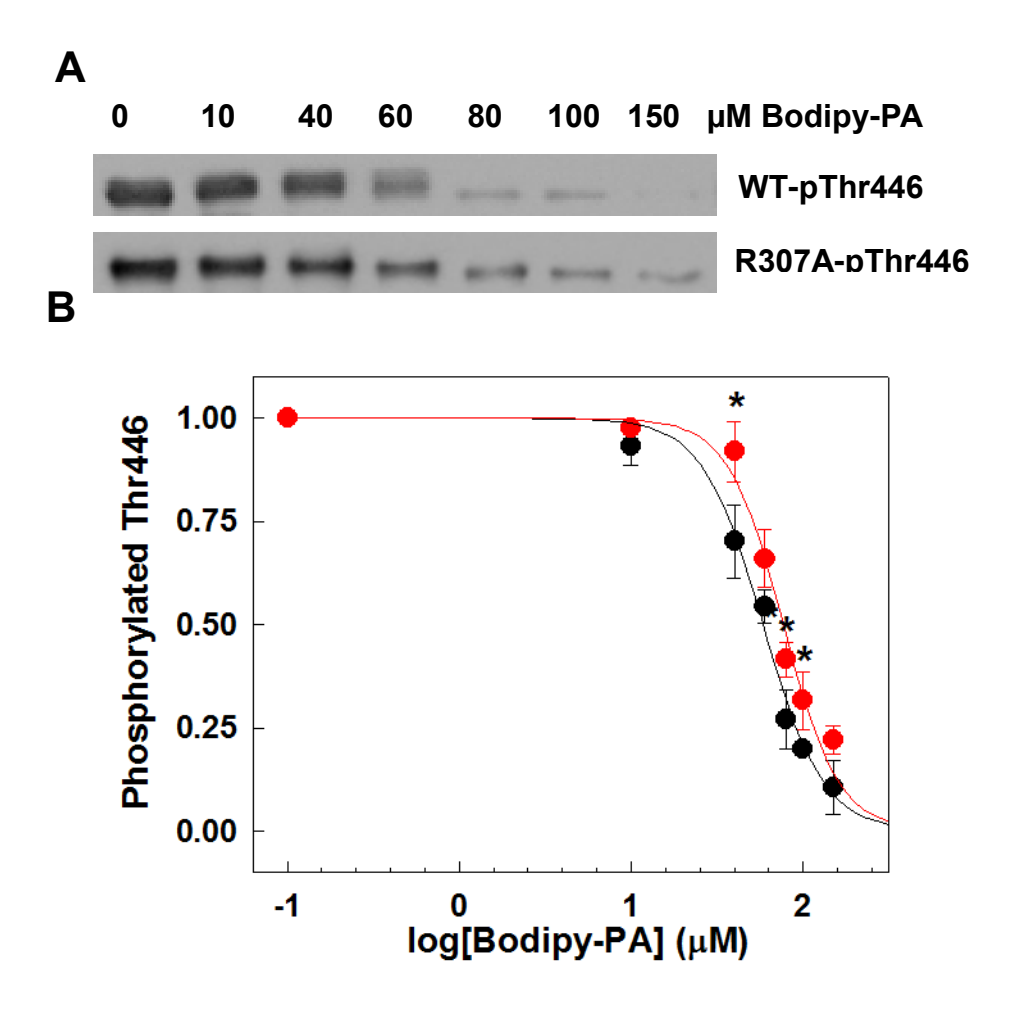


Figure 3.8. Bodipy-PA binding to PKR-WT and mutant proteins. 10 nM of Bodipy-PA was mixed with 50 nM of the PKR proteins in PBS buffer (pH 7.4) at room temperature. After 10 min of incubation, fluorescence polarization measurements were performed at 488 nm/515 nm using a spectrofluorometer. Each error bar represents the mean of triplicates \pm SD. The * indicates statistically different results compared to the WT protein (p<0.05).



3.9. Inhibitory effects of Bodipy-PA PKR-WT PKR-R307A on and autophosphorylation. (A): In-vitro competition assay with Western blot analysis. In the presence of 100 µM ATP and 1 µM PKR proteins, Bodipy-PA at the indicated concentrations was added to the phosphorylation buffer. After the kinase reaction, the phosphorylated fractions were visualized by Western blot analysis using anti-pT446. (B): Quantification of the phosphorylated T446. From Figure 6A, the phosphorylation levels of PKR-WT and PKR-R307A were quantified and normalized against the levels in the negative control (without Bodipy-PA) for each protein. Data shown are the means and standard deviations from three independent experiments. * indicates statistically significant different values for the mutant vs. WT protein at the same condition (p<0.05).

kinase inhibition by Bodipy-PA is observed with the R307A mutation as compared with the WT, with a significant increase in the half-maximum inhibitory concentration (WT (IC $_{50} = 48.29 \pm 8.57 \mu$ M, Hill coefficient = 2.47); R307A (IC $_{50} = 80.34 \pm 5.63 \mu$ M, Hill coefficient = 2.70)). Thus, the experimental results strongly suggest that palmitic acid binding at or near R307 is capable of inhibiting the autophosphorylation of the PKR protein.

3.5. Discussion and Conclusions

PKR is a major signaling enzyme that plays diverse roles in cellular functions. It is well established that PKR is activated by viral double-stranded RNA (dsRNA) and the activation of PKR regulates its dimerization and autophosphorylation [167]. Furthermore, PKR is involved in signal transduction pathways such as the MAPK and NF-κB pathways [167, 179]. Recently, our group proposed that PKR can also regulate the Bcl-2-JNK pathway to mediate the apoptotic response of palmitate. In this scenario, palmitate decreases the autophosphorylation level of PKR at Thr451, which down-regulates the phosphorylation of Bcl-2 at Ser70 [173] and anti-apoptosis. The latter is possible given that PKR does not have upstream kinases, thus upon autophosphorylation it is able to modulate the activity of other proteins. In this study, we address how palmitate may decrease the autophosphorylation level of PKR and suggest, based on computational and experimental results, that palmitate interacts with the ATP-binding site of WT PKR proteins to interfere with PKR autophosphorylation. This novel mechanism may provide an explanation of how palmitate reduces the autophosphorylation of PKR in HepG2 cells.

In the latent state, PKR exists in a weak monomer-dimer equilibrium with a KD of

 μ M, but the dimerization of the PKR proteins increases significantly upon either HIV TARRNA (HIV-1 trans-activation responsive region-RNA) binding ($K_D \sim 75~\mu$ M) or phosphorylation of PKR ($K_D \sim 20~\mu$ M) [161, 175]. In addition, phosphorylated WT protein serves as a potent activator of latent PKR, increasing the autophosphorylation reaction rate by 20-fold [161]. Although dimerization of PKR is very important for autophosphorylation, (0.5 μ M is sufficient to induce the autophosphorylation reaction [175]), this reaction rate increases significantly by its product, phosphorylated PKR. Thus, phosphorylated PKR is clearly more potent in autophosphorylating PKR. Interestingly, we found that the binding affinity of palmitate to the phosphorylated PKR is similar to the unphosphorylated PKR. Their similar binding affinity helps to block the autophosphorylation of both the unphosphorylated WT and the phosphorylated WT. In addition, we demonstrated that palmitate binds to unphosphorylated PKR to inhibit access of ATP to the PKR protein, thereby significantly reducing the autophosphorylation reaction (Figure 3.5 and Figure 3.7). These multiple lines of evidence support an inhibitory role of palmitate on PKR autophosphorylation.

The binding mode of ATP to other kinase is similar to that observed with PKR [159, 160]. Recently, the structure of 15 kinases were aligned and the ATP-binding site was found to be highly conserved [180]. It was computationally demonstrated that the kinases share a consensus structure that stabilizes the ATP molecule and correctly coordinates ATP for phosphotransfer. Similar to these results for ATP, our computational results suggest that palmitate also may be binding to the ATP-binding site of multiple kinases, likely near the Lys296 and Asp432 of the PKR protein, and homologous sites of the other kinases, Akt1, CDK4, and MAKAPK3, studied here. We further demonstrated that palmitate can physically interact with these other kinases based on the FP-based interaction assay. In addition, our binding studies show the mutant PKR

proteins, K296A and D432A, significantly decrease the binding affinity of Bodipy-C16 to the PKR protein, suggesting that palmitate likely locates near the ATP-binding site. Based upon our results, we propose that palmitate may broadly affect many soluble kinases. In future, if one were interested in a specific signaling pathway, a kinase library could be developed with the palmitic acid binding assay to identify kinases that strongly interact with palmitate and thereby help elucidate potential kinase signaling networks mediated by palmitate. Further studies are needed to fully understand all of the interactions of palmitate with kinases and the signaling pathways mediated by palmitate.

Along with the K296 and D432 residues, we additionally confirmed that R307 on the αChelix is important for palmitic acid-binding. Interestingly, R307 stabilizes the activation loop by binding to the phosphorylated T446 residue (see Figure 3.4). Palmitate's interaction with the R307 residue on the unphosphorylated PKR could block the phosphate transfer to the T446 residue, subsequently reducing the phosphorylation levels on T446. Indeed, mutation on either K296A or D432A blocks the autophosphorylation in E.coli cells, generating the unphosphorylated form of the PKR mutant protein, while the R307A protein maintains the phosphorylated state similar to the WT protein (Data not shown). Thus the reduction in the binding of palmitate to the mutant proteins (K296A and D432A) could result from local conformation changes around the ATP binding site. For instance, the conformation of the ATP binding site in the K296A and D432A mutant proteins could change affecting the αC-helix (for example, E308 on the α C-helix is involved in stabilizing the conformation of the ATP binding site; see Figure 3.1 and 3.4, thus changes in the ATP binding site could impact the αC-helix), and if palmitate interacts with the αC-helix, then the binding affinity of palmitate on both mutants could concomitantly be affected. Therefore any changes (e.g. decrease) in the interactions with

the mutants cannot be exclusively attributed to palmitate's interaction. In contrast, since R307A does not change the phosphorylation state as compared to the WT protein, this suggests a lower likelihood of a conformational change with R307A as compared to both the K296A and D432A mutants. Therefore if palmitate locates in and around the R307 residue and the mutation R307A modulates the phophosphorylation of PKR, it could suggest a possibility that the inhibition of PKR activity is due to palmitate's interaction with that residue. In addition, K296 and D432 were predicted from docking experiments that have two major limitations; a rigid structure of the PKR protein and a biased search for the hypothesized binding sites. However, R307 was identified by extensive unbiased MD simulations that started from 25 random palmitate locations around the dynamic receptor molecule. Thus the data from the MD simulations provides more reliable binding modes of palmitate on the PKR protein. Although it is apparent that palmitate localizes to the areas (αC-helix and near the ATP binding site) between the N- and C-lobes, in future, it would be useful to have PKR-palmitate co-crystal structures to obtain the actual binding modes.

In summary, we uncovered how palmitate may modulate PKR phosphorylation. Palmitate is binding on the α C-helix (near the ATP binding site), to interfere and inhibit the autophosphorylation of PKR. In addition, due to the conserved ATP-binding site, palmitate can non-specifically bind to other kinases. However, the binding affinity of palmitate to the kinases may differ, depending on both the specific configuration around the ATP-binding site and the active/inactive conformation. This novel mechanism provides potential insight into how palmitate may modulate the signaling of PKR and, more broadly, other kinases.

CHAPTER 4. ROLES OF TRYPTOPHAN ON THE OLIGOMERIZATION OF THE TRANSMEMBRANE DOMAIN OF IRE1 α

Publications:

- (1) **Cho H**, Lamarca R, Chan C. Oligomerization of the transmembrane domain of IRE1α in SDS micelles. Biochem Biophys Res Commun. (2012) 427(4):764-7.
- (2) **Cho H***, Stanzione F*, Yerneni S, Sum AK, Chan C. Tryptophan457 regulates the oligomerization and activity of the IRE1α protein. (In preparation).

4.1. Abstract

Activation of ER stress sensor proteins is an indispensable step to remedy cellular stresses associated with the accumulation of unfolded/misfolded protein in the ER lumen. IRE1α, a Type I transmembrane (TM) protein possessing both kinase and endonuclease functions, is the most conserved and well characterized ER stress sensor protein. Like other single-spanning membrane protein kinases, activation of the IRE1α protein can be fully achieved through the dimerization/oligomerization process. While the oligomerization of both the luminal and cytosolic domains has been studied, the functional role of the TM oligomerization is currently unclear. Using computational and experimental tools, we systematically investigated the potential dimerization interfaces and found that a Tryptophan residue plays a critical role on regulating the TM dimerization. Tryptophan as an aromatic and amphipathic residue serves as a driving force on the TM helix-helix packing process, which is stabilized by aromatic interactions

and hydrogen bonds. Further cellular experiments would help to address whether the TM domain is functionally connected to the cytosolic domain.

4.2. Introduction

The Endoplasmic Reticulum (ER) is a cellular compartment responsible for protein folding, lipid synthesis, and calcium storage. Physiological conditions such as elevated levels of free fatty acids (FFAs) and glucose, oxidative stress, and inflammatory cytokines are known to perturb ER homeostasis, leading to the accumulation of unfolded/misfolded proteins in the ER lumen. [16]. Cellular adaptation to ER stress is achieved through activation of the unfolded protein response (UPR), an integrated signal transduction pathway mediated by three ER stress sensor proteins, IRE1 (Inositol-requiring enzyme 1), PERK (protein kinase R (PKR)-like ER kinase), and ATF6 (activating transcription factor 6) [14]. UPR signaling coordinates the cellular response by down-regulating protein translation, enhancing the expression of ER chaperone proteins that promote protein refolding, and activating proteases involved in the degradation of misfolded proteins. When these adaptive processes are insufficient to attenuate ER stress, the UPR triggers apoptosis [15].

In mammals, IRE1 has two isoforms: IRE1- α possesses the most conserved signaling pathways of the UPR and is expressed ubiquitously, whereas IRE1- β is expressed in intestinal epithelial cells. [17]. IRE1 α is a type I transmembrane protein with a N-terminal luminal domain as an ER stress sensor and a C-terminal cytosolic domain carrying protein Ser/Thr kinase and endoribonuclease activities. Under the ER stress conditions, the luminal domain of IRE1 α

oligmerizes in the lumen, promoting self-association of the whole molecule [18]. The face-to-face dimerization of the kinase domain facilitates trans-autophosphorylation, subsequently activating the RNase domain [19]. The active form of IRE1α catalyzes the unconventional processing of the mRNA encoding the transcriptional factor X-Box binding protein-1 (XBP1), by splicing a 26-nucleotide intron from the XBP1 mRNA which generates an active transcription factor (XBP1s) [20]. The spliced XBP1s controls the upregulation of UPR-targeted genes involved in enhancing ER protein-folding capacity and degrading unfolded or misfolded ER proteins [20, 21].

The dimerization/oligomerization of IRE1 α is known to upregulate IRE1 α activity. The dimerization interface of the luminal domain is stabilized by hydrogen bonds and hydrophobic interactions and disruption of these interactions prevents the self-association of the molecule, subsequently reducing both the autophosphorylation and the RNase activities of IRE1 α in the cells [23, 181]. Furthermore, like other Ser/Thr kinases, the IRE1 α kinase domain performs the dimerization-dependent phosphorylation of the activation segment in trans to promote kinase activation and the face-to-face dimerization interface on the kinase domain is also functionally and structurally connected to the RNase domain [19]. Thus the dimerization of either the luminal or the cytosolic domain is crucial for regulating IRE1 α enzymatic activities. In contrast to the luminal or cytosolic domains, the roles of the transmembrane (TM) domain on the IRE1 α protein have been barely studied. Our group previously showed that, in the absence of the luminal domain and cytosolic domain, the TM domain of the IRE1 α protein oligomerizes in a membrane-like environment [182]. In addition, it has been recently suggested that the IRE1 α molecule lacking the luminal domain is able to sense the lipid perturbation and contribute to UPR

activation through the TM domain [55]. However, molecular mechanism of the oligomerization and activation of IRE1 α mediated by the TM domain has thus far not been studied.

IRE1 α is thought to have similar activation mechanisms to receptor tyrosine kinases (RTKs), the largest group of Type I transmembrane proteins, that transmit signaling from the extracellular domain to the cytosolic domain through the dimerization of the TM domain [183, 184]. Furthermore, the kinase domain of IRE1 α is structurally similar to one of RTKs, epidermal growth factor receptor (EGFR) [185]. Disturbing the TM dimerization of RTKs, i.e., EGFR and fibroblast growth factor receptor 3 (FGFR3), has been well known to reduce their kinase activities [186, 187]. Thus, here we hypothesized that the TM domain of IRE1 α is functionally linked to its cytosolic domain.

In the present study, we used MD (molecular dynamics) simulations to provide a possible mechanism of the TM dimerization by studying the residues at the interface between the TM peptides. Further biophysical and biochemical experiments provided evidence that the TM peptide is capable of dimerizing in the membrane. With mutation studies, we elucidated the physical functions of the particular residue in the dimerization process.

4.3. Materials and Methods

4.3.1. Peptide synthesis and purification

Unlabeled peptide and N-terminal labeled-peptides with FITC (Fluorescein isothiocyanate), Rhodamine B, and Carboxytetramethylrhodamine (TAMRA) were synthesized from Peptide 2.0 Inc (Chantilly, VA, USA). The peptide sequences are following:

For SDS micelles,

- 1) 435APVDSMLKDMATIILSTFLLIGWVAFIITYPLSMH469
- 2) FITC-APVDSMLKDMATIILSTFLLIGWVAFIITYPLSMH
- 3) Rhodamin B- APVDSMLKDMATIILSTFLLIGWVAFIITYPLSMH

For POPC (1-palmitoyl 2-oleoyl phosphatidylcholine) liposome, three flanking residues (lysine) were attached.

- 1) K-452KDMATIILSTFLLIGWVAFIITYPLS467-KK
- 2) FITC-K-KDMATIILSTFLLIGWVAFIITYPLS-KK
- 3) TAMRA-K- KDMATIILSTFLLIGWVAFIITYPLS-KK

The peptides were purified using reverse-phase HPLC and confirmed by MALDI-TOF mass spectrometry.

4.3.2. Circular dichroism (CD) spectroscopy

CD spectra were recorded with ChirascanTM CD Spectrometer (Applied Photophysics) in the 190–260 nm regions (0.5 nm step, 10 nm/min, 1 nm slit width). The 1 mm path-length quartz cell (Starna Cells, Inc) was used for the measurements. Baseline was measured for TFE, SDS, and liposomes without the peptide and subtracted from the corresponding sample spectrum.

4.3.3. Förster resonance energy transfer (FRET) measurements

For a donor/acceptor pair, the excitation wavelength was set at 439 nm and emission spectra were collected from 480 to 650 nm. FRET efficiency was calculated from measurements of donor fluorescence intensity at 515 nm in the absence and presence of the acceptor: FRET efficiency = (ID - IDA)/(ID), where ID and IDA are the donor fluorescence intensities of

samples containing only donor-labeled peptides and samples with both donor- and acceptor-labeled peptides, respectively. The contribution to the emission at 515 nm from the direct excitation of the acceptor was removed by subtracting the spectra of samples containing only acceptor-labeled peptides. In addition, the background noise from lipid was eliminated by subtracting the spectra of liposome samples without any peptide.

4.3.4. Sample Preparation for SDS micelles

To prepare TM peptides in aqueous solutions of SDS, the peptides were initially dissolved in TFE and dried under a stream of nitrogen. The dried peptides were then mixed with a freshly made 20 mM SDS solution containing 10 mM Tris-HCl (pH 7.0) and 50 mM NaCl. The samples were sonicated for 15 min and incubated for 1 hr at room temperature before further experiments.

4.3.5. Preparation of Liposome containing TM peptides

Unlabeled TM peptide and N-terminal labeled-TM peptides with FITC or TAMRA were dissolved in TFE and POPC were dissolved in chloroform. Both peptides and POPC were mixed and then the organic solvents were removed using nitrogen gas stream. The peptide/lipid mixture was reconstituted in 10 mM phosphate buffer (pH7) containing 500 mM NaCl. Samples were then freeze-thawed three times. For FRET experiments, the samples were equilibrated at RT for 1 hr before the measurement. For CD measurements, probe sonication was performed to produce small unilamellar vesicles and reduce light scattering, which is a critical factor for CD measurements in the far UV region.

4.3.6. TOXCAT Chimera Constructions

The TOXCAT vectors, pccKAN (TM deficient negative control), pccGpA-WT (positive control), and pccGpA-G83I (negative control), along with NT326 (malE-) *E.Coli* strain, were kindly provided by Dr. Donald M. Engelman (Yale University, New Haven, CT) [188]. DNA fragment coding for IRE1α-TM residues (444-466 aa) was amplified from the plasmid pcDNA-hIRE1α (a gift originally from Randal J. Kaufman (University of Michigan, MI, USA)) and then was inserted into in-frame to the NheI and BamHI sites of pccKAN to generate the ToxR-IRE1-TM-MBP fusion protein. Individual mutants of IRE1-TM domain were created via mutation of the pcc-IRE1-WT plasmid using the QuikChange Lightning site-directed mutagenesis kit (Agilent Technologies, Inc.). The sequences of mutations were confirmed by DNA sequencing services (Eurofins MWG Operon).

4.3.7. TOXCAT assay

The TOXCAT chimeras were transformed into NT326 cells and grown at 37 °C until A600 is 0.6. The harvested cells were lysed using the xTractor Cell Lysis Buffer (Clontech) containing 0.2 mg/mL Lysozyme. The cell extract was assayed for quantification of the CAT concentration using the CAT enzymelinked immunosorbent assay kit (Roche Applied Science), according to its product manual. Chimera protein expression was quantified from Western blotting using anti-MBP antibody and used to normalized CAT activity by various constructs.

4.3.8. MalE Complementation Assay

To confirm correct membrane insertion, NT326 cells expressing the TOXCAT chimeras were grown overnight in LB media. The cells were inoculated in M9 minimal media and cultured

for 8 hrs. The cells were streaked onto M9 minimal media agar plates containing 0.4 % maltose as the only carbon source and incubated for 3 days at 37 °C. The images of the agar plates were collected using the Molecular Imager ChemiDoc XRS System (Bio Rad).

4.4. Results

4.4.1. Prediction of IRE1 α Transmembrane (TM) Segment from various prediction methods

The sequence of the IRE1a TM domain has not been experimentally determined but its potential sequence (444-464 aa) was obtained from UniProt data base using three prediction methods (ESKW [189], **MEMSAT** [190]. **TMHMM** [191]) (http://www.uniprot.org/uniprot/O75460) (Table 3). We additionally simulated the potential TM domain with several web-based programs, i.e. DAS [192], HMMTOP [193], OCTOPUS [194], Phobius [195], SOSUI [196], TMHMM [191]. The N-terminus of the TM domain was predicted to begin at M444 except with DAS which predicted A445, but the C-terminal residue varied from I462 to L466, depending on the prediction method (Table 3). Residues 444 to 466 were chosen as the transmembrane domain, thus an extended TM model peptide was designed (A435-H469) that included several N-terminal and C-terminal flanking residues in IRE1α.

4.4.2. Oligomerization of the transmembrane domain of IRE1α in SDS micelles

SDS is a well-characterized system applied to mimic transmembrane proteins, and is commonly used to uncover helix-helix interactions of TM domains given its ability to maintain the native secondary and tertiary structures of the TM segments [197-200]. However, long

Table 3. Prediction of IRE1 α Transmembrane Segment from various prediction programs

Source	Sequence
UniProt	435APVDSMLKD <u>MATIILSTFLLIGWVAFIITY</u> PLSMH469
DAS	435APVDSMLKDM <u>ATIILSTFLLIGWVAFIITYP</u> LSMH469
HMMTOP	435APVDSMLKD <u>MATIILSTFLLIGWVAFIITYPL</u> SMH469
OCTOPUS	435APVDSMLKD <u>MATIILSTFLLIGWVAFIITY</u> PLSMH469
Phobius	435APVDSMLKD <u>MATIILSTFLLIGWVAFIITYPL</u> SMH469
SOSUI	435APVDSMLKD <u>MATIILSTFLLIGWVAFIITYPL</u> SMH469
TMHMM	435APVDSMLKD <u>MATIILSTFLLIGWVAFII</u> TYPLSMH469

hydrophobic peptides frequently result in (non-native) β -sheet characteristics, which can lead to insolubility and unstable peptide solutions. Using CD spectroscopy, we checked whether the model peptides are helical in the SDS micelles. The CMC (critical micelle concentration) of SDS at 50 mM NaCl is reported to be 2.25 mM [201]. Therefore we used 20 mM SDS, which is well above the CMC, in a buffer solution (10 mM Tris (pH 7.0), 50 mM NaCl). In addition, TFE (2,2,2-trifluoroethanol), known to promote α -helix formation, was used as a positive control environment for the TM peptide. The CD spectra of the TM peptide in TFE showed a characteristic α -helical profile with minima at 208 and 222 nm (Figure 4.1). Likewise, the CD spectrum of the TM peptide in 20 mM SDS also showed α -helical conformation. CDNN (the CD spectrum deconvolution software) analysis [202] of the spectra revealed a high helical content of the TM peptide in SDS and TFE, 43.97±0.47 % and 54.80 ±3.63 %, respectively.

Since SDS-PAGE is commonly used to qualitatively examine the oligomeric states of the TM domain, we performed SDS-PAGE to determine whether the IRE1α TM domain oligomerizes in SDS. The results at different peptide concentrations (2, 4, 6, 10 μM) are presented in Figure 4.2. The TM peptides migrated as three distinct forms, corresponding to a monomer (3.91 kDa), dimer (7.82 kDa) and tetramer (15.64 kDa) fractions on 12 % NuPAGE gel. In addition, the dimer and tetramer fractions increased with peptide concentration, suggestive of the existence of dimeric and tetrameric TM peptide species. These results support that IRE1α TM domain oligomerizes in SDS in the absence of the luminal and cytosolic domains.

To confirm the oligomerization status, we further employed FRET analysis. FRET is used to evaluate the self-association of the TM peptides in SDS micelles [200, 203, 204]. The selected fluorophores (FITC and Rhodamine B) are a well-known donor-acceptor pair with a R_0 (Förster radius that is a distance where FRET efficiency is 50 %) of ~55Å. SDS-PAGE results

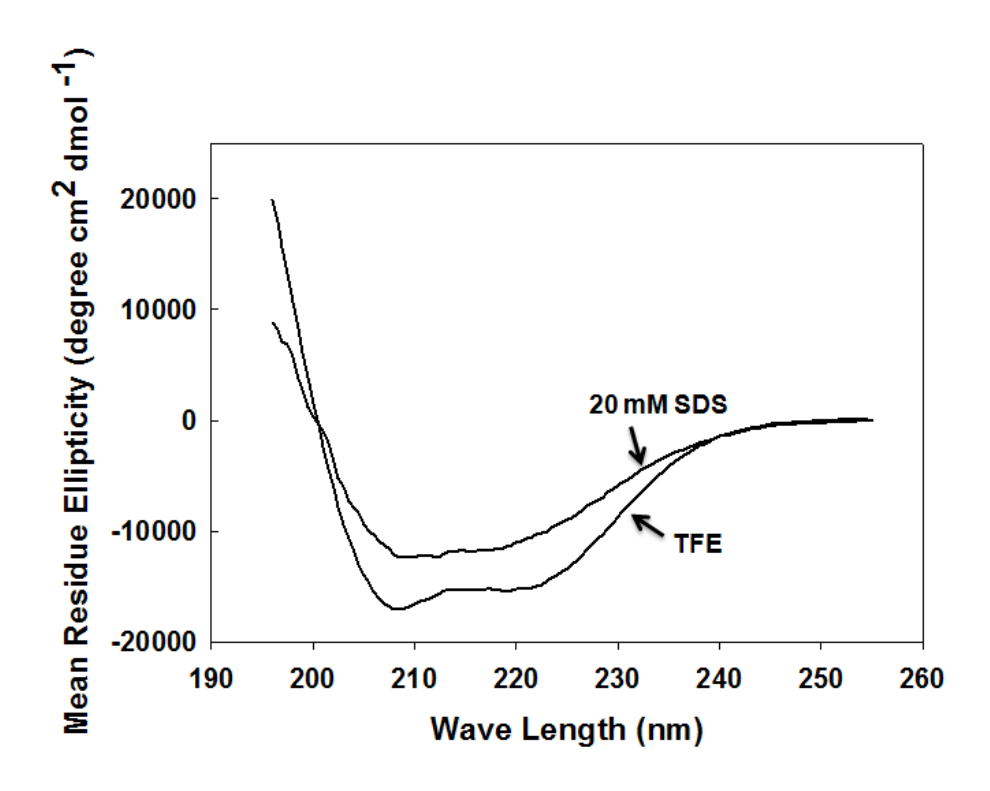


Figure 4.1. Secondary structure of IRE1 α TM model peptide determined by circular dichroism spectroscopy. CD spectra are shown for the peptide in TFE and in detergent buffer containing 20 mM SDS, 10 mM Tris-HCl (pH 7.0), 50 mM NaCl. The peptide concentration was 40 μ M in each case.

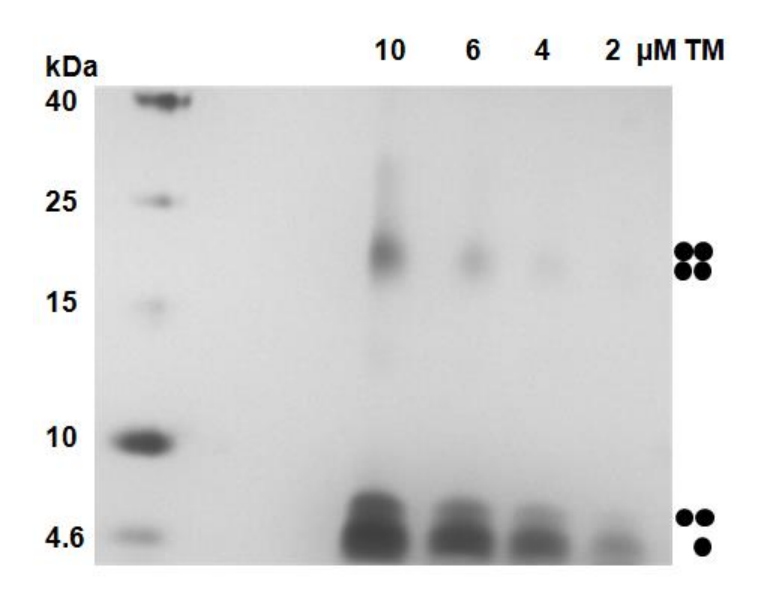


Figure 4.2. Oligomer formation of IRE1 α TM model peptide by SDS-PAGE. IRE1 α TM model peptide dissolved in 20 mM SDS-containing sample buffer were loaded onto 12% NuPage gel at different concentrations (2, 4, 6, 10 μ M). Bands were visualized using silver staining.

indicated similar migration of the unlabeled-TM peptide and labeled-TM peptides (FITC-TM and Rhodamine B-TM) (data not shown), demonstrating that the attachment of the fluorophores did not influence the oligomerization ability of the peptide. Figure 4.3A shows typical emission spectra of the donor-only sample (FITC-labeled TM peptide) (dashed line) and the acceptor-only sample (Rhodamine-labled TM peptide) (dotted line) in SDS micelles. However, when both the donor and acceptor are present in the sample, FRET occurs as indicated by the decrease in donor fluorescence and the appearance of sensitized acceptor fluorescence (Figure 4.3A). Thus, the results suggest that the FITC- and Rhodamine B-labeled TM peptides could self-associate in SDS micelles.

To further estimate the oligomer status, FRET efficiency was measured as a function of the molar fraction of the acceptor (Pa), while the concentrations of the donor and total peptide remained constant. According to the equation (FRET efficiency = $K(1-(1-Pa)^{n-1})$), where Pa is the molar fraction of the acceptor, n is the number of molecule, K is a constant), a linear dependence between the FRET efficiency and the molar fraction of the acceptor is indicative of dimer formation and deviation from linearity represents the formation of high-order oligmers [205]. As shown in Figure 4.3B, the non-linear increase in FRET efficiency in the SDS micelles approximates a tetrameric state (n=4.33±0.187 and K = 0.58±0.01 with R = 0.997), suggesting the IRE1 α TM peptides is possibly forming tetramers. The FRET analysis (Figure 4.3B) agrees with the SDS-PAGE results in Figure 4.2, indicating the isolated TM domains have a propensity to oligomerize.

4.4.3. Oligomerization of the transmembrane domain of IRE1α in POPC liposome

We previously showed that the TM domain of IRE1 α maintains α -helical structure in

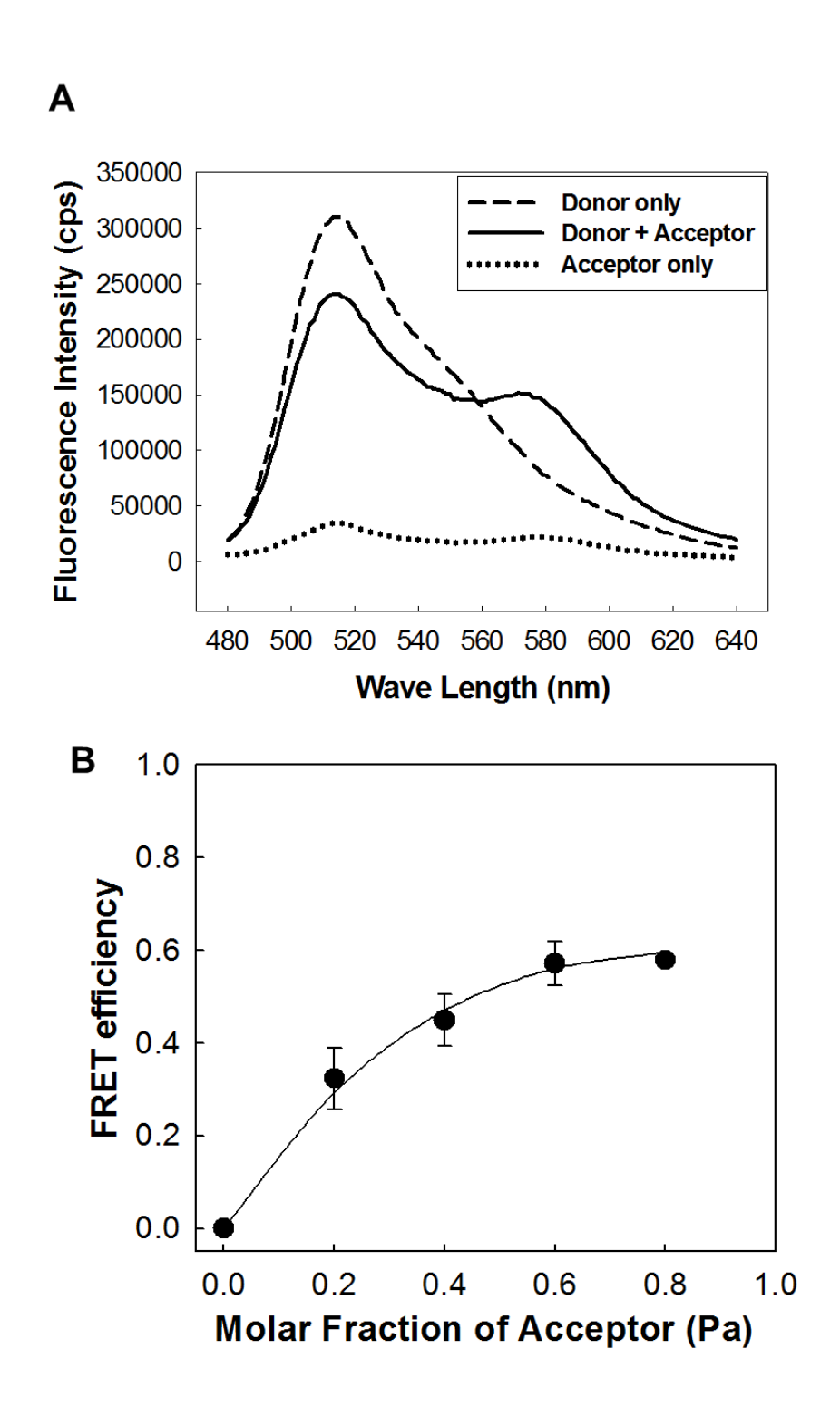


Figure 4.3. Oligomer formation of IRE1α TM model peptide by FRET. (A) Fluorescence spectra of FITC/Rhodamine B-labeled TM peptides in SDS micelles. 0.75 μM of donor (FITC-TM) or/and acceptor (Rhodamine B-TM) peptides were dissolved in 20mM SDS, 10mM Tris-HCl (pH 7.0), and 50mM NaCl. The excitation was fixed at 439 nm such that only the FITC was

(Figure 4.3 cont'd) directly excited and the emission was scanned from 480 to 640 nm. The spectra were measured for the samples containing the donor and acceptor peptides (solid line), as well as control samples containing only the donor (dash line) and only the acceptor peptides (dotted line). (B) FRET analysis of IRE1 α TM interactions in SDS micelles. FITC-labeled peptides (donor) at 0.75 μ M were titrated with an increasing mole fraction of Rhodamine B-labeled peptides (acceptor) in 20mM SDS, 10mM Tris-HCl (pH 7.0), and 50mM NaCl. The total peptide concentration was kept constant at 4 μ M with the addition of unlabeled peptide. The FITC-labeled peptides were excited at 439 nm and the fluorescence intensity was measured from 480 to 640 nm. FRET efficiency was calculated and data fitted as described in the Materials and methods. Error bars correspond to the standard deviation of four experiments.

SDS micelles [182]. Since no structural information of the IRE1 α -TM domain in phospholipid bilayers is available, we further examined whether the TM domain is α -helical in our model phospholipid, POPC. As shown in Figure 4.4, the CD data of the TM model peptide in POPC liposomes seems consistent with α -helix formation, as evidenced by the presence of a minimum around either 208 or 222 nm.

FRET is often used to evaluate the dimerization/oligomerization of TM peptides in micelles and liposomes [200, 206]. When both the donor (Fluorescein isothiocyanate (FITC)) and acceptor (Carboxytetramethylrhodamine (TAMRA)) are present in the POPC liposome, FRET clearly occurs as indicated by a decrease in the donor fluorescence and the appearance of sensitized acceptor fluorescence (Figure 4.5A). We further confirmed that the measured FRET efficiency as a function of the total peptide concentration in a fixed amount of POPC liposome (FITC-TM/TAMRA-TM = 1) is concentration-dependent and exceeds the random proximity effects [207], indicating a propensity of self-association in the liposome (Figure 4.5B). We further confirmed that the label fluorophores (FITC or TAMRA) at the N-terminus on the TM peptide does not alter the secondary conformation in TFE (2,2,2-trifluoroethanol), an organic solvent known to promote α-helix formation (Figure 4.6).

4.4.4. Trp457 mutations reduce the self-association of IRE1α-TM domain

We used the TOXCAT assay, in which association between TM domains in the inner membrane of *E. coli* drives expression of the reporter gene chloramphenicol acetyltransferase (CAT) [188]. CAT activity was normalized to a positive control (the TM domain of glycophorin A (GpA)), which is known to dimerize strongly [208] while GpA-G86I served as a dimerization-impaired mutant (a negative control). As shown in Figure 4.7A, the WT TM domain has

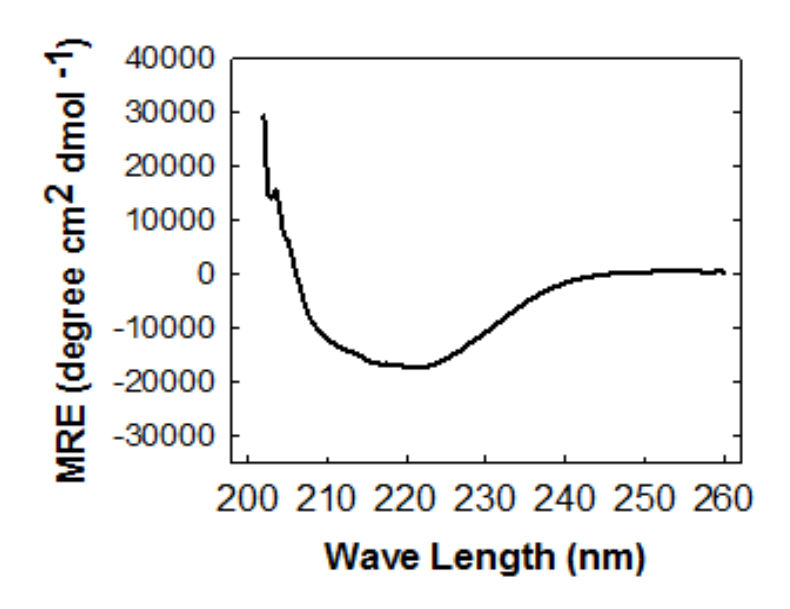


Figure. 4.4. CD spectrum of IRE1-TM peptide in POPC liposome. Secondary structure of IRE1α TM model peptide determined by circular dichroism spectroscopy. CD spectrum is shown for the peptide inserted POPC liposome in 10 mM phosphate buffer (pH7), 500 mM NaCl.

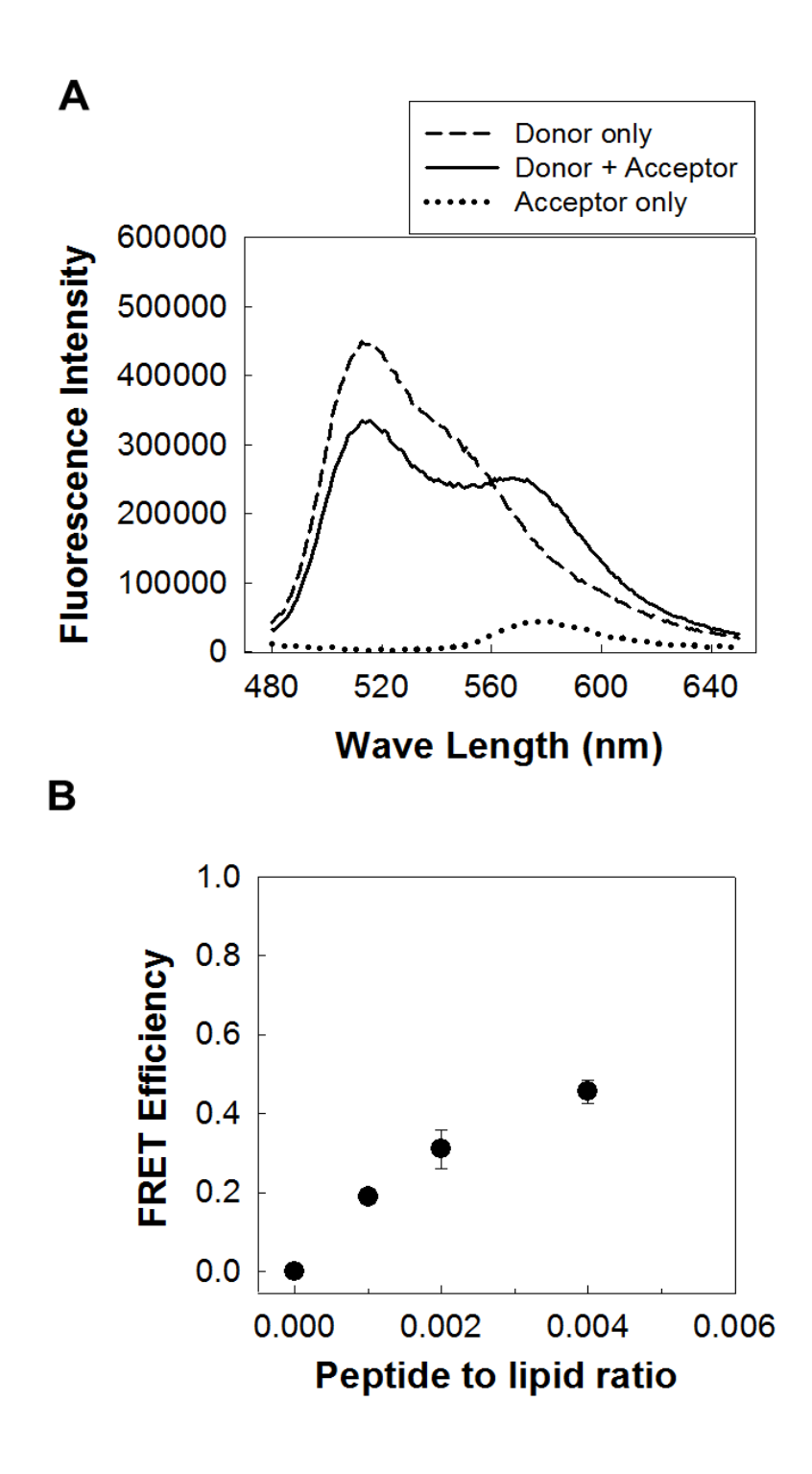


Figure 4.5. FRET analysis of IRE1 α -TM interactions in POPC liposomes. (A) Fluorescence spectra of FITC/TAMRA-labeled TM peptides inserted in POPC liposomes. 0.1 mol% of donor (FITC-TM) or/and 0.1 mol% of acceptor (TAMRA-TM) peptides were reconstituted in 400 μ M of the lipid. The excitation was fixed at 439 nm such that only the FITC was directly excited and

(Figure 4.5 cont'd) the emission was scanned from 480 to 650 nm. The spectra were measured for the samples containing the donor and acceptor peptides (solid line), as well as control samples containing only the donor (dash line) and only the acceptor peptides (dotted line). (B) Dependence of the energy transfer from the peptide/lipid molar ratio. The ratio of donor-labeled to acceptor-labeled peptides was kept at 1 while the total peptide concentration to lipid ratio varied. The final concentration of Lipid was fixed at 400 μ M. The FRET efficiency was calculated as described in Materials and Methods.

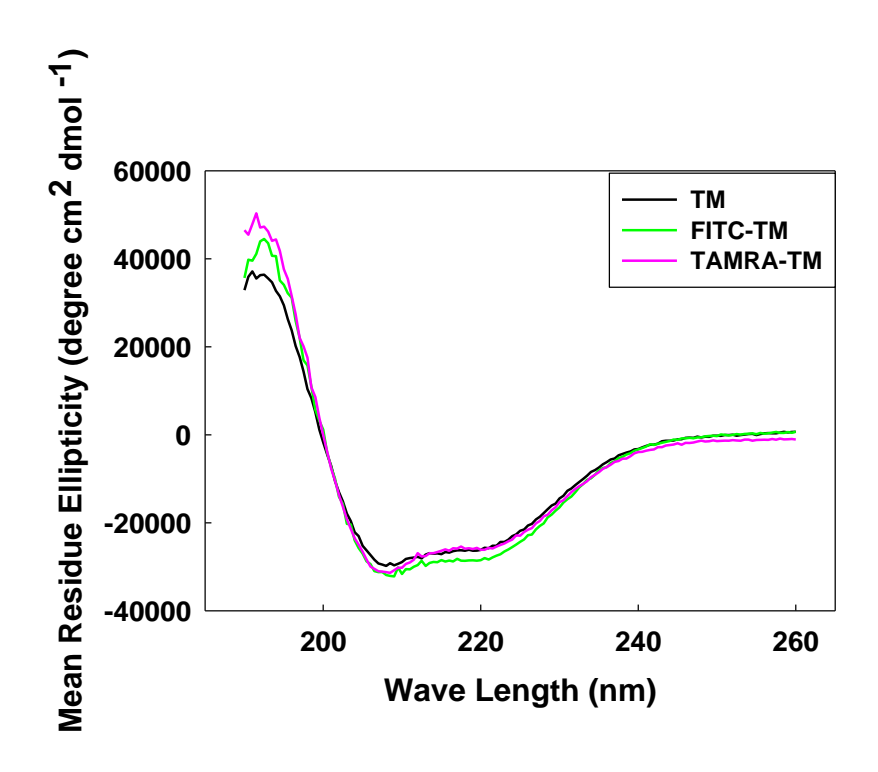


Figure. 4.6. CD spectra of IRE1α-TM peptides in TFE. The N-terminal attached fluorescent dyes (FITC and TAMRA) do not perturb the helical secondary structure of the model peptide.

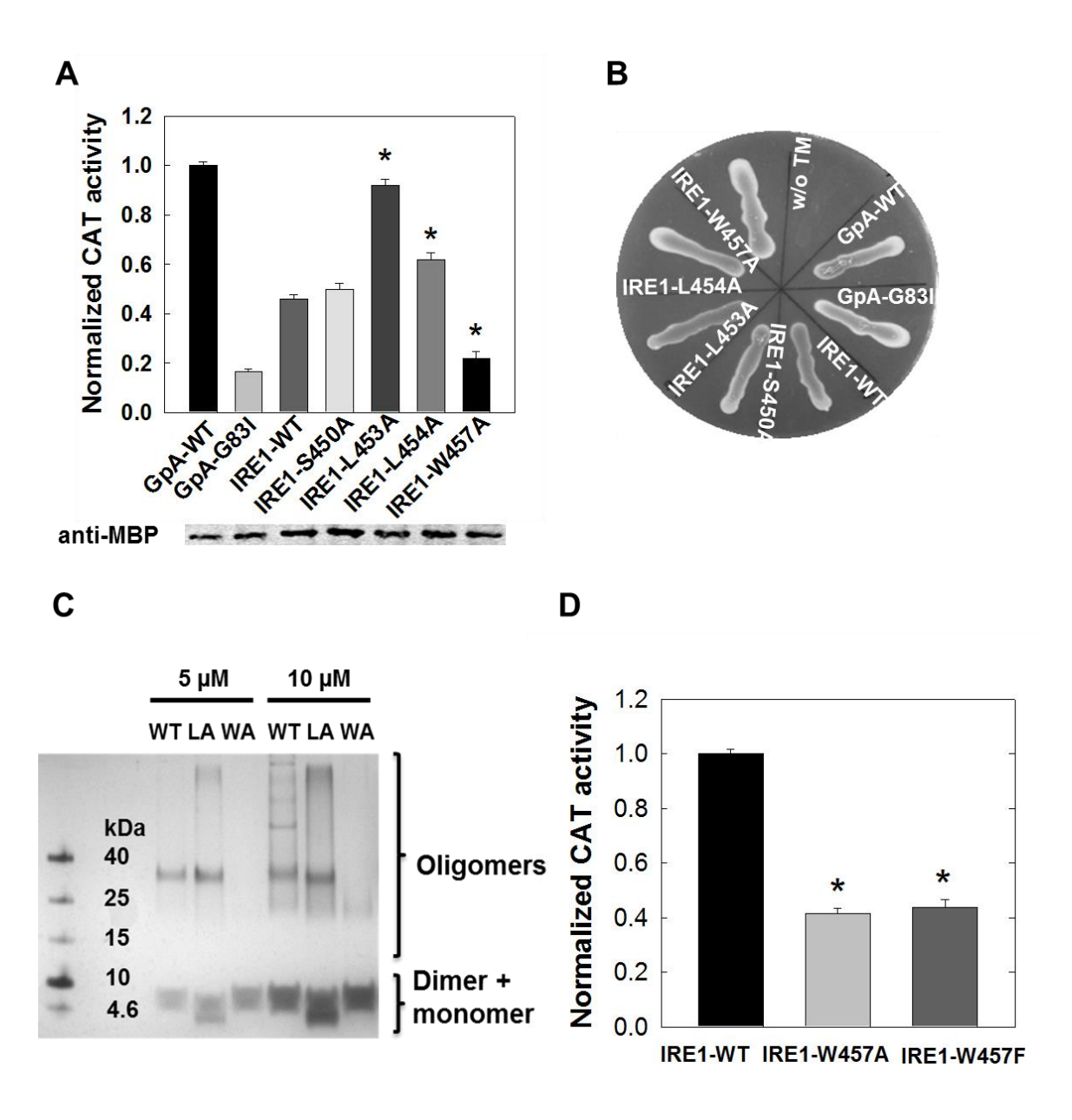


Figure 4.7. TOXCAT and SDS-PAGE analyses of IRE1 α -TM oligomerization. (A) (Upper) TOXCAT assays. CAT activities from cells expressing ToxR-TM-MBP were quantified and normalized to GpA-WT. GpA-WT and its disruptive mutant (GpA-G83I) serve as positive and negative controls. Error bars show standard deviation of six independent values: *p < 0.001. (Lower) Western Blotting analysis. The expression levels of ToxR-TM-MBP proteins were

(Figure 4.7 cont'd) measured using anti-MBP antibody. The expression levels were also normalized to correct the CAT activity. (B) MalE complementation assay. The TOXCAT chimeric proteins (ToxR-TM-MBP) were plated on M9 agar containing 0.4 % maltose. The MalE activity is used to show an appropriate TM topology. (C) SDS-PAGE analyses of the wild-type and mutants of IRE1-TM peptide. IRE1 α TM model peptides dissolved in 1x LDS sample loading buffer were loaded onto 9% Tris-glycine gel at different concentrations (5 and 10 μ M). Bands were visualized using silver staining. (D) TOXCAT assay with W457 mutants. CAT activities from cells expressing ToxR-TM-MBP were quantified and normalized to IRE1-WT. Error bars show standard deviation of six independent values: *p < 0.001.

approximately 45 % CAT activity as compared with the signal generated by GpA-WT, indicating that the IRE1 a TM domain dimerizes in the biological membrane. Our collaborator (Dr. Amadeu K. Sum's group, Colorado School of Mines) performed MD simulations to predict the residues at the interface between two TM model peptides, which could provide a possible mechanism of the TM dimerization and further provide a representative model for the assembly of dimeric building blocks on the TM oligomerization. Since the MD simulation results suggested that Ser450, Leu453, Leu454, and Trp457 might be localized in the dimerization interface on the TM domain of IRE1α protein, we further tested whether the mutation on those residues alters the selfassociation of IRE1α-TM domain. The mutation of Trp457 to Alanine results in a significant reduction in the CAT activity, whereas the L453A mutant dramatically increases the CAT activity (Figure 4.7A). Furthermore, as shown in Figure 4.7B, when maltose was the sole carbon source (MalE complementation), each construct containing the TM domains is able to facilitate the growth of an MBP-deficient strain of E. coli, indicating that the MBP domain of the chimeric protein was located in the bacterial periplasmic space. To determine whether the W457A and L453A mutants are capable of modulating the oligomerization driven by the IRE1α-TM domain, the model peptides were further analyzed through SDS-PAGE, which is commonly used for detecting the oligomerization status of TM domains. As shown in Figure 4.7C, the WT model peptide has several oligomeric states, as evident by the smeared bands on the SDS-PAGE image. The monomeric and dimeric states did not separate clearly, possibly reflecting the dynamic equilibrium between the two states during the electrophoresis, which is frequently observed in short TM domain peptides [209]. In addition, the W457A mutant dramatically decreased the oligomerization of the model peptide, but the L453A mutant slightly increased its oligomerization as compared with the WT model peptide. Thus, taken together with the results of Figure 4.7A, we concluded that the Trp457 residue plays a critical role on regulating the oligomerization of the IRE1 α -TM domain.

Of the aromatic residues, the side chain of tryptophan is unique, with its amphipathic nature enabling it to participate in both aromatic interactions (NH- π and CH- π) and hydrogen bonding [210]. The multi-functional side-chain makes the tryptophan residue an important contributor, both to the process of protein folding and stabilization of the folded protein structures. To address whether the tryptophan residue is a unique feature in the 457 position for the TM dimerization, Trp457 was also mutated to Phenylalanine, an aromatic residue which does not provide a hydrogen bond donor. As shown in Figure 4.7D, the CAT activities of W457A and W457F were compared with that of the WT. Along with W457A, W457F also dramatically decreased the **CAT** activity, suggesting that W457F disrupts mutant the dimerization/oligomerization of the TM domain in the E.coli cell membrane. Interestingly, the W457A and W457F mutants do not show any significant difference between them with respect to the CAT activity. Thus the experimental results suggest that the aromatic characteristic alone is not sufficient to prevent the self-association and thus the H-bond or/and dipole moments on the tryptophan residue could play a critical role on regulating the TM dimerization.

4.5. Discussion and Conclusions

It has been shown that both the luminal and the cytosolic domains can oligomerize [19, 23, 181, 211]. The oligomeric form of the luminal domain was identified by detecting exogeneously expressing proteins on SDS-PAGE gel [211]. In addition, structural and functional studies found that disruption of the dimer interface interaction on the luminal domain blocked the

phosphorylation of the cytosolic domain, suggesting that dimerization of the luminal domain promotes dimerization and activation of the cytosolic domain [23]. In addition to dimers, the cytosolic domain also has been shown to form high-order oligomers (tetra-, hexa-, octomer as an even number oligomers) by velocity-analytical ultracentrifugation experiments, indicating the assembly of dimeric building blocks is important to the oligomerization process [181]. The enzymatic assay additionally suggested that the endoribonuclease activity of the human IRE1 α is activated by self-association of four or more IRE1 α monomers, presumably similar to that observed with yeast Ire1 [181, 212]. Thus this higher-order oligomerization plays a crucial role in IRE1 α activation. Similarly, our findings showed that the TM domain of IRE1 α also is able to form dimers, tetramers, and higher oligomers, suggesting that the TM domain could participate in the oligomerization of the IRE1 α protein.

In membrane proteins, it is well known that tryptophan preferentially localizes in the membrane interface, due to its aromaticity of the indole moiety and the overall amphipathic nature [213]. Tryptophan has the largest hydrophobic interface among all natural amino acids, but its NH group is also capable of forming hydrogen bonds with the lipid carbonyl groups or the interfacial water molecules [213, 214]. These physical characteristics of Tryptophan specifically contribute to the functions and structures of the ion channel proteins extensively reviewed in [215]. Interestingly, Tryptophan has a heptad repeat pattern which supports self-association of the helical transmembrane segments [216]. Furthermore, Sal-Man *et al.* suggested that the aromatic-XX-aromatic motif (W-XX-W motif) regulates the transmembrane helix-helix interactions [217]. However, to the best of our knowledge, the molecular mechanisms by which tryptophan mediates the transmembrane helix-helix interactions is still unclear.

MD simulations (From Dr. Sum's group) and experimental results showed that Trp457 could provide a driving force for the dimerization process. In the MD simulation data, initially the two Trp457 residues were located in the opposite side of the two TM peptides. However, they rapidly changed orientation to allocate in the center of the interface forming a stable aromatic interaction. Unlike tryptophan, phenylalanine does not have dipole moments and it is not able to form any H-bonds. MD simulations and the TOXCAT analyses showed that the mutation W457F significantly reduced the TM dimerization (Figure 4.7D), indicating both the dipole moments and H-bonds could be crucial for the dimerization process. The TM segment of IRE1 α contains a W457-XX-F460 sequence, possibly suggesting that the dimerization could be mediated by the W-XX-W motif. In the motif, the aromatic residues could be replaced by other aromatic amino acids, without significantly reducing the protein functions [217]. In our study, the mutation of Trp457 to phenylalanine dramatically reduced the self-association of the IRE1α TM segments (Figure 4.7D), suggesting that Trp457 is not replaceable by Phenylalanine. Thus, the TM dimerization of the IRE1α protein is not mediated by the W-XX-W motif, but Trp itself is critical to the dimerization process. Furthermore, MD simulation of a non-natural amino acid, 1-methyl-tryptophan (1-Me-Trp) that contains a methyl group on the NH of the indole group was performed. 1-Me-Trp retains the aromaticity and dipole moments of the indole rings, but does not have the H-bond interactions. Since indole and 1-Me-Trp have dipole moments of similar direction and magnitude (2.1 Debye for Trp and 2.2 Debye for 1-Me-Trp) [218], the only difference between Tryptophan and 1-Me-Trp is the ability to form H-bonds. The MD simulations showed there is no significant difference in the dimerization pattern between Trp and 1-Me-Trp, suggesting the H-bond alone is not likely critical for the TM dimerization of IRE1α, but could be useful for correct stacking of the aromatic rings. The tryptophan residue could

mediate the TM dimerization through aromatic interactions (π - π interactions) and stabilize the TM association through H-bonding.

In addition to the aromatic residue, MD simulation results predicted that the interface of IRE1α TM domain includes Ser450, Leu453, and Leu454 in the involvement of H-bonds and hydrophobic interactions and indeed L453A mutation enhanced dimerization (Figure 4.7). Interestingly, those residues are located as a leucine-zipper-like motif (S450xxL453xxx motif). The heptad repeat SxxLxxx motif was previously observed in the parallel TM dimerization on the mouse erythropoietin receptor (EpoR) protein [219]. Since the mouse EpoR protein contains two repeats of SxxLxxx sequence, but the human has only one of the motif, the mouse EpoR TM domain has a stronger association than its human homologue [220]. Like the human EpoR protein, the IRE1α contains only one heptad SxxLxxx motif, which nevertheless could be sufficient to support the Trp-Trp interaction on the dimerization interface.

Surprisingly, yeast Ire1 does not have either a Tryptophan residue or the SxxLxxx motif on the TM domain (Figure 4.8). However, the TM domain on the human IRE1 α is highly homologous with the mouse IRE1 α : only one residue Ile455 in human is different from Val455 in mouse. Since the Tryptophan residue and the SxxLxxx sequence are conserved in the mouse protein and the structure and hydrophobicity between Isoleucine and Valine are similar, the molecular mechanisms of the TM dimerization for the mouse IRE1 α could be very similar to the human IRE1 α protein. The yeast Ire1 has a longer TM segment than the human IRE1 α protein, which reflects the different lipid compositions in the ER membranes [221]. In addition, since the different sensing mechanisms between human IRE1 α and yeast Ire1 luminal domains (reviewed in [222, 223]) were observed, it would be interesting to determine in future how the dimerization mechanisms of the yeast Ire1-TM domain differ from those of the human IRE1 α . Interestingly,

Yeast Ire1 LLKFGSLVYRIIETGVFLLLFLIFCAIL
Human IRE1 α MATIILSTFLLIGWVAFIITY
Mouse IRE1 α MATIILSTFLLVGWVAFIITY
Human PERK PVLLLHWWKEIVATILFCIIA
Mouse PERK PILLLHWWKEIFGTILLCIVA

Figure 4.8. TM Sequence comparison of IRE1 and PERK proteins. The TM sequences were obtained from Uniprot website (http://www.uniprot.org/).

human PERK and mouse PERK contains two tryptophan residues (Trp521 and Trp522) in sequence (Figure 4.8). These two Tryptophan residues are localized in different locations (closer to the N-terminus) as compared to the IRE1 α protein (where it is closer to the C-terminus). Furthermore, the Tryptophan residues have adjacent polar residues (Lys523 and Glu524 localized in the TM center) on PERK. Along with the π - π (aromatic-aromatic) interactions mediated by the Tryptophan residue, the cation- π interaction is known to enhance the strength of oligomerization of TM helices [224]. It still remains a question whether the two Tryptophan residues could partition into the π - π interaction or cation- π interactions with Lys523. In addition to the Tryptophan residue, since the Glutamic acid residue buried in the hydrophobic core of the TM helices was shown to promote the dimerization of RTKs through the H-bond [225], Glu524 or Lys523 could be important for PERK dimerization. Although there are many open questions, from sequence alignments (Figure 4.8), we speculate that the molecular mechanism of the TM dimerization might not be conserved among the UPR sensor proteins.

In summary, we provide evidence that the TM domain of the IRE1 α protein oligomerizes in the membrane-mimic environments, and maintains its helical structure. With combining to the computational study, we found that the tryptophan residue plays a critical role on regulating the dimerization/oligomerization of the IRE1 α protein.

CHAPTER 5. ROLES OF PALMITIC ACID ON THE IRE1a PROTEIN

5.1. Introduction

IRE1α is one of the main arms in the UPR, an evolutionarily conserved intracellular signaling pathway triggered when unfolded or misfolded proteins accumulate in the endoplasmic reticulum (ER) [226]. To minimize the ER stress caused by perturbation of the protein folding environments, IRE1α is activated upon autophosphorylation and the active form catalyzes the unconventional processing of the mRNA encoding the transcription factor XBP1, by splicing a 26-nucleotide intron from the XBP1 mRNA which generates an active transcription factor (XBP1s) [20]. The spliced XBP1s controls the upregulation of UPR-targeted genes involved in enhancing ER protein-folding capacity and degrading unfolded or misfolded ER proteins [20, 21]. Furthermore, the active IRE1α can induce apoptosis through interaction with tumor necrosis factor-receptor-associated factor 2 (TRAF2), leading to activation of c-JUN N-terminal kinase (JNK) through apoptosis signal-regulating kinase 1 (ASK1) [22].

Like other Ser/Thr kinases, all features around the ATP binding site are conserved in the IRE1 α protein (See Figure 5.1). From the N-terminal lobe, two conserved residues, Glu612 within the α C helix and Lys599, assist to optimally position the α - and β -phosphate groups. The DFG motif is in the 'in' conformation and the side chain of Asp711 in the motif provides a direct ligand interaction with the Mg²⁺ ion. In addition to the kinase domain, a small helix in the C-terminal RNase domain (α 3') contributes the catalytic function of the RNase domain, and is conserved in the other RNaseL ribonuclease family [227].

Small ligand molecules have been found to regulate the enzymatic activities of the IRE1a

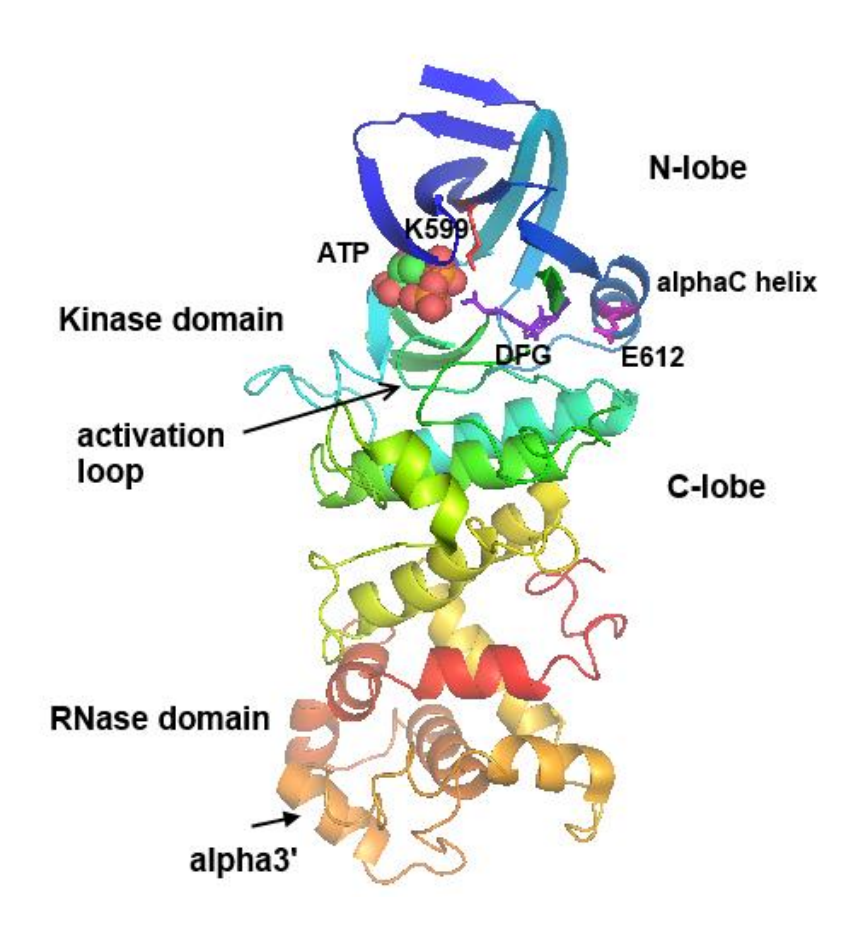


Figure. 5.1. Cytosolic domain of human IRE1 α . The structure is rainbow colored blue to red, N to C-terminus. ATP molecule is shown in balls. Two helices (α C and α 3') important for the catalytic functions of kinase and RNase are shown in the figure. PDB id: 3P23.

protein. ATP-competitive inhibitor 1NM-PP1 is well known to allosterically activate the RNase domain though binding of kinase-dead IRE1 α mutants [228, 229]. In contrast, another ATP-competitive inhibitor, Sunitinib, inhibits the IRE1 α autophosphorylation, subsequently blocking the RNase activity [19]. In addition to the kinase domain targeting molecules, a hydrophobic Q-site at the dimer interface on the RNase domain of yeast Ire was identified by one of the flavonols, Quercetin, which enhanced the RNA activity by stabilizing the back-to-back dimer conformation of the enzyme [230]. Thus, there could be possibilities that other biological small molecules may bind on either the ATP binding site or the hydrophobic site on the IRE1 α protein.

Palmitic acid, one of the saturated free fatty acids, activates the IRE1 α activity in various cell lines [231-233]. However, the molecular mechanisms by which palmitic acid regulates the IRE1 α activity have not been uncovered. Interestingly, a recent publication suggested that palmitic acid activates the kinase and RNase activity of the IRE1 α through its transmembrane domain although the detail molecular mechanism is still unclear [55]. In addition, our group recently showed that palmitic acid directly interacts with the PKR kinase protein, thus regulating autophosphorylation [150]. Since the kinase domain around the ATP-binding domain is mostly conserved on kinases [180] and the yeast Ire1protein has similar dimer configurations with the PKR kinase protein [234], we hypothesize that palmitate might interact with the human IRE1 α , thus directly regulating the protein activities in the cells.

5.2. Materials and Methods

5.2.1. Western blot analysis

The HepG2 cells were washed twice with cold PBS and treated with RIPA buffer (50 mM Tris (pH 8.0), 150 mM NaCl, 1% NP-40, 0.5% sodium deoxycholate, 0.1% SDS) supplemented with protease inhibitor cocktail (Sigma-Aldrich) for 10 min on ice. The cell lysate was clarified by centrifugation at 13000 rpm for 10 min, and the supernatant was collected. Total protein levels were quantified by Bradford assay (Bio-Rad). Thirty micrograms of total protein was loaded onto 9% SDS-PAGE gel, transferred to nitrocellulose membranes, and probed with antibodies for the IRE1α protein.

5.2.2. RT-PCR

Total RNA was extracted from cells with the RNeasy mini kit (Qiagen). One microgram of total mRNA was reverse-transcribed using an iScript cDNA synthesis kit (Bio-RAD). The cDNA of XBP1 was resolved in 3 % agarose.

5.2.3. Protein expression and purification of the IRE1 α protein constructions

DNA plasmid containing the full length of human IRE1α gene was kindly provided by Dr. David Ron's group (University of Cambridge). The luminal domain (19-446 aa), cytosolic domain (562-962 aa), and kinase domain (562-833 aa) were cloned into pEcoli-Nterm 6xHN vector (Clontech).

The plasmids were transformed into *E. coli* Tuner (DE3) (Novagen). Cells were grown in LB media at 37 °C until the OD at 600 nm reaches 0.6 and then protein expression was induced with 1 mM IPTG overnight at 18 °C. The cells were collected by centrifugation at 4,000 rpm for 10 min and re-suspended in lysis buffer (50 mM HEPES, 500 mM NaCl, 5 % glycerol (pH 7.0), and 7 mM β–mercaptoethanol) containing protease inhibitor cocktail (Roche). The CelLyticB

buffer (Sigma) was added into the lysis buffer and the cells were incubated for 20 min at RT. The supernatant was loaded onto the HisTALONTM Superflow Column and the proteins were eluted with an imidazole gradient using ÄKTATM FPLC system (GE Healthcare). High salt contents in the fractions were removed using HiTrapTM Desalting column (GE Healthcare). All purified proteins were confirmed by SDS-PAGE and Western blotting analysis.

5.2.4. *In-vitro* XBP1 cleavage assay

The reactions were performed using RNase reaction buffer (20 mm HEPES, pH 7.5, 5 mM KOAc, 0.01mM DTT) supplemented with various concentration of MgCl₂ (0 to 5 mM) and 200 nM IRE1-CD proteins. For fluorescence intensity-based assay, the intensity values were measured at 488/515 nm using a spectrofluorometer. In addition, 15% urea-acrylamide gels were prepared and the samples were run in the gel using TBE buffer. The images were obtained from an imager equipped with a fluorescein filter (GE Healthcare).

5.2.5. Protein expression in Drosophila Schneider 2 (S2) Cells

The cytosolic domain (residues 547–977) was cloned into a pMT/V5-HisB vector (Addgene plasmid 17589: CG4845/pMT/V5-HisB) at Xho I and Kpn I restriction sites. The plasmid (PMT/V5-HisB-IRE1α-CD) and pCOPuro (Addgene plasmid 17533 [235]) was transfected into S2 cells using calcium phosphate transfection kit (Life Technologies). To generate the stable cell line, the transfected cells were maintained at 4 μg/mL of puromycin. 500 μM CuSO₄ were added in the flask containing the stably expressed cells. The protein expression level was quantified using western blotting analysis.

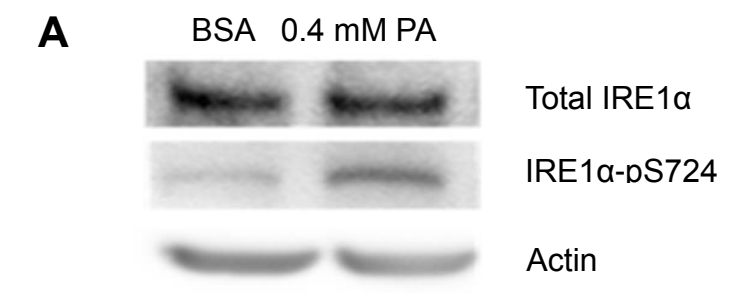
5.3. Results

5.3.1. Palmitic acid elevates the levels of both IRE1 α phosphorylation and XBP1 splicing in HepG2 cells

We first tested whether palmitate affects the IRE1α activity in HepG2 cells. As shown in Figure 5.2A, 0.4 mM palmitate significantly increases the phosphorylation level at S724 that is responsible for the activation of the protein. Figure 5.2B shows the quantification of the phosphorylation level at S724. We further confirmed that 0.7 mM palmitate enhances the activity of IRE1α RNase, by increasing the spliced XBP1 mRNA (Figure 5.2C). However, the cells did not respond to 0.4 mM, suggesting that the XBP1 requires a higher palmitate concentration in HepG2 cells.

5.3.2. Palmitic Acid binds to the cytosolic domain (CD) of IRE1α protein

To determine whether palmitate interacts with the luminal domain (LD) or cytosolic domain (CD), two recombinant proteins, the IRE1α-LD and IRE1α-CD, were expressed in Tuner (DE3) *E.coli* cells and purified using affinity chromatography. As shown in Figure 5.3A, the IRE1α-LD proteins expressed in BL21(DE3) *E.coli* cells were soluble while IRE1α-CD is insoluble, mostly locating in inclusion body. Thus we performed optimization experiments to obtain soluble forms of IRE1α-CD and we successfully extracted the soluble protein using Tuner (DE3) *E.coli* cells and CelLyticB lysis buffer (Sigma) (Figure 5.3B). In our previous study [150], we developed a fluorescence polarization (FP)-based palmitate interaction assay using fluorescently labeled palmitate molecule, Bodipy-PA. At the constant concentration of Bodipy-PA (10 nM), the Bodipy-PA binding assay was performed with increasing concentrations of the



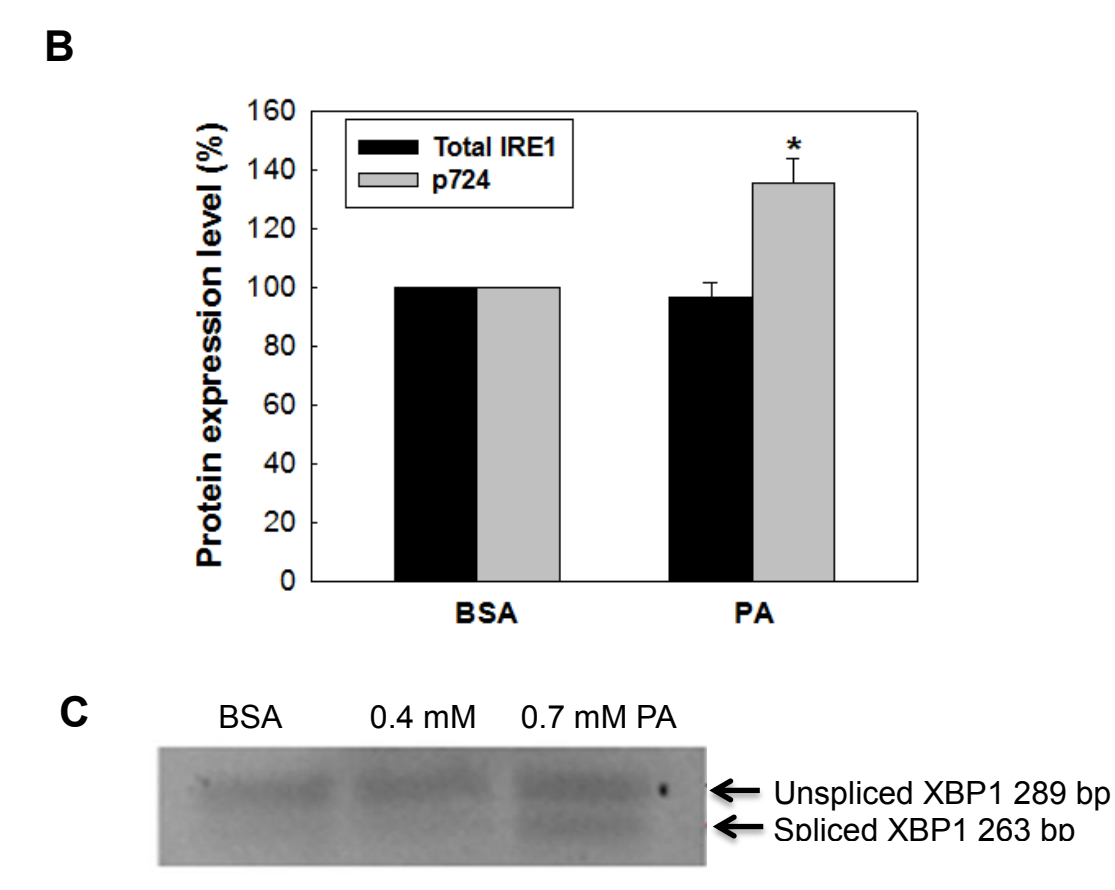


Figure. 5.2. Effect of palmitate on the phosphorylation of IRE1α and XBP1 splicing. HepG2 cells were cultured in regular medium until reaching 90% confluency and then exposed to palmitate for 24 hr. 2% BSA was used as a negative control. After treatment, the cells were harvested for further analyses. (A) Western blot of the IRE1α protein. The levels of both the total and phosphorylated IRE1α proteins were measured using anti-IRE1α and anti-IRE1α (pS724) antibodies. (B) Quantification of the western blotting data. The protein levels from data (A) were quantified using the Molecular Imager ChemiDoc XRS System. (C) Measurement of XBP1 splicing level. The spliced hXBP1 was reverse-transcribed and then resolved in 3 % agarose gel.

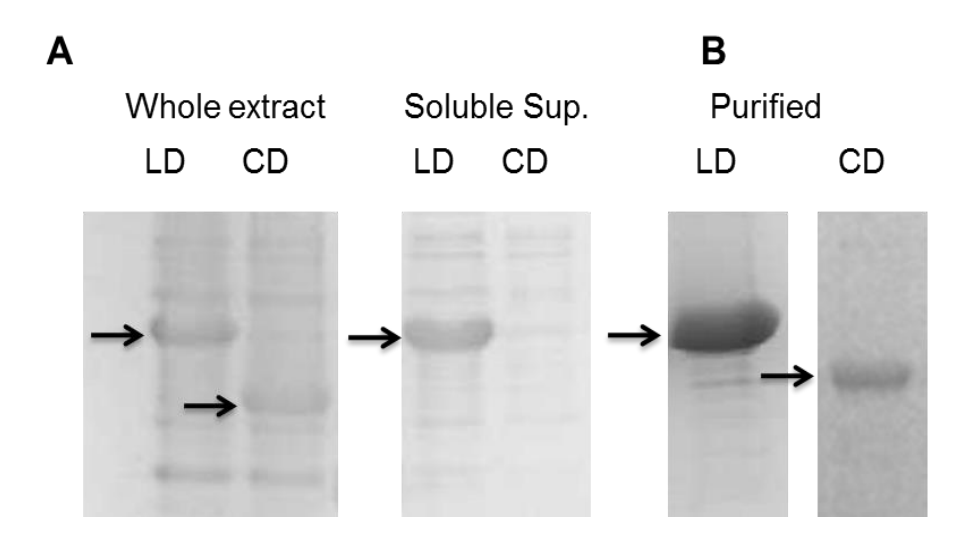


Figure 5.3. Purification of IRE1 α -LD and IRE1 α -CD proteins. (A) Solubility test of IRE1 α -LD and IRE1 α -CD expressed in *E.coli* cells. The proteins obtained from the whole extract and soluble supernatants were marked by arrows on the SDS-PAGE images (B) Purified IRE1 α -LD and IRE α -CD. The recombinant proteins were marked by arrows on the SDS-PAGE images.

IRE1 α proteins. As shown in Figure 5.4, only IRE1 α -CD showed significant increases in FP values. Also, assuming a 1:1 stoichiometry binding, we estimated the K_D value of IRE1 α -CD to be 53.7 nM. While the K_D values of BSA and PKR proteins have 29 nM and 25 nM [149, 150], respectively, FABPs have about 50 to 1 μ M depending on the detection method used [59-61], suggesting that the K_D value of IRE1 α -CD (53.7 nM) is reasonable for the palmitate-binding proteins. Thus, these results show that palmitate is directly associated with the cytosolic domain, but not the luminal domain.

5.3.3. Palmitic Acid binds to the alphaC helix on IRE1a protein

To predict potential palmitate binding sites on the IRE1α-CD protein, our collaborator (Dr. Michael Feig's group at MSU) performed MD simulations. The MD simulation results showed palmitate may bind to Arg611 and Lys716 on the phosphorylated IRE1α-CD (w/o phosphates groups), Arg727 and Arg728 on the unphosphorylated IRE1α-CD, and to Arg864 and Arg887 on the phosphorylated IRE1α-CD (w/ phosphates groups). The locations of all the residues are shown in Figure.5.5. Arg611 is located on the αC helix and Lys716, Arg727, and Arg728 are on the activation loop. In addition, while both Arg864 and Arg887 are on the RNase domain, Arg887 on the α3′ is involved in the RNase catalytic function. Since the predictions (Arg864 and Arg887) were recently completed, we first performed the alanine mutation on four residues (Arg611, Lys716, Arg727, and Arg728) using a site-directed mutation. As shown in Figure 5.6A, while R611A did not alter the phosphorylation statues as compared to the WT, K716A dramatically reduced the phosphorylation level. In addition, since Arg726 and Arg728 are located on the activation loop and close to the phosphorylation sites (Ser724 and Ser726), the phosphorylation level was completely abolished. Since the Arg726 and Arg728 residues were

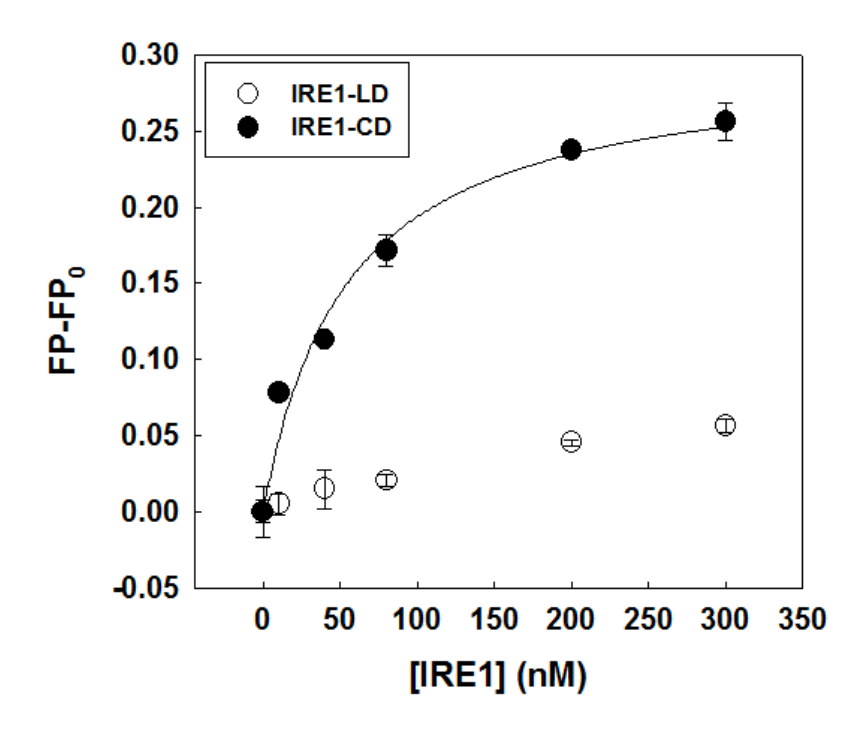


Figure 5.4. Binding affinity of Bodipy-PA to the luminal domain (LD) and cytosolic domain (CD) of the IRE1 α protein. 10 nM of Bodipy-PA was added to PBS buffer with increasing concentrations the proteins. After 5 min of incubation, the fluorescence polarization was measured at 488/515 nm using a spectrofluorometer. The solid lines represent fitting of the data to the quadratic binding equation described in Materials and Methods (see Chapter 3.2). Each error bar represents the mean of triplicates \pm SD.

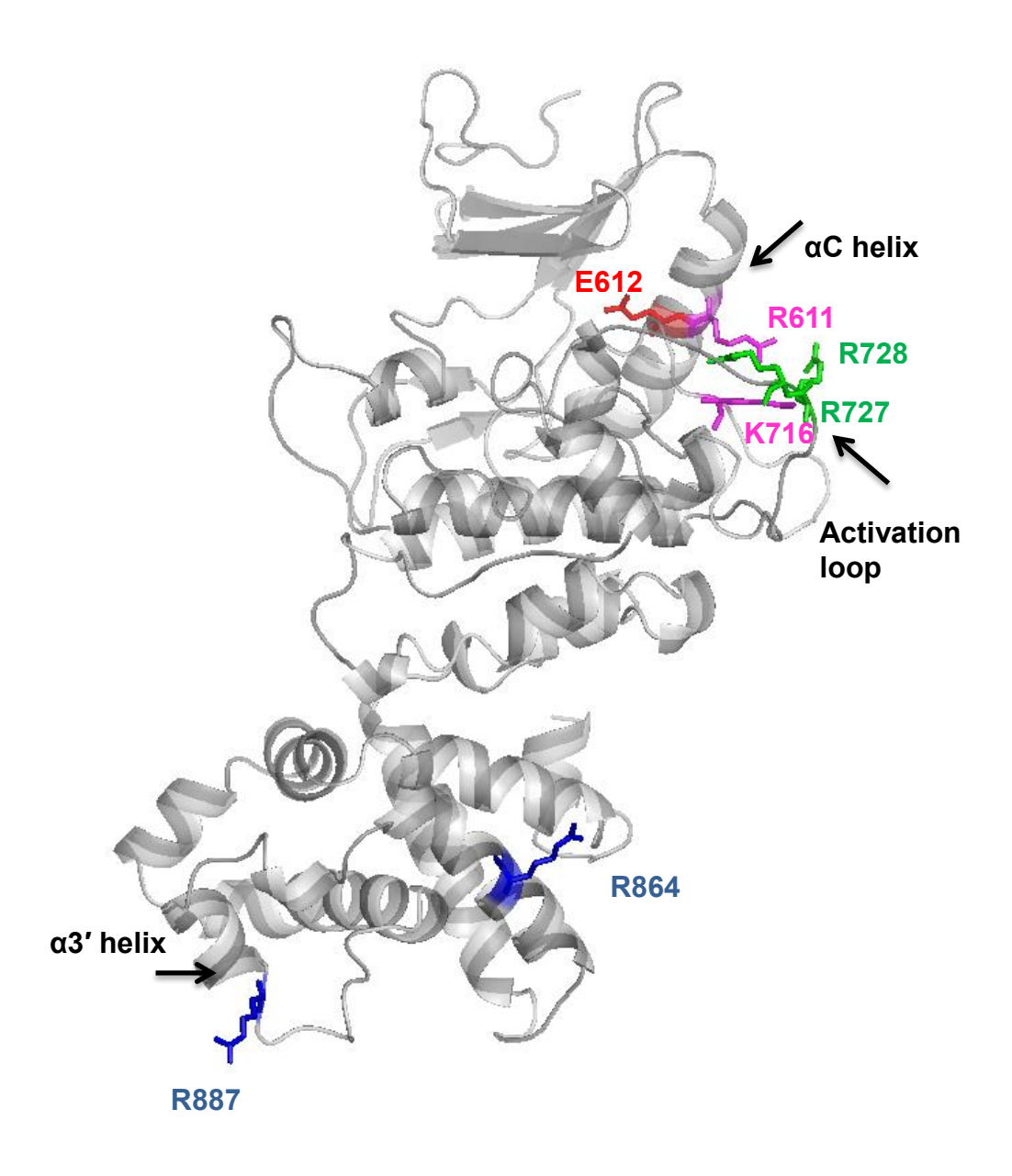


Figure 5.5. Potential residues identified from the MD simulation. R727 and R728 (Green: unphosphorylated IRE1 model) are in the activation loop. Along with E612 (Red), R611 is on the alphaC helix and K716 is localized in the activation loop (Pink: phosphorylated IRE1 α model w/o phosphate group). R864 and R887 are located on the RNase domain (Blue: phosphorylated IRE1 α model w/ phosphate group).

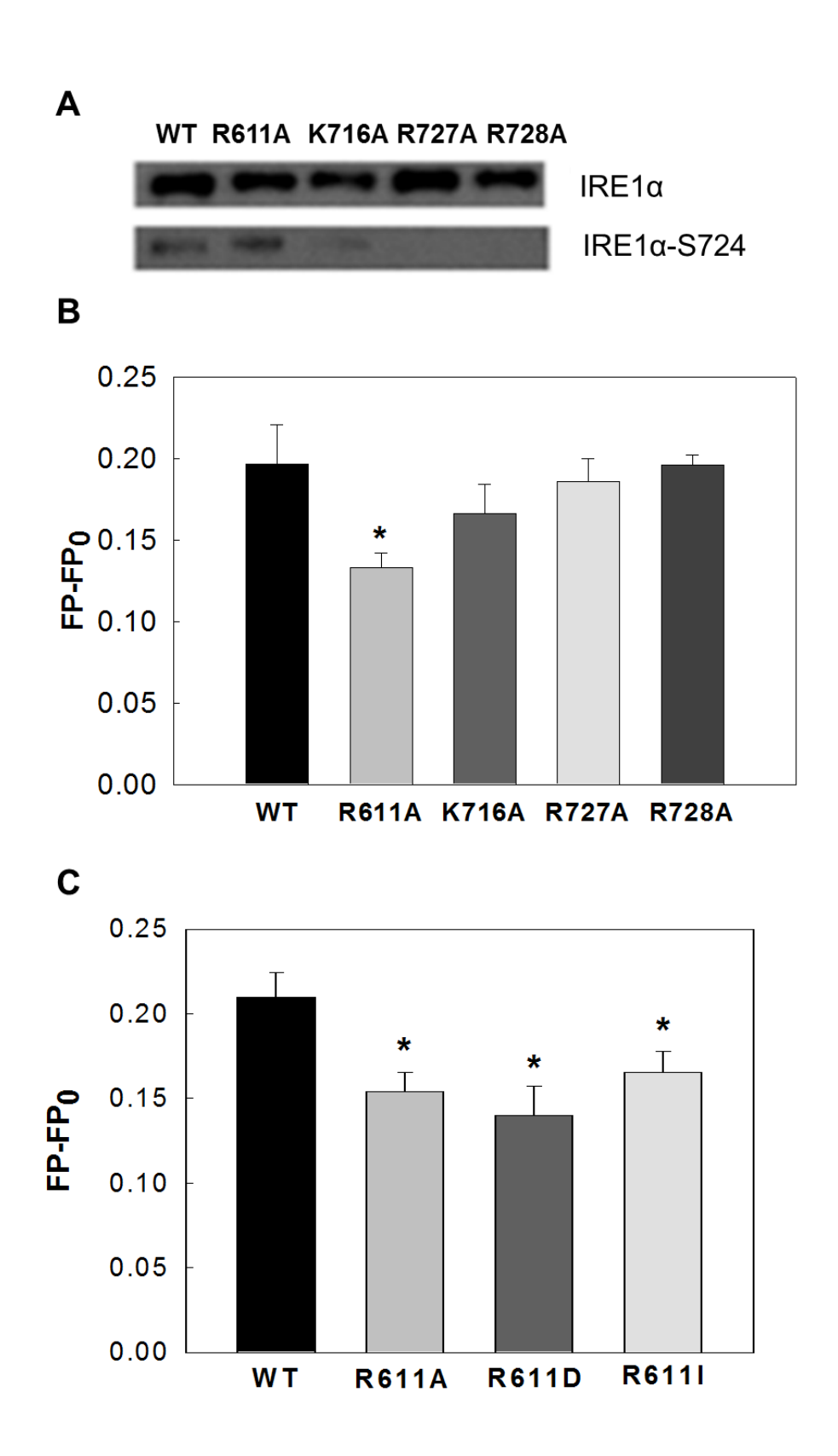
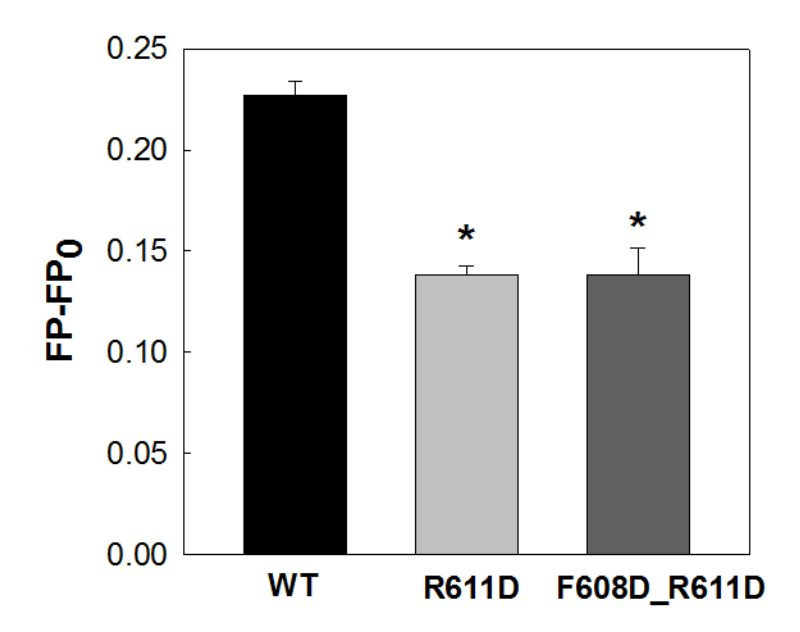


Figure 5.6. Effects of the mutants on the palmitic acid binding to IRE1 α .

Figure 5.6 (cont'd)

D



(A) Western blotting analyses. The total protein and phosphorylation (S724) levels of purified IRE1 α -CD-WT and mutants were measured using antibodies. (B), (C), and (D) Fluorescence polarization measurement of IRE1 α mutants. 10 nM of Bodipy-PA was added to 40 nM of proteins in PBS buffer. After 5 min of incubation, the fluorescence polarization was measured at an excitation wavelength of 488 nm and an emission wavelength of 515 nm using a spectrofluorometer. * (p<0.001) indicates statistically different to wild-type proteins.

predicted from the unphosphorylated model, the purified mutant proteins (R727A and R728A) could be representative model proteins for the unphosphorylated state. The FP-based palmitic acid binding assay shows that only the R611A mutant significantly decreased the palmitate binding affinity as compared to the WT (Figure 5.6B). To evaluate the physical characteristics of the Arg611 residue on the palmitate-binding, we further performed mutations, R611D and R611I. As shown in Figure 5.6C, neither a negative charged (Asp) or hydrophobic residues (Ile) induced a significant difference from the R611A mutation, suggesting that palmitate could bind or interact with another residues surrounding the alphaC helix and a single site mutation likely would not completely inhibit the palmitate's interaction with the protein. We further mutated another residue (Phe608), which is located on the alphaC helix which is supposed to interact with the tail of palmitate molecule (From MD simulation data), on the R611D mutant. The double mutant (R611D_F608D) also did not show a significant difference from the R611D mutant (Figure 5.6D).

Since we confirmed that palmitate localizes in the kinase domain, likely on the alphaC helix, we prepared the IRE1α-KD protein (kinase domain containing 562-833 aa), expressed in the *E. coli* cells. As shown in Figure 5.7, the FP-based palmitate binding assay supports that palmitate interacts with the kinase domain of IRE1α. The estimated binding constant is about 120 nM, which is higher than with IRE1α-CD (53 nM). In other words, the binding affinity of palmitate to IRE1α-KD molecule is lower than to IRE1α-CD, suggesting that there could be another binding site in the cytosolic domain to which palmitate preferentially interacts, possibly the RNase domain. Thus further mutations on Arg864 and Arg887 residues could provide clearer information on the palmitate binding sites.

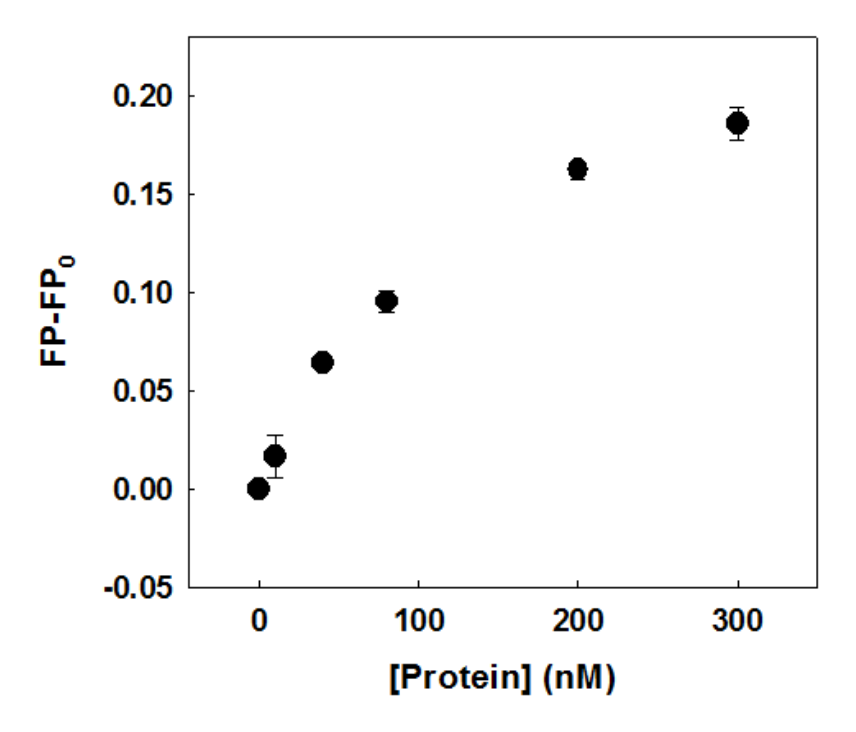
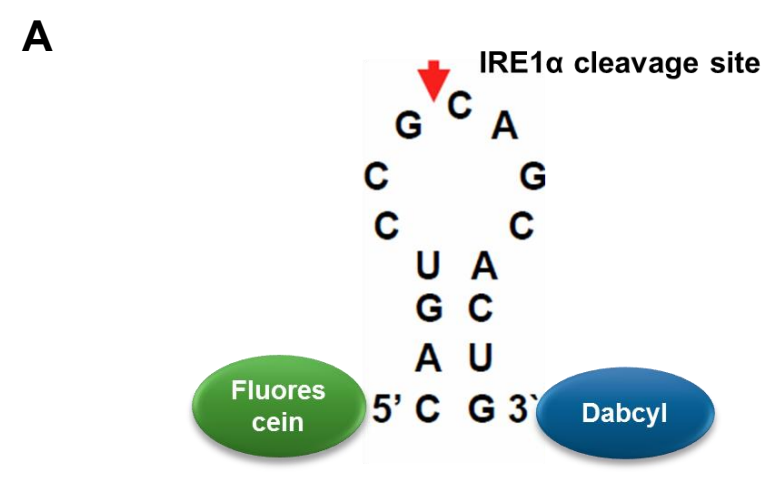


Figure 5.7. Fluorescence polarization measurements of the IRE1α-KD protein. 10 nM of Bodipy-PA was added to PBS buffer with increasing concentrations the proteins. After 5 min of incubation, the fluorescence polarization was measured at 488/515 nm using a spectrofluorometer. Each error bar represents the difference on the FP values between duplicate samples.

5.3.4. IRE1 α -CD protein expressed in the *E. coli* cells retains weak RNase activity Since IRE1 α -CD proteins were extensively phosphorylated in the *E.coli* cells, the protein is primarily in a phosphorylated form (Figure 5.6A), potentially activating the RNase. To further confirm whether the phosphorylated IRE α -CD is able to catalyze the XBP1 RNA substrate, we modified an *in-vitro* XBP1 cleavage assay (see Figure 5.8A) [236]. The mini-XBP-1 RNA substrate was labeled with fluorescein at 5' end and dabcyl at 3' end. Cleavage of the substrate by IRE1 α -CD releases the dabcyl-dependent quenching of fluorescein, enabling the green fluorescence. To eliminate chances of contaminations from other nucleases, we used nuclease-free water for the assay and confirmed that BSA (as a negative control protein) does not have any RNase activity (Figure 5.8B). We observed an IRE1 α -CD concentration-dependent cleavage of the labeled substrate suggesting that the assay is suitable for quantification of RNase activity (Figure 5.8B).

Although the fluorescence intensity-based XBP1 cleavage assay is useful for confirming whether IRE1 α -CD induces cleavage of the XBP1 RNA substrate, most of the prior studies used urea-PAGE gel to visualize the uncleaved and cleaved forms of the RNA substrate [19, 237]. Therefore, we performed the *in-vitro* cleavage assay using the mini-XBP-1 RNA substrate (Figure 5.8A), followed by urea-PAGE analysis. As shown in Figure 5.9, the Mg²⁺ ion is necessary for the RNase reaction. In addition, the purified IRE1 α -CD from *E.coli* cells cleave the XBP1 RNA substrate very weakly while other studies that obtained the purified IRE1 α -CD from insect cells showed cleavage of 40 – 90 % of the XBP1 RNA substrate [19, 237]. Nevertheless we confirmed that the IRE1 α -CD protein expressed in the *E. coli* cells retains a weak RNase activity. Thus further experiments using insect cells could help to increase the protein activity.



Mini-XBP1 stem-loop RNA substrate

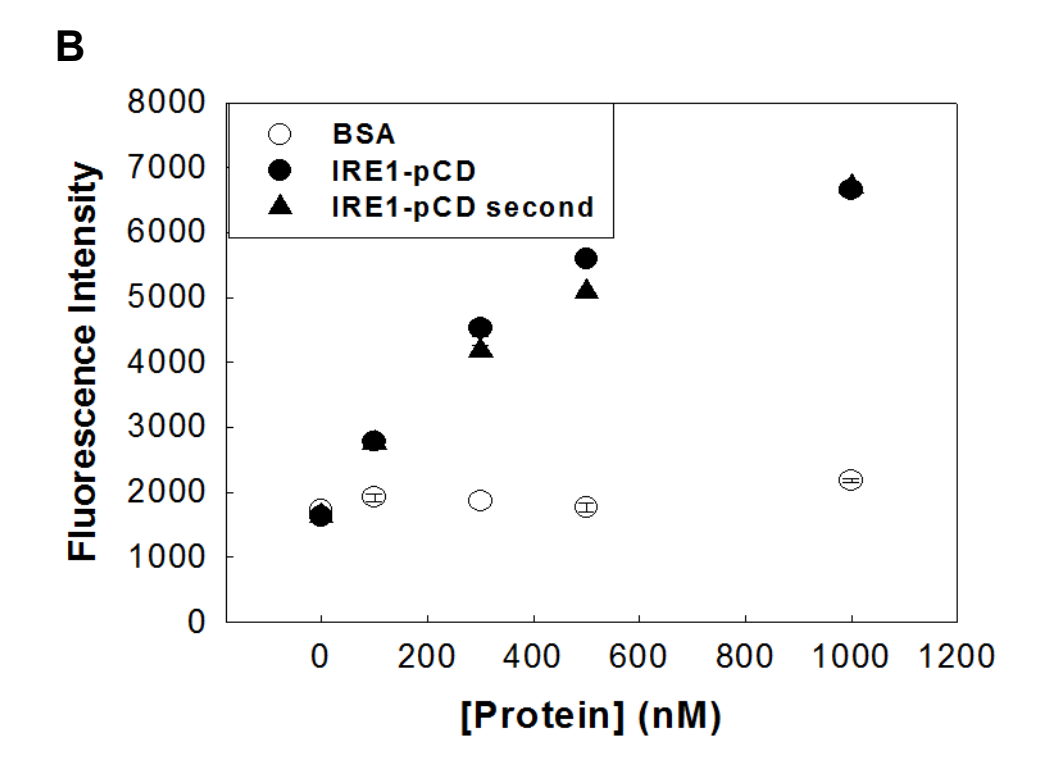


Figure 5.8. Fluorescence intensity-based XBP1 cleavage assay. (A) Schematic of the mini-XBP-1 stem-loop used as the IRE1 α -CD substrate. The Fluorescein fluorophore was linked to the 5 end and Dabcyl was linked to the 3 end. The red arrow represents the cleavage site. (B) Fluorescence intensity measurements of the mini-XBP1 substrate cleavage. In the presence of 100 nM RNA substrate, proteins (BSA or IRE1 α -CD) were added, followed by the measurement of fluorescence intensity at 488/515 nm.

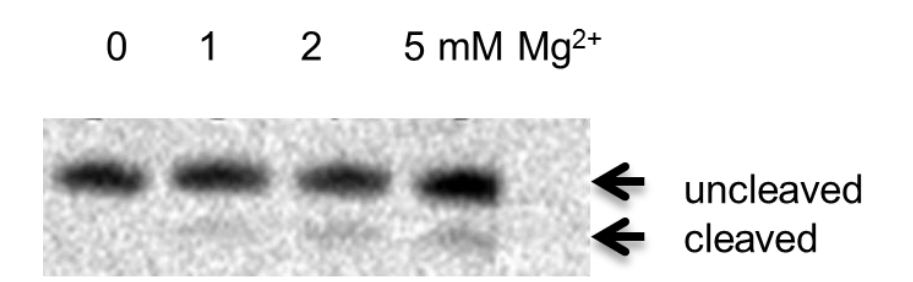


Figure 5.9. Urea-PAGE of XBP1 mini-substrate cleavage by IRE1 α -CD. In-vitro XBP1 cleavage assay was performed at the various concentrations of Mg²⁺ ions. Cleavage by IRE1 α -CD generates a fluorescent species with higher gel mobility.

5.4. Discussion and Future works.

Over the years, several indirect mechanisms by which palmitate activates the UPR sensor proteins have been suggested. Calcium depletion in the ER or disruption of the ER-to-Golgi trafficking were thought to increase the activity of the UPR sensor proteins [50, 51, 54]. Paradoxically, a recent study showed that palmitate is more directly involved in the IRE1 activation process [55]. A mutant lacking the luminal domain of IRE1 α responded to palmitate similar to the WT protein. In other words, palmitate is able to modulate the activity of the mutant IRE1 α protein, suggesting the luminal domain is not essential for the palmitate-induced IRE1 α activation. Interestingly, we found that palmitate does not interact with the luminal domain of IRE1 α , which is consistent with this previous work [55], but directly binds to the cytosolic domain (Figure 5.4). Thus these observations indicate that IRE1 α can be activated through luminal-independent signals in the palmitate-treated cells.

The α C-helix has been shown to modulate the oligomeric state and the RNase activity of yeast phosphorylated Ire1 [238]. In the active form of the IRE1 proteins, the Glu612 residue on the α C-helix positions into the ATP-binding site, stabilizing the interaction with the nucleotide. The inactive (unphosphorylated) form changes the α C-helix to an "out" position, which creates a steric clash between the α C-helix and a partnering Ire1 monomer [239]. Our experiments showed that palmitate interacts with the Arg611 residue. Although more experiments are required, we believe that palmitate-binding on the Arg611 residue may stabilize the α C-helix, maintaining a favorable active conformation for the RNase activity.

To gain more detail mechanisms of palmitate on the IRE1 α protein, more mutant proteins on the RNase domain need to be evaluated. In addition, since we found that the IRE1 α protein

produced from $E.\ coli$ cells have much lower activity than ones from insect cells (Figure 5.9), the next step would be to express the protein in insect cells. As shown in Figure 5.10, we have successfully expressed the IRE1 α -CD protein in insect cells. It is apparent that more mutation studies on the RNase domain and enzyme assays are needed to elucidate the roles of palmitate on the IRE1 α protein to obtain a clear understanding of their interactions.

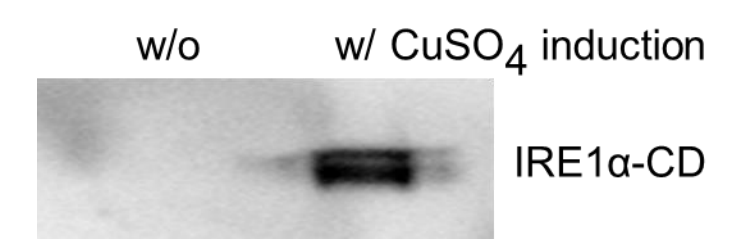


Figure 5.10. Protein expression of IRE1 α -CD in insect cells. Drosophila Schneider 2 (S2) Cells were transfected with both pMT-V5/HisB- IRE1 α -CD and pCOPuro plasmids to generate stable cell line. 0.5 mM CuSO₄ (an inducer for pMT (metallothionein) promoter) was added in the cells to induce the protein expression. The protein expression level was measured using anti-IRE1 α antibody. In the absence of CuSO₄, there was no protein observed in the western blotting image. In contrast, CuSO₄ significantly increased the IRE1 α -CD expression in the stable cell line.

CHAPTER 6. CONCLUSIONS AND FUTURE DIRECTIONS

Palmitic acid mostly interacts with carrier proteins such as serum albumin proteins and FABPs, which promote fatty acid uptake and transport to sites for metabolisms [58]. In our study, we showed that palmitate binds to several kinase proteins, e.g. PKR and IRE1 α , near the α C helix. Palmitate-binding on the α C helix significantly reduces PKR autophosphorylation, suggesting palmitate acts as an allosteric inhibitor of the PKR protein. In addition, we showed that palmitate interacts with the kinase domain of IRE1 α , however questions remain. 1) Does palmitate regulate the phosphorylation of the IRE1 α protein? 2) Does palmitate interact with the RNase domain of IRE1 α , subsequently regulating the RNase activity? Nevertheless, this study is the first to suggest a novel functional role of palmitate with kinase proteins, highlighting a new research area.

6.1. A potential for palmitate to interact with the PERK protein

In addition to the IRE1α, PERK, as one of the eIF2α kinases, shares a similar functional role as the PKR protein. As shown in Figure 6.1, our study showed that palmitate increases the phosphorylation level of PERK (at Ser 713) in HepG2 cells [40]. Since we found that palmitate interacts with PKR-R307 residue on the αC helix, we hypothesize that palmitate could also bind to the PERK protein due to the structural similarity between the PERK and PKR proteins. Since a co-crystalized structure of human PERK with an ATP competitive inhibitor was recently resolved [240], we further compared the human PERK structure (PDB: 4G31) with the unphosphorylated PKR homology model built from the unphosphorylated GCN2 protein

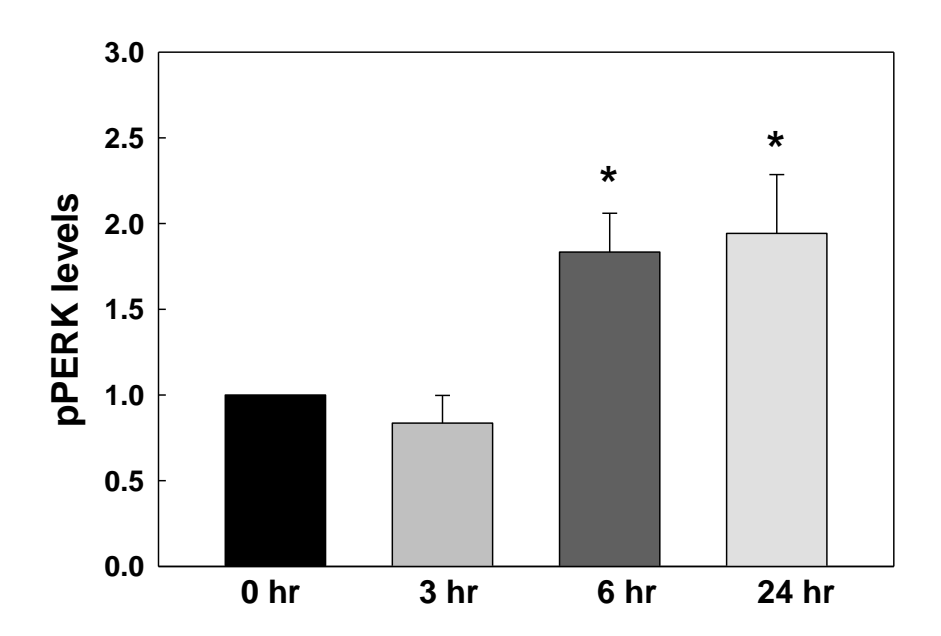


Figure. 6.1. Effects of palmitate on the PERK activity. HepG2 cells were treated with 2 % BSA (as a negative control) and 700 μ M Palmitate. After 3, 6, 24 hrs, the cell extracts were collected and subjected to immunoblot analysis for total PERK (both phosphorylated and non-phosphorylated proteins), p-PERK (phosphorylated proteins). Actin served as a loading control. The phosphorylation levels of PERK were quantified and normalized to the total protein levels of PERK, respectively. The fold changes on the phosphorylation level were calculated at each time point using the following equation: (phosphorylation level)palmitate/(phosphorylation level)BSA. Data represent the mean and standard deviation of three independent experiments: *p < 0.01 vs. the control at each time point.

structure (PDB: 1ZY4). The major difference found in the structure of the N-lobe of PERK as compared with that of PKR is that PERK has a longer a helix than PKR (Figure 6.2). Nonetheless, the location of R307 on PKR is conserved on the PERK protein (R637) and the carboxyl group of the palmitate molecule is located between R307 on PKR and R637 on PERK (see Figure 6.2), suggesting that palmitate could potentially interact with R637 on the human PERK protein. In the C-lobe, four short alpha helices were observed on the PERK structure which may results from the differences in the sequence length between the two proteins, i.e., the PERK kinase domain (593-1077 aa) is longer than the PKR kinase domain (267-538 aa). Since the homology model of PKR is adapted from the GCN2 protein, at this point, we are not able to obtain clear evidence on how the PERK structure differs from PKR. However, in future, it would be useful to determine if palmitate regulates the phosphorylation level of the PERK kinase domain using an *in-vitro* kinase assay. Additionally, PERK-R637A mutant can be prepared to compare the palmitate binding affinity and kinase activity with that of PERK-WT. These experiments could provide information on how palmitate interacts differently on the ER transmembrane kinase (PERK) vs. the cytosolic kinase (PKR) protein.

6.2. Myristoylation of the kinase proteins

Using PDB (http://www.rcsb.org/pdb/home/home.do) database, we searched for any fatty acids that can be ligands for kinases in addition to the UPR kinase proteins. Surprisingly, two kinases, PKA Serine/Theorine and c-Abl Tyrosine Kinase, interact with myristic acid (a C14-saturated fatty acid) in their kinase domains [241-243]. The kinase structures of the two proteins are compared in Figure 6.3. PKA has an additional alpha helix domain (Helix A) as compared

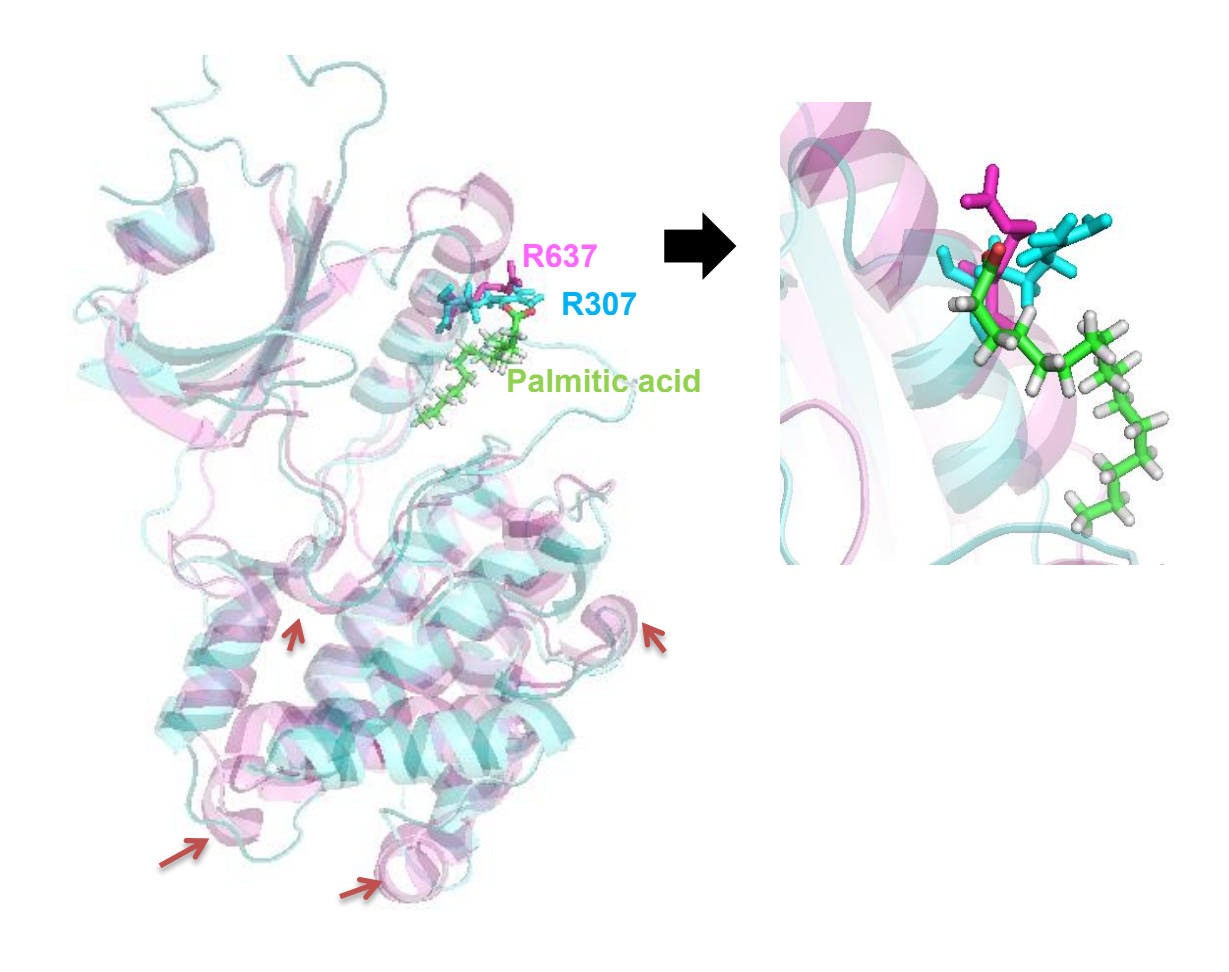


Figure. 6.2. Superimposition of the kinase domains of PERK and PKR. Unphosphorylated PERK (pink, PDB: 4G31) and unphosphorylated PKR (cyan, homology modeling based on GCN2 (PDB ID: 1ZY4)) were compared. Along with the palmitate molecule (green), R307 (PKR) and R637 (PERK) residues were shown in the figure. PERK has more short helices than PKR (marked by arrows). The closer view on the αC helix is shown in the left panel.

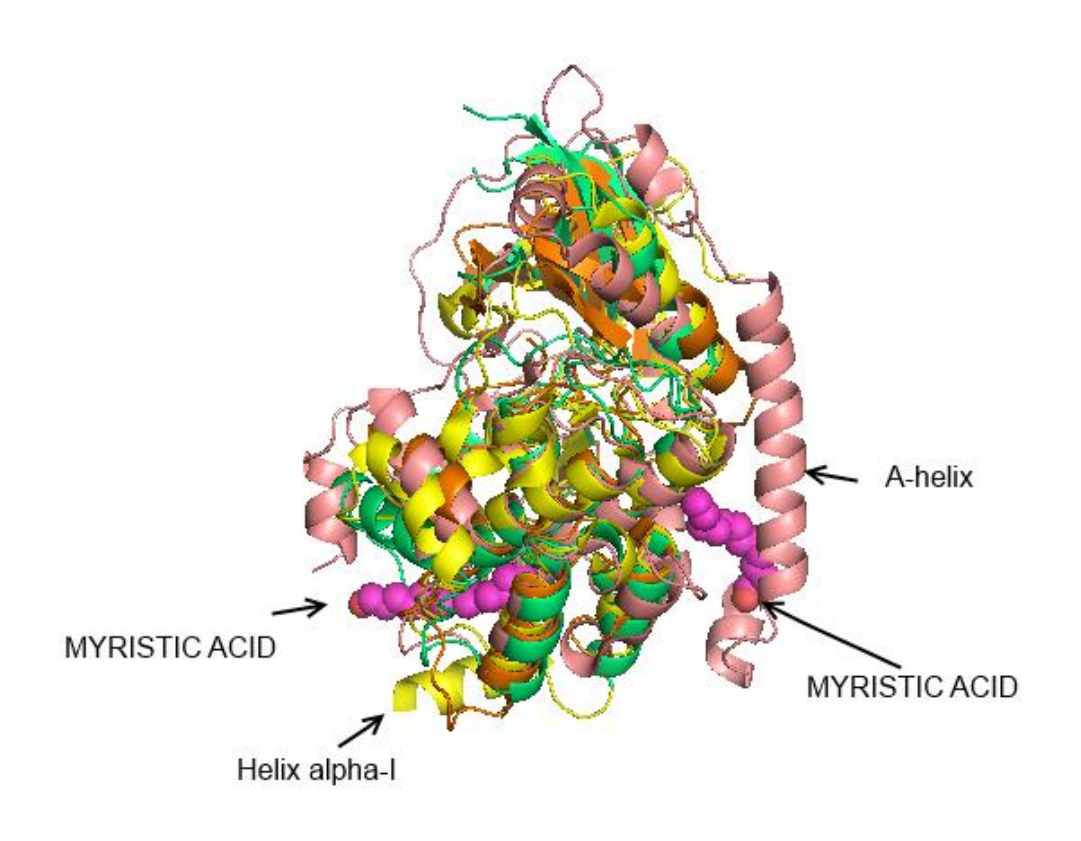


Figure. 6.3. Superimposition of the kinase domains of four proteins. PKR (green, PDB: 2A19), IRE1α (orange, PDB: 3P23), PKA (light pink, PDB: 1CTP), c-Abl (yellow, 2FO0) were shown in the figure. The myristic acid is in balls and in pink color.

with the other three kinases (PKR, IRE1α, c-Abl) and the helix A provides a myristate-binding cavity in the kinase domain. The c-Abl kinase has an additional short helix (αI-helix) at the bottom of its kinase domain, which provides a cap for myristate binding on the protein. Due to the high structural similarity of c-Abl with PKR and IRE1α, we further checked whether palmitate could localize in the same binding pocket (around the αI-helix) in the PKR and IRE1α proteins (see Figure 6.3). The MD simulation data showed that none of palmitate molecules from the simulated models (unphosphorylated and phosphorylated PKR and IRE1α) are located in the same binding pocket as myristrate. The myristate binding on PKA and c-Abl is a non-reversible covalent bond through myristoylation, which is a covalent attachment of myristate to the N-terminal glycine of the kinases. Generally myristoylation helps proteins to translocate to the membrane for proper function of the proteins, however myristoylation of the PKA and c-Abl tyrosine kinases regulates their kinase activities through local conformational changes [243, 244].

6.3. Palmitoylation of the kinase proteins

Due to the structural similarity between palmitate and myristate, it raises the question; could palmitate covalently bind to these kinase proteins? In other words, are there any kinases which could be palmitoylated? Along with myristoylation, some of the Src family kinases (SFKs), a membrane bound tyrosine kinase family, are known to be palmitoylated through a covalent attachment on the cysteine residue of the proteins [245]. Furthermore, a proteomic analysis recently identified several palmitoylated kinases including Ser/Thr kinases AMPKα, integrin-linked kinase (ILK1), MAPK1 (ERK2), and PKA (regulatory subunit) [246]. Thus it questions whether the potential palmitate-binding sites on either PKR or IRE1α, containing a

cysteine residue, could be involved in a palmitoylation reaction. Using the software (CSS-Palm: http://csspalm.biocuckoo.org/), we first predicted potential palmitoylation sites on both PKR and IRE1 α . The prediction results showed that C186 (in the dsRNA binding domain) and C551 (the last C-terminal residue in the kinase domain) on the PKR protein could be palmitoylated. Since we already confirmed that palmitate does not bind to the dsRNA binding domain, palmitate's binding on the PKR protein is unlikely due to palmitoylation. In addition, CSS-Palm predicted four residues on the IRE1 α protein; C538 is located in a linker and the other three residues (C605, C790 C794) are in the kinase domain. Of these only the C605 residue in the α C helix shares a palmitic acid binding site with the R611 residue. Since the palmitoylation sites on the kinase proteins are typically located in another functional group rather than the kinase domain or are far from the active site [245], the binding of palmitate to the α C helix is not likely due to the palmitoylation reaction.

6.4. Human IRE1 α vs. yeast Ire1

Human IRE1 α is relatively less studied than yeast Ire1. It is known that there are different sensing mechanisms between human IRE1 α and yeast Ire1 luminal domains (reviewed in [222, 223]). In addition to the luminal domain, the cytosolic domain of human IRE1 α has different structural features from the yeast Ire1 (mostly on the kinase domain) [19]. Two helical segments (α D' and α E') observed in the yeast Ire1 structure (PDB ID: 3FVB) do not occur in human IRE1 α . In addition, the α C helix of the human IRE1 α is partially unwound and shorter than the one on the yeast Ire1 protein. Furthermore, the transmembrane domain between the human IRE1 α and yeast Ire1 does not have homologues sequences (Figure 4.8). Thus gaining more functional and

structural information on the human IRE1 α would help our understanding of mammalian UPR activation.

6.5. Roles of palmitate on the transmembrane domain of IRE1a

In addition, a recent study claimed that lipid saturation in the transmembrane domain is critical for IRE1 α activation [55]. Our lab previously confirmed that palmitate changes the physical characteristic of the lipid bilayers, by reducing the membrane fluidity [247]. As discussed in reference [55], α -helical transmembrane peptides preferentially localize in the liquid phase and the higher gel phase (lower fluidity) induced by palmitate would promote diffusion of the peptides into the liquid phase (a smaller area), thereby favoring dimerization [221]. Since there is no evidence to date on how palmitate increases the TM dimerization in the membrane, it would be useful to perform MD simulations with the TM peptides and palmitate, and the lipid bilayer and evaluate the effects of palmitate on the TM dimerization through biophysical experiments. Since we found that the W457 residue is critical for TM dimerization, the computational and experimental data could help determine whether palmitate directly influences the aromatic interactions formed by W457 or whether palmitate indirectly promotes the TM dimerization by altering the physical properties of the phospholipid membrane.

6.6. FABPs-mediated transport mechanisms

Due to the low solubility of palmitate in aqueous solution, palmitate mostly interacts with FABPs in the cytosol. Under normal physiological condition, cytosolic FABPs can accommodate

up to 150~300 mM fatty acids, helping long-chain fatty acids to overcome their low aqueous concentration [248]. A key question that remains, however, is how palmitate solubilizes and transports through an essentially aqueous cytosol in order to bind the target kinase proteins, PKR and IRE1 α . Interestingly, the liver FABP, known to interact with palmitate, directly interacts with PPAR α , and is involved in nucleo-cytoplasmic shuttling of lipids [249]. Thus one could determine whether PKR and IRE1 α proteins are involved in protein-protein interactions with FABPs. Furthermore, the molecular mechanism by which FABPs transport fatty acids to other proteins is not well established, thus the possibility of direct protein-protein interactions does not preclude the involvement of other delivery mechanisms.

6.7. Future works and conclusions

The binding affinities of PKR and IRE1α (several tens of nanomolar) are comparable with most palmitic acid binding proteins and higher than some of the FABPs (several tens of nano molar to hundred nanomolar). Although the direct effects of palmitate on those kinases in cells are currently under investigation, it would be worthwhile to obtain an x-ray crystal structure of palmitate and either PKR or IRE1α. Since the kinase domain is highly conserved among many kinase proteins, the detail binding mode of palmitate on those kinases could provide conserved palmitate-binding sites, reinforcing a functional role of palmitate on many kinase proteins. Furthermore, more mechanistic studies could identify the critical sites that interact with palmitate on the kinase proteins. Through mutation studies in cells, one could test whether palmitate's binding on the kinase proteins further regulates their enzymatic activities and downstream signaling events. Especially for IRE1α, mutation on either the transmembrane or cytosolic

domains could help to address questions of whether palmitate synergically induces IRE1 activity through both domains or whether one domain is more critical than the other in regulating the palmitate-mediated activation.

In summary, although many open questions remain, the current studies suggested a novel functional role of palmitic acid on kinase proteins. Further biophysical and computational studies could provide more insights on the molecular mechanisms by which palmitate regulates the enzymatic activity of kinase proteins. A better understanding of the molecular mechanisms could help to address the causes of ER-stress associated diseases as well as potential implications on the efficacy of current drug therapies that target kinases.

REFERENCES

REFERENCES

- 1. Cohen JC, Horton JD, Hobbs HH: Human fatty liver disease: old questions and new insights. *Science* 2011, 332(6037):1519-1523.
- 2. Musso G, Gambino R, Cassader M: Non-alcoholic fatty liver disease from pathogenesis to management: an update. *Obesity Reviews* 2010, 11(6):430-445.
- 3. Vernon G, Baranova A, Younossi ZM: Systematic review: the epidemiology and natural history of non-alcoholic fatty liver disease and non-alcoholic steatohepatitis in adults. *Alimentary Pharmacology & Therapeutics* 2011, 34(3):274-285.
- 4. Boden G: Obesity, insulin resistance and free fatty acids. *Curr Opin Endocrinol Diabetes Obes* 2011, 18(2):139-143.
- 5. Takamura T, Misu H, Ota T, Kaneko S: Fatty liver as a consequence and cause of insulin resistance: lessons from type 2 diabetic liver. *Endocr J* 2012, 59(9):745-763.
- 6. Bhatia LS, Curzen NP, Calder PC, Byrne CD: Non-alcoholic fatty liver disease: a new and important cardiovascular risk factor? *Eur Heart J* 2012, 33(10):1190-1200.
- 7. Listenberger LL, Schaffer JE: Mechanisms of lipoapoptosis: implications for human heart disease. *Trends Cardiovasc Med* 2002, 12(3):134-138.
- 8. Reddy JK, Rao MS: Lipid metabolism and liver inflammation. II. Fatty liver disease and fatty acid oxidation. *Am J Physiol Gastrointest Liver Physiol* 2006, 290(5):G852-858.
- 9. Feldstein AE, Canbay A, Angulo P, Taniai M, Burgart LJ, Lindor KD, Gores GJ: Hepatocyte apoptosis and Fas expression are prominent features of human nonalcoholic steatohepatitis. *Gastroenterology* 2003, 125(2):437-443.
- 10. de Almeida IT, Cortez-Pinto H, Fidalgo G, Rodrigues D, Camilo ME: Plasma total and free fatty acids composition in human non-alcoholic steatohepatitis. *Clin Nutr* 2002, 21(3):219-223.
- 11. Borradaile NM, Han X, Harp JD, Gale SE, Ory DS, Schaffer JE: Disruption of endoplasmic reticulum structure and integrity in lipotoxic cell death. *Journal of Lipid Research* 2006, 47(12):2726-2737.
- 12. Malhi H, Kaufman RJ: Endoplasmic reticulum stress in liver disease. *J Hepatol* 2011, 54(4):795-809.
- 13. Braakman I, Bulleid NJ: Protein folding and modification in the mammalian endoplasmic reticulum. *Annu Rev Biochem* 2011, 80:71-99.

- 14. Kaufman RJ: Stress signaling from the lumen of the endoplasmic reticulum: coordination of gene transcriptional and translational controls (vol 13, pg 1211, 1999). *Genes & Development* 1999, 13(14):1898-1898.
- 15. Groenendyk J, Michalak M: Endoplasmic reticulum quality control and apoptosis. *Acta Biochim Pol* 2005, 52(2):381-395.
- 16. Wang S, Kaufman RJ: The impact of the unfolded protein response on human disease. *J Cell Biol* 2012, 197(7):857-867.
- 17. Tirasophon W, Welihinda AA, Kaufman RJ: A stress response pathway from the endoplasmic reticulum to the nucleus requires a novel bifunctional protein kinase/endoribonuclease (Ire1p) in mammalian cells. *Genes Dev* 1998, 12(12):1812-1824.
- 18. Oikawa D, Kimata Y, Kohno K, Iwawaki T: Activation of mammalian IRE1alpha upon ER stress depends on dissociation of BiP rather than on direct interaction with unfolded proteins. *Exp Cell Res* 2009, 315(15):2496-2504.
- 19. Ali MMU, Bagratuni T, Davenport EL, Nowak PR, Silva-Santisteban MC, Hardcastle A, McAndrews C, Rowlands MG, Morgan GJ, Aherne W *et al*: Structure of the Ire1 autophosphorylation complex and implications for the unfolded protein response. *Embo Journal* 2011, 30(5):894-905.
- 20. Yoshida H, Matsui T, Yamamoto A, Okada T, Mori K: XBP1 mRNA is induced by ATF6 and spliced by IRE1 in response to ER stress to produce a highly active transcription factor. *Cell* 2001, 107(7):881-891.
- 21. Lee AH, Iwakoshi NN, Glimcher LH: XBP-1 regulates a subset of endoplasmic reticulum resident chaperone genes in the unfolded protein response. *Molecular and Cellular Biology* 2003, 23(21):7448-7459.
- 22. Urano F, Wang XZ, Bertolotti A, Zhang YH, Chung P, Harding HP, Ron D: Coupling of stress in the ER to activation of JNK protein kinases by transmembrane protein kinase IRE1. *Science* 2000, 287(5453):664-666.
- 23. Zhou J, Liu CY, Back SH, Clark RL, Peisach D, Xu Z, Kaufman RJ: The crystal structure of human IRE1 luminal domain reveals a conserved dimerization interface required for activation of the unfolded protein response. *Proceedings of the National Academy of Sciences of the United States of America* 2006, 103(39):14343-14348.
- 24. Harding HP, Zhang YH, Ron D: Protein translation and folding are coupled by an endoplasmic-reticulum-resident kinase (vol 397, pg 271, 1999). *Nature* 1999, 398(6722):90-90.
- 25. Karpinski BA, Morle GD, Huggenvik J, Uhler MD, Leiden JM: Molecular cloning of human CREB-2: an ATF/CREB transcription factor that can negatively regulate

- transcription from the cAMP response element. *Proc Natl Acad Sci U S A* 1992, 89(11):4820-4824.
- 26. Harding HP, Novoa I, Zhang Y, Zeng H, Wek R, Schapira M, Ron D: Regulated translation initiation controls stress-induced gene expression in mammalian cells. *Mol Cell* 2000, 6(5):1099-1108.
- 27. Scheuner D, Song B, McEwen E, Liu C, Laybutt R, Gillespie P, Saunders T, Bonner-Weir S, Kaufman RJ: Translational control is required for the unfolded protein response and in vivo glucose homeostasis. *Mol Cell* 2001, 7(6):1165-1176.
- 28. Novoa I, Zeng HQ, Harding HP, Ron D: Feedback inhibition of the unfolded protein response by GADD34-mediated dephosphorylation of eIF2 alpha. *Journal of Cell Biology* 2001, 153(5):1011-1021.
- 29. McCullough KD, Martindale JL, Klotz LO, Aw TY, Holbrook NJ: Gadd153 sensitizes cells to endoplasmic reticulum stress by down-regulating Bc12 and perturbing the cellular redox state. *Molecular and Cellular Biology* 2001, 21(4):1249-1259.
- 30. Kilberg MS, Shan J, Su N: ATF4-dependent transcription mediates signaling of amino acid limitation. *Trends in Endocrinology and Metabolism* 2009, 20(9):436-443.
- 31. Cazanave SC, Elmi NA, Akazawa Y, Bronk SF, Mott JL, Gores GJ: CHOP and AP-1 cooperatively mediate PUMA expression during lipoapoptosis. *American Journal of Physiology-Gastrointestinal and Liver Physiology* 2010, 299(1):G236-G243.
- 32. Haze K, Okada T, Yoshida H, Yanagi H, Yura T, Negishi M, Mori K: Identification of the G13 (cAMP-response-element-binding protein-related protein) gene product related to activating transcription factor 6 as a transcriptional activator of the mammalian unfolded protein response. *Biochem J* 2001, 355(Pt 1):19-28.
- 33. Haze K, Yoshida H, Yanagi H, Yura T, Mori K: Mammalian transcription factor ATF6 is synthesized as a transmembrane protein and activated by proteolysis in response to endoplasmic reticulum stress. *Mol Biol Cell* 1999, 10(11):3787-3799.
- 34. Yoshida H, Matsui T, Yamamoto A, Okada T, Mori K: XBP1 mRNA is induced by ATF6 and spliced by IRE1 in response to ER stress to produce a highly active transcription factor. *Cell* 2001, 107(7):881-891.
- 35. Wei YR, Wang D, Topczewski F, Pagliassotti MJ: Saturated fatty acids induce endoplasmic reticulum stress and apoptosis independently of ceramide in liver cells. *American Journal of Physiology-Endocrinology and Metabolism* 2006, 291(2):E275-E281.

- 36. Wei Y, Wang D, Pagliassotti MJ: Saturated fatty acid-mediated endoplasmic reticulum stress and apoptosis are augmented by trans-10, cis-12-conjugated linoleic acid in liver cells. *Molecular and Cellular Biochemistry* 2007, 303(1-2):105-113.
- 37. Ibrahim SH, Akazawa Y, Cazanave SC, Bronk SF, Elmi NA, Werneburg NW, Billadeau DD, Gores GJ: Glycogen synthase kinase-3 (GSK-3) inhibition attenuates hepatocyte lipoapoptosis. *Journal of Hepatology* 2011, 54(4):765-772.
- 38. Akazawa Y, Cazanave S, Mott JL, Elmi N, Bronk SF, Kohno S, Charlton MR, Gores GJ: Palmitoleate attenuates palmitate-induced Bim and PUMA up-regulation and hepatocyte lipoapoptosis. *Journal of Hepatology* 2010, 52(4):586-593.
- 39. Jung TW, Lee YJ, Lee MW, Kim SM: Full-length adiponectin protects hepatocytes from palmitate-induced apoptosis via inhibition of c-Jun NH2 terminal kinase. *Febs Journal* 2009, 276(8):2278-2284.
- 40. Cho H, Wu M, Zhang L, Thompson R, Nath A, Chan C: Signaling dynamics of palmitate-induced ER stress responses mediated by ATF4 in HepG2 cells. *BMC Syst Biol* 2013, 7:9.
- 41. Cao J, Dai DL, Yao L, Yu HH, Ning B, Zhang Q, Chen J, Cheng WH, Shen W, Yang ZX: Saturated fatty acid induction of endoplasmic reticulum stress and apoptosis in human liver cells via the PERK/ATF4/CHOP signaling pathway. *Mol Cell Biochem* 2012, 364(1-2):115-129.
- 42. Cnop M, Ladriere L, Igoillo-Esteve M, Moura RF, Cunha DA: Causes and cures for endoplasmic reticulum stress in lipotoxic beta-cell dysfunction. *Diabetes Obesity & Metabolism* 2010, 12:76-82.
- 43. Lu J, Wang Q, Huang L, Dong H, Lin L, Lin N, Zheng F, Tan J: Palmitate causes endoplasmic reticulum stress and apoptosis in human mesenchymal stem cells: prevention by AMPK activator. *Endocrinology* 2012, 153(11):5275-5284.
- 44. Leroy C, Tricot S, Lacour B, Grynberg A: Protective effect of eicosapentaenoic acid on palmitate-induced apoptosis in neonatal cardiomyocytes. *Biochim Biophys Acta* 2008, 1781(11-12):685-693.
- 45. Jiang H, Liang C, Liu X, Jiang Q, He Z, Wu J, Pan X, Ren Y, Fan M, Li M *et al*: Palmitic acid promotes endothelial progenitor cells apoptosis via p38 and JNK mitogen-activated protein kinase pathways. *Atherosclerosis* 2010, 210(1):71-77.
- 46. Lee E-S, Yoon C-H, Kim Y-S, Bae Y-S: The double-strand RNA-dependent protein kinase PKR plays a significant role in a sustained ER stress-induced apoptosis. *Febs Letters* 2007, 581(22):4325-4332.

- 47. Shimazawa M, Ito Y, Inokuchi Y, Hara H: Involvement of double-stranded RNA-dependent protein kinase in ER stress-induced retinal neuron damage. *Investigative Ophthalmology & Visual Science* 2007, 48(8):3729-3736.
- 48. Singh M, Fowlkes V, Handy I, Patel CV, Patel RC: Essential Role of PACT-Mediated PKR Activation in Tunicamycin-induced Apoptosis. *Journal of Molecular Biology* 2009, 385(2):457-468.
- 49. Yang X, Chan C: Repression of PKR mediates palmitate-induced apoptosis in HepG2 cells through regulation of Bcl-2. *Cell Research* 2009, 19(4):469-486.
- 50. Cunha DA, Hekerman P, Ladriere L, Bazarra-Castro A, Ortis F, Wakeham MC, Moore F, Rasschaert J, Cardozo AK, Bellomo E *et al*: Initiation and execution of lipotoxic ER stress in pancreatic beta-cells. *Journal of Cell Science* 2008, 121(14):2308-2318.
- 51. Wei YR, Wang D, Gentile CL, Pagliassotti MJ: Reduced endoplasmic reticulum luminal calcium links saturated fatty acid-mediated endoplasmic reticulum stress and cell death in liver cells. *Molecular and Cellular Biochemistry* 2009, 331(1-2):31-40.
- 52. Karaskov E, Scott C, Zhang L, Teodoro T, Ravazzola M, Volchuk A: Chronic palmitate but not oleate exposure induces endoplasmic reticulum stress, which may contribute to INS-1 pancreatic beta-cell apoptosis. *Endocrinology* 2006, 147(7):3398-3407.
- 53. Gwiazda KS, Yang TL, Lin Y, Johnson JD: Effects of palmitate on ER and cytosolic Ca2+ homeostasis in beta-cells. *Am J Physiol Endocrinol Metab* 2009, 296(4):E690-701.
- 54. Preston AM, Gurisik E, Bartley C, Laybutt DR, Biden TJ: Reduced endoplasmic reticulum (ER)-to-Golgi protein trafficking contributes to ER stress in lipotoxic mouse beta cells by promoting protein overload. *Diabetologia* 2009, 52(11):2369-2373.
- 55. Volmer R, van der Ploeg K, Ron D: Membrane lipid saturation activates endoplasmic reticulum unfolded protein response transducers through their transmembrane domains. *Proc Natl Acad Sci U S A* 2013, 110(12):4628-4633.
- 56. Bhattacharya AA, Grune T, Curry S: Crystallographic analysis reveals common modes of binding of medium and long-chain fatty acids to human serum albumin. *Journal of Molecular Biology* 2000, 303(5):721-732.
- 57. Chmurzynska A: The multigene family of fatty acid-binding proteins (FABPs): Function, structure and polymorphism. *Journal of Applied Genetics* 2006, 47(1):39-48.
- 58. Furuhashi M, Hotamisligil GS: Fatty acid-binding proteins: role in metabolic diseases and potential as drug targets. *Nature Reviews Drug Discovery* 2008, 7(6):489-503.

- 59. Richieri GV, Anel A, Kleinfeld AM: INTERACTIONS OF LONG-CHAIN FATTY-ACIDS AND ALBUMIN DETERMINATION OF FREE FATTY-ACID LEVELS USING THE FLUORESCENT-PROBE ADIFAB. *Biochemistry* 1993, 32(29):7574-7580.
- 60. Richieri GV, Ogata RT, Zimmerman AW, Veerkamp JH, Kleinfeld AM: Fatty acid binding proteins from different tissues show distinct patterns of fatty acid interactions. *Biochemistry* 2000, 39(24):7197-7204.
- 61. Veerkamp JH, van Moerkerk HTB, Prinsen CFM, van Kuppevelt TH: Structural and functional studies on different human FABP types. *Molecular and Cellular Biochemistry* 1999, 192(1-2):137-142.
- 62. Majava V, Polverini E, Mazzini A, Nanekar R, Knoll W, Peters J, Natali F, Baumgärtel P, Kursula I, Kursula P: Structural and functional characterization of human peripheral nervous system myelin protein P2. *PLoS One* 2010, 5(4):e10300.
- 63. Fujishiro T, Shoji O, Nagano S, Sugimoto H, Shiro Y, Watanabe Y: Crystal structure of H2O2-dependent cytochrome P450SPalpha with its bound fatty acid substrate: insight into the regioselective hydroxylation of fatty acids at the alpha position. *J Biol Chem* 2011, 286(34):29941-29950.
- 64. Zhu G, Koszelak-Rosenblum M, Malkowski MG: Crystal Structures of α-Dioxygenase from Oryza sativa: Insights into Substrate Binding and Activation by Hydrogen Peroxide. *Protein Sci* 2013.
- 65. Aparna V, Dileep KV, Mandal PK, Karthe P, Sadasivan C, Haridas M: Anti-inflammatory property of n-hexadecanoic acid: structural evidence and kinetic assessment. *Chem Biol Drug Des* 2012, 80(3):434-439.
- 66. Takai Y, Kishimoto A, Iwasa Y, Kawahara Y, Mori T, Nishizuka Y: CALCIUM-DEPENDENT ACTIVATION OF A MULTIFUNCTIONAL PROTEIN-KINASE BY MEMBRANE PHOSPHOLIPIDS. *Journal of Biological Chemistry* 1979, 254(10):3692-3695.
- 67. Lemmon MA: Membrane recognition by phospholipid-binding domains. *Nature Reviews Molecular Cell Biology* 2008, 9(2):99-111.
- 68. Diskin R, Engelberg D, Livnah O: A novel lipid binding site formed by the MAP kinase insert in p38 alpha. *Journal of Molecular Biology* 2008, 375(1):70-79.
- 69. Wenk MR: Lipidomics: new tools and applications. *Cell* 2010, 143(6):888-895.
- 70. Brown PH, Balbo A, Schuck P: Characterizing protein-protein interactions by sedimentation velocity analytical ultracentrifugation. *Curr Protoc Immunol* 2008, Chapter 18:Unit 18.15.

- 71. Ford MG, Pearse BM, Higgins MK, Vallis Y, Owen DJ, Gibson A, Hopkins CR, Evans PR, McMahon HT: Simultaneous binding of PtdIns(4,5)P2 and clathrin by AP180 in the nucleation of clathrin lattices on membranes. *Science* 2001, 291(5506):1051-1055.
- 72. Gorman PM, Kim S, Guo M, Melnyk RA, McLaurin J, Fraser PE, Bowie JU, Chakrabartty A: Dimerization of the transmembrane domain of amyloid precursor proteins and familial Alzheimer's disease mutants. *BMC Neurosci* 2008, 9:17.
- 73. Tsujita K, Suetsugu S, Sasaki N, Furutani M, Oikawa T, Takenawa T: Coordination between the actin cytoskeleton and membrane deformation by a novel membrane tubulation domain of PCH proteins is involved in endocytosis. *J Cell Biol* 2006, 172(2):269-279.
- 74. Ishii M, Fujita S, Yamada M, Hosaka Y, Kurachi Y: Phosphatidylinositol 3,4,5-trisphosphate and Ca2+/calmodulin competitively bind to the regulators of G-protein-signalling (RGS) domain of RGS4 and reciprocally regulate its action. *Biochem J* 2005, 385(Pt 1):65-73.
- 75. Lee SH, Jin JB, Song J, Min MK, Park DS, Kim YW, Hwang I: The intermolecular interaction between the PH domain and the C-terminal domain of Arabidopsis dynamin-like 6 determines lipid binding specificity. *J Biol Chem* 2002, 277(35):31842-31849.
- 76. Dalton AK, Murray PS, Murray D, Vogt VM: Biochemical characterization of rous sarcoma virus MA protein interaction with membranes. *J Virol* 2005, 79(10):6227-6238.
- 77. Tsujita K, Itoh T, Kondo A, Oyama M, Kozuka-Hata H, Irino Y, Hasegawa J, Takenawa T: Proteome of acidic phospholipid-binding proteins: spatial and temporal regulation of Coronin 1A by phosphoinositides. *J Biol Chem* 2010, 285(9):6781-6789.
- 78. Schroit AJ, Madsen J, Ruoho AE: Radioiodinated, photoactivatable phosphatidylcholine and phosphatidylserine: transfer properties and differential photoreactive interaction with human erythrocyte membrane proteins. *Biochemistry* 1987, 26(7):1812-1819.
- 79. Benfenati F, Greengard P, Brunner J, Bähler M: Electrostatic and hydrophobic interactions of synapsin I and synapsin I fragments with phospholipid bilayers. *J Cell Biol* 1989, 108(5):1851-1862.
- 80. Haberkant P, van Meer G: Protein-lipid interactions: paparazzi hunting for snap-shots. *Biol Chem* 2009, 390(8):795-803.
- 81. Gubbens J, de Kroon AI: Proteome-wide detection of phospholipid-protein interactions in mitochondria by photocrosslinking and click chemistry. *Mol Biosyst* 2010, 6(10):1751-1759.

- 82. Wiseman T, Williston S, Brandts JF, Lin LN: Rapid measurement of binding constants and heats of binding using a new titration calorimeter. *Anal Biochem* 1989, 179(1):131-137.
- 83. Hughes E, Clayton JC, Middleton DA: Cytoplasmic residues of phospholamban interact with membrane surfaces in the presence of SERCA: a new role for phospholipids in the regulation of cardiac calcium cycling? *Biochim Biophys Acta* 2009, 1788(2):559-566.
- 84. Hoernke M, Schwieger C, Kerth A, Blume A: Binding of cationic pentapeptides with modified side chain lengths to negatively charged lipid membranes: Complex interplay of electrostatic and hydrophobic interactions. *Biochim Biophys Acta* 2012, 1818(7):1663-1672.
- 85. Bhunia A, Mohanram H, Bhattacharjya S: Structural determinants of the specificity of a membrane binding domain of the scaffold protein Ste5 of budding yeast: Implications in signaling by the scaffold protein in MAPK pathway. *Biochim Biophys Acta* 2012, 1818(5):1250-1260.
- 86. Hundertmark M, Dimova R, Lengefeld J, Seckler R, Hincha DK: The intrinsically disordered late embryogenesis abundant protein LEA18 from Arabidopsis thaliana modulates membrane stability through binding and folding. *Biochim Biophys Acta* 2011, 1808(1):446-453.
- 87. Marsh D, Horváth LI: Structure, dynamics and composition of the lipid-protein interface. Perspectives from spin-labelling. *Biochim Biophys Acta* 1998, 1376(3):267-296.
- 88. Marsh D: Electron spin resonance in membrane research: protein-lipid interactions from challenging beginnings to state of the art. *Eur Biophys J* 2010, 39(4):513-525.
- 89. D'Errico G, Ercole C, Lista M, Pizzo E, Falanga A, Galdiero S, Spadaccini R, Picone D: Enforcing the positive charge of N-termini enhances membrane interaction and antitumor activity of bovine seminal ribonuclease. *Biochim Biophys Acta* 2011, 1808(12):3007-3015.
- 90. Vitiello G, Grimaldi M, Ramunno A, Ortona O, De Martino G, D'Ursi AM, D'Errico G: Interaction of a beta-sheet breaker peptide with lipid membranes. *J Pept Sci* 2010, 16(2):115-122.
- 91. Reyes Mateo C, G*mez Perez J, Villala*n J, Gonzal*z Ros JM: Protein-Lipid Interactions New Approaches and Emerging Concepts. In: *Springer Series in Biophysics series*. New York: Springer; 2005: xiv, 236 p. ill.
- 92. Romoser V, Ball R, Smrcka AV: Phospholipase C beta2 association with phospholipid interfaces assessed by fluorescence resonance energy transfer. G protein betagamma subunit-mediated translocation is not required for enzyme activation. *J Biol Chem* 1996, 271(41):25071-25078.

- 93. Nomikos M, Mulgrew-Nesbitt A, Pallavi P, Mihalyne G, Zaitseva I, Swann K, Lai FA, Murray D, McLaughlin S: Binding of phosphoinositide-specific phospholipase C-zeta (PLC-zeta) to phospholipid membranes: potential role of an unstructured cluster of basic residues. *J Biol Chem* 2007, 282(22):16644-16653.
- 94. Radhakrishnan A, Stein A, Jahn R, Fasshauer D: The Ca2+ affinity of synaptotagmin 1 is markedly increased by a specific interaction of its C2B domain with phosphatidylinositol 4,5-bisphosphate. *J Biol Chem* 2009, 284(38):25749-25760.
- 95. Gilbert GE, Furie BC, Furie B: Binding of human factor VIII to phospholipid vesicles. *J Biol Chem* 1990, 265(2):815-822.
- 96. Pap EH, Bastiaens PI, Borst JW, van den Berg PA, van Hoek A, Snoek GT, Wirtz KW, Visser AJ: Quantitation of the interaction of protein kinase C with diacylglycerol and phosphoinositides by time-resolved detection of resonance energy transfer. *Biochemistry* 1993, 32(48):13310-13317.
- 97. Petrescu AD, Gallegos AM, Okamura Y, Strauss JF, Schroeder F: Steroidogenic acute regulatory protein binds cholesterol and modulates mitochondrial membrane sterol domain dynamics. *J Biol Chem* 2001, 276(40):36970-36982.
- 98. Gray A, Olsson H, Batty IH, Priganica L, Peter Downes C: Nonradioactive methods for the assay of phosphoinositide 3-kinases and phosphoinositide phosphatases and selective detection of signaling lipids in cell and tissue extracts. *Anal Biochem* 2003, 313(2):234-245.
- 99. Dixon MJ, Gray A, Schenning M, Agacan M, Tempel W, Tong Y, Nedyalkova L, Park HW, Leslie NR, van Aalten DM *et al*: IQGAP proteins reveal an atypical phosphoinositide (aPI) binding domain with a pseudo C2 domain fold. *J Biol Chem* 2012.
- 100. Bazin H, Trinquet E, Mathis G: Time resolved amplification of cryptate emission: a versatile technology to trace biomolecular interactions. *J Biotechnol* 2002, 82(3):233-250.
- 101. Zigoneanu IG, Yang YJ, Krois AS, Haque E, Pielak GJ: Interaction of α-synuclein with vesicles that mimic mitochondrial membranes. *Biochim Biophys Acta* 2012, 1818(3):512-519.
- 102. Kobashigawa Y, Harada K, Yoshida N, Ogura K, Inagaki F: Phosphoinositide-incorporated lipid-protein nanodiscs: A tool for studying protein-lipid interactions. *Anal Biochem* 2011, 410(1):77-83.
- 103. Qiu L, Lewis A, Como J, Vaughn MW, Huang J, Somerharju P, Virtanen J, Cheng KH: Cholesterol modulates the interaction of beta-amyloid peptide with lipid bilayers. *Biophys J* 2009, 96(10):4299-4307.

- 104. Mustafa AK, van Rossum DB, Patterson RL, Maag D, Ehmsen JT, Gazi SK, Chakraborty A, Barrow RK, Amzel LM, Snyder SH: Glutamatergic regulation of serine racemase via reversal of PIP2 inhibition. *Proc Natl Acad Sci U S A* 2009, 106(8):2921-2926.
- 105. Guillén J, González-Alvarez A, Villalaín J: A membranotropic region in the C-terminal domain of hepatitis C virus protein NS4B interaction with membranes. *Biochim Biophys Acta* 2010, 1798(3):327-337.
- 106. Sanchez SA, Bagatolli LA, Gratton E, Hazlett TL: A two-photon view of an enzyme at work: Crotalus atrox venom PLA2 interaction with single-lipid and mixed-lipid giant unilamellar vesicles. *Biophys J* 2002, 82(4):2232-2243.
- 107. Melo AM, Prieto M, Coutinho A: The effect of variable liposome brightness on quantifying lipid-protein interactions using fluorescence correlation spectroscopy. *Biochim Biophys Acta* 2011, 1808(10):2559-2568.
- 108. Temmerman K, Nickel W: A novel flow cytometric assay to quantify interactions between proteins and membrane lipids. *J Lipid Res* 2009, 50(6):1245-1254.
- 109. Zhu H, Bilgin M, Bangham R, Hall D, Casamayor A, Bertone P, Lan N, Jansen R, Bidlingmaier S, Houfek T *et al*: Global analysis of protein activities using proteome chips. *Science* 2001, 293(5537):2101-2105.
- 110. Feng L: Probing lipid-protein interactions using lipid microarrays. *Prostaglandins Other Lipid Mediat* 2005, 77(1-4):158-167.
- 111. Borch J, Torta F, Sligar SG, Roepstorff P: Nanodiscs for immobilization of lipid bilayers and membrane receptors: kinetic analysis of cholera toxin binding to a glycolipid receptor. *Anal Chem* 2008, 80(16):6245-6252.
- 112. Bally M, Bailey K, Sugihara K, Grieshaber D, Vörös J, Städler B: Liposome and lipid bilayer arrays towards biosensing applications. *Small* 2010, 6(22):2481-2497.
- 113. Hélix-Nielsen C: Biomimetic membranes for sensor and separation applications. In: *Biological and medical physics, Biomedical engineering,*. Dordrecht; New York: Springer,; 2012: 1 online resource (xv, 292 p.).
- 114. Stevenson JM, Perera IY, Boss WF: A phosphatidylinositol 4-kinase pleckstrin homology domain that binds phosphatidylinositol 4-monophosphate. *J Biol Chem* 1998, 273(35):22761-22767.
- 115. Dowler S, Kular G, Alessi DR: Protein lipid overlay assay. *Sci STKE* 2002, 2002(129):pl6.

- 116. Kanter JL, Narayana S, Ho PP, Catz I, Warren KG, Sobel RA, Steinman L, Robinson WH: Lipid microarrays identify key mediators of autoimmune brain inflammation. *Nat Med* 2006, 12(1):138-143.
- 117. Gallego O, Betts MJ, Gvozdenovic-Jeremic J, Maeda K, Matetzki C, Aguilar-Gurrieri C, Beltran-Alvarez P, Bonn S, Fernández-Tornero C, Jensen LJ *et al*: A systematic screen for protein-lipid interactions in Saccharomyces cerevisiae. *Mol Syst Biol* 2010, 6:430.
- 118. Linman MJ, Culver SP, Cheng Q: Fabrication of fracture-free nanoglassified substrates by layer-by-layer deposition with a paint gun technique for real-time monitoring of protein-lipid interactions. *Langmuir* 2009, 25(5):3075-3082.
- 119. Linman MJ, Abbas A, Roberts CC, Cheng Q: Etched glass microarrays with differential resonance for enhanced contrast and sensitivity of surface plasmon resonance imaging analysis. *Anal Chem* 2011, 83(15):5936-5943.
- 120. Phillips KS, Cheng Q: Microfluidic immunoassay for bacterial toxins with supported phospholipid bilayer membranes on poly(dimethylsiloxane). *Anal Chem* 2005, 77(1):327-334.
- 121. Wang Z, Wilkop T, Han JH, Dong Y, Linman MJ, Cheng Q: Development of air-stable, supported membrane arrays with photolithography for study of phosphoinositide-protein interactions using surface plasmon resonance imaging. *Anal Chem* 2008, 80(16):6397-6404.
- 122. Deng Y, Wang Y, Holtz B, Li J, Traaseth N, Veglia G, Stottrup BJ, Elde R, Pei D, Guo A *et al*: Fluidic and air-stable supported lipid bilayer and cell-mimicking microarrays. *J Am Chem Soc* 2008, 130(19):6267-6271.
- 123. Taylor JD, Phillips KS, Cheng Q: Microfluidic fabrication of addressable tethered lipid bilayer arrays and optimization using SPR with silane-derivatized nanoglassy substrates. *Lab Chip* 2007, 7(7):927-930.
- 124. Losey EA, Smith MD, Meng M, Best MD: Microplate-based analysis of protein-membrane binding interactions via immobilization of whole liposomes containing a biotinylated anchor. *Bioconjug Chem* 2009, 20(2):376-383.
- 125. Chandra H, Reddy PJ, Srivastava S: Protein microarrays and novel detection platforms. *Expert Rev Proteomics* 2011, 8(1):61-79.
- 126. Ray S, Mehta G, Srivastava S: Label-free detection techniques for protein microarrays: prospects, merits and challenges. *Proteomics* 2010, 10(4):731-748.
- 127. Moran-Mirabal JM, Edel JB, Meyer GD, Throckmorton D, Singh AK, Craighead HG: Micrometer-sized supported lipid bilayer arrays for bacterial toxin binding studies through total internal reflection fluorescence microscopy. *Biophys J* 2005, 89(1):296-305.

- 128. Smith KA, Gale BK, Conboy JC: Micropatterned fluid lipid bilayer arrays created using a continuous flow microspotter. *Anal Chem* 2008, 80(21):7980-7987.
- 129. Joubert JR, Smith KA, Johnson E, Keogh JP, Wysocki VH, Gale BK, Conboy JC, Saavedra SS: Stable, ligand-doped, poly(bis-SorbPC) lipid bilayer arrays for protein binding and detection. *ACS Appl Mater Interfaces* 2009, 1(6):1310-1315.
- 130. Rowland MM, Gong D, Bostic HE, Lucas N, Cho W, Best MD: Microarray analysis of Akt PH domain binding employing synthetic biotinylated analogs of all seven phosphoinositide headgroup isomers. *Chem Phys Lipids* 2012, 165(2):207-215.
- 131. Consonni SV, Gloerich M, Spanjaard E, Bos JL: cAMP regulates DEP domain-mediated binding of the guanine nucleotide exchange factor Epac1 to phosphatidic acid at the plasma membrane. *Proc Natl Acad Sci U S A* 2012, 109(10):3814-3819.
- 132. Gong D, Smith MD, Manna D, Bostic HE, Cho W, Best MD: Microplate-based characterization of protein-phosphoinositide binding interactions using a synthetic biotinylated headgroup analogue. *Bioconjug Chem* 2009, 20(2):310-316.
- 133. Phillips KS, Han JH, Martinez M, Wang Z, Carter D, Cheng Q: Nanoscale glassification of gold substrates for surface plasmon resonance analysis of protein toxins with supported lipid membranes. *Anal Chem* 2006, 78(2):596-603.
- 134. Liu Y, Cheng Q: Detection of membrane-binding proteins by surface plasmon resonance with an all-aqueous amplification scheme. *Anal Chem* 2012, 84(7):3179-3186.
- 135. Junghans A, Champagne C, Cayot P, Loupiac C, Köper I: Probing Protein-Membrane Interactions Using Solid Supported Membranes. *Langmuir* 2011.
- 136. Terrettaz SS, Thierry. Duschl, Claus and Vogel, Horst: Protein Binding to Supported Lipid Membranes: Investigation of the Cholera Toxin-Ganglioside Interaction by Simultaneous Impedance Spectroscopy and Surface Plasmon Resonance. *Langmuir* 1993, 9:1361-1369.
- 137. Das A, Base C, Manna D, Cho W, Dubreuil RR: Unexpected complexity in the mechanisms that target assembly of the spectrin cytoskeleton. *J Biol Chem* 2008, 283(18):12643-12653.
- 138. Gheorghiu M, Olaru A, Tar A, Polonschii C, Gheorghiu E: Sensing based on assessment of non-monotonous effect determined by target analyte: case study on pore-forming compounds. *Biosens Bioelectron* 2009, 24(12):3517-3523.
- 139. Phillips KS, Wilkop T, Wu JJ, Al-Kaysi RO, Cheng Q: Surface plasmon resonance imaging analysis of protein-receptor binding in supported membrane arrays on gold substrates with calcinated silicate films. *J Am Chem Soc* 2006, 128(30):9590-9591.

- 140. Taylor JD, Linman MJ, Wilkop T, Cheng Q: Regenerable tethered bilayer lipid membrane arrays for multiplexed label-free analysis of lipid-protein interactions on poly(dimethylsiloxane) microchips using SPR imaging. *Anal Chem* 2009, 81(3):1146-1153.
- 141. Harkewicz R, Dennis EA: Applications of mass spectrometry to lipids and membranes. *Annu Rev Biochem* 2011, 80:301-325.
- 142. D'Santos C, Lewis EA: Functional Proteomics: Mapping Lipid-Protein Interactomes. In: *Integrative Proteomics*. InTech, Published; 2012: 363-378.
- 143. Giannakis E, Pacífico J, Smith DP, Hung LW, Masters CL, Cappai R, Wade JD, Barnham KJ: Dimeric structures of alpha-synuclein bind preferentially to lipid membranes. *Biochim Biophys Acta* 2008, 1778(4):1112-1119.
- 144. Park JH, Kwon EY, Jung HI, Kim DE: Direct force measurement of the interaction between liposome and the C2A domain of synaptotagmin I using atomic force microscopy. *Biotechnol Lett* 2006, 28(7):505-509.
- 145. Baksh MM, Kussrow AK, Mileni M, Finn MG, Bornhop DJ: Label-free quantification of membrane-ligand interactions using backscattering interferometry. *Nat Biotechnol* 2011, 29(4):357-360.
- 146. Glatz JF, Veerkamp JH: A radiochemical procedure for the assay of fatty acid binding by proteins. *Anal Biochem* 1983, 132(1):89-95.
- 147. Thumser AE, Storch J: Characterization of a BODIPY-labeled fluorescent fatty acid analogue. Binding to fatty acid-binding proteins, intracellular localization, and metabolism. *Molecular and cellular biochemistry* 2007, 299(1-2):67-73.
- 148. Richieri GV, Kleinfeld AM: Unbound free fatty acid levels in human serum. *Journal of lipid research* 1995, 36(2):229-240.
- 149. Elmadhoun BM, Wang GQ, Templeton JF, Burczynski FJ: Binding of [3H]palmitate to BSA. *The American journal of physiology* 1998, 275(4 Pt 1):G638-644.
- 150. Cho H, Mukherjee S, Palasuberniam P, Pillow L, Bilgin B, Nezich C, Walton SP, Feig M, Chan C: Molecular Mechanism by Which Palmitate Inhibits PKR Autophosphorylation. *Biochemistry* 2011, 50(6):1110-1119.
- 151. Stark GR, Kerr IM, Williams BR, Silverman RH, Schreiber RD: How cells respond to interferons. *Annual review of biochemistry* 1998, 67:227-264.
- 152. Dey M, Cao C, Dar AC, Tamura T, Ozato K, Sicheri F, Dever TE: Mechanistic link between PKR dimerization, autophosphorylation, and eIF2alpha substrate recognition. *Cell* 2005, 122(6):901-913.

- 153. Gale M, Jr., Katze MG: Molecular mechanisms of interferon resistance mediated by viral-directed inhibition of PKR, the interferon-induced protein kinase. *Pharmacology & therapeutics* 1998, 78(1):29-46.
- 154. Xu Z, Williams BR: The B56alpha regulatory subunit of protein phosphatase 2A is a target for regulation by double-stranded RNA-dependent protein kinase PKR. *Molecular and cellular biology* 2000, 20(14):5285-5299.
- 155. Williams BR: PKR; a sentinel kinase for cellular stress. *Oncogene* 1999, 18(45):6112-6120.
- 156. Nanduri S, Carpick BW, Yang Y, Williams BR, Qin J: Structure of the double-stranded RNA-binding domain of the protein kinase PKR reveals the molecular basis of its dsRNA-mediated activation. *The EMBO journal* 1998, 17(18):5458-5465.
- 157. Nanduri S, Rahman F, Williams BR, Qin J: A dynamically tuned double-stranded RNA binding mechanism for the activation of antiviral kinase PKR. *The EMBO journal* 2000, 19(20):5567-5574.
- 158. Dar AC, Dever TE, Sicheri F: Higher-order substrate recognition of eIF2alpha by the RNA-dependent protein kinase PKR. *Cell* 2005, 122(6):887-900.
- 159. Johnson LN, Noble ME, Owen DJ: Active and inactive protein kinases: structural basis for regulation. *Cell* 1996, 85(2):149-158.
- 160. Nolen B, Taylor S, Ghosh G: Regulation of protein kinases; controlling activity through activation segment conformation. *Molecular cell* 2004, 15(5):661-675.
- 161. McKenna SA, Lindhout DA, Kim I, Liu CW, Gelev VM, Wagner G, Puglisi JD: Molecular framework for the activation of RNA-dependent protein kinase. *The Journal of biological chemistry* 2007, 282(15):11474-11486.
- 162. Kornev AP, Haste NM, Taylor SS, Eyck LF: Surface comparison of active and inactive protein kinases identifies a conserved activation mechanism. *Proceedings of the National Academy of Sciences of the United States of America* 2006, 103(47):17783-17788.
- 163. Lee SB, Esteban M: The interferon-induced double-stranded RNA-activated protein kinase induces apoptosis. *Virology* 1994, 199(2):491-496.
- 164. Takizawa T, Ohashi K, Nakanishi Y: Possible involvement of double-stranded RNA-activated protein kinase in cell death by influenza virus infection. *Journal of virology* 1996, 70(11):8128-8132.
- 165. Kibler KV, Shors T, Perkins KB, Zeman CC, Banaszak MP, Biesterfeldt J, Langland JO, Jacobs BL: Double-stranded RNA is a trigger for apoptosis in vaccinia virus-infected cells. *Journal of virology* 1997, 71(3):1992-2003.

- 166. Yeung MC, Chang DL, Camantigue RE, Lau AS: Inhibitory role of the host apoptogenic gene PKR in the establishment of persistent infection by encephalomyocarditis virus in U937 cells. *Proceedings of the National Academy of Sciences of the United States of America* 1999, 96(21):11860-11865.
- 167. Garcia MA, Gil J, Ventoso I, Guerra S, Domingo E, Rivas C, Esteban M: Impact of protein kinase PKR in cell biology: from antiviral to antiproliferative action. *Microbiol Mol Biol Rev* 2006, 70(4):1032-1060.
- 168. Kim SH, Forman AP, Mathews MB, Gunnery S: Human breast cancer cells contain elevated levels and activity of the protein kinase, PKR. *Oncogene* 2000, 19(27):3086-3094.
- 169. Kim SH, Gunnery S, Choe JK, Mathews MB: Neoplastic progression in melanoma and colon cancer is associated with increased expression and activity of the interferon-inducible protein kinase, PKR. *Oncogene* 2002, 21(57):8741-8748.
- 170. Hiasa Y, Kamegaya Y, Nuriya H, Onji M, Kohara M, Schmidt EV, Chung RT: Protein kinase R is increased and is functional in hepatitis C virus-related hepatocellular carcinoma. *The American journal of gastroenterology* 2003, 98(11):2528-2534.
- 171. Delgado Andre N, De Lucca FL: Knockdown of PKR expression by RNAi reduces pulmonary metastatic potential of B16-F10 melanoma cells in mice: possible role of NF-kappaB. *Cancer letters* 2007, 258(1):118-125.
- 172. Li Z, Srivastava S, Mittal S, Yang X, Sheng L, Chan C: A Three Stage Integrative Pathway Search (TIPS) framework to identify toxicity relevant genes and pathways. *BMC bioinformatics* 2007, 8:202.
- 173. Yang X, Chan C: Repression of PKR mediates palmitate-induced apoptosis in HepG2 cells through regulation of Bcl-2. *Cell research* 2009, 19(4):469-486.
- 174. Bevilacqua PC, Cech TR: Minor-groove recognition of double-stranded RNA by the double-stranded RNA-binding domain from the RNA-activated protein kinase PKR. *Biochemistry* 1996, 35(31):9983-9994.
- 175. Lemaire PA, Lary J, Cole JL: Mechanism of PKR activation: dimerization and kinase activation in the absence of double-stranded RNA. *Journal of molecular biology* 2005, 345(1):81-90.
- 176. Jammi NV, Beal PA: Phosphorylation of the RNA-dependent protein kinase regulates its RNA-binding activity. *Nucleic acids research* 2001, 29(14):3020-3029.
- 177. Matsui T, Tanihara K, Date T: Expression of unphosphorylated form of human double-stranded RNA-activated protein kinase in Escherichia coli. *Biochemical and biophysical research communications* 2001, 284(3):798-807.

- 178. Lemaire PA, Tessmer I, Craig R, Erie DA, Cole JL: Unactivated PKR exists in an open conformation capable of binding nucleotides. *Biochemistry* 2006, 45(30):9074-9084.
- 179. Barber GN: The dsRNA-dependent protein kinase, PKR and cell death. *Cell death and differentiation* 2005, 12(6):563-570.
- 180. Knight JD, Qian B, Baker D, Kothary R: Conservation, variability and the modeling of active protein kinases. *PloS one* 2007, 2(10):e982.
- 181. Li H, Korennykh AV, Behrman SL, Walter P: Mammalian endoplasmic reticulum stress sensor IRE1 signals by dynamic clustering. *Proc Natl Acad Sci U S A* 2010, 107(37):16113-16118.
- 182. Cho H, Lamarca R, Chan C: Oligomerization of the transmembrane domain of IRE1α in SDS micelles. *Biochem Biophys Res Commun* 2012, 427(4):764-767.
- 183. Schlessinger J: Cell signaling by receptor tyrosine kinases. *Cell* 2000, 103(2):211-225.
- 184. Li E, Hristova K: Role of receptor tyrosine kinase transmembrane domains in cell signaling and human pathologies. *Biochemistry* 2006, 45(20):6241-6251.
- 185. Zhang X, Gureasko J, Shen K, Cole PA, Kuriyan J: An allosteric mechanism for activation of the kinase domain of epidermal growth factor receptor. *Cell* 2006, 125(6):1137-1149.
- 186. Li E, Hristova K: Receptor tyrosine kinase transmembrane domains: Function, dimer structure and dimerization energetics. *Cell Adh Migr* 2010, 4(2):249-254.
- 187. Dosch DD, Ballmer-Hofer K: Transmembrane domain-mediated orientation of receptor monomers in active VEGFR-2 dimers. *FASEB J* 2010, 24(1):32-38.
- 188. Russ WP, Engelman DM: TOXCAT: a measure of transmembrane helix association in a biological membrane. *Proc Natl Acad Sci U S A* 1999, 96(3):863-868.
- 189. Eisenberg D, Schwarz E, Komaromy M, Wall R: Analysis of membrane and surface protein sequences with the hydrophobic moment plot. *J Mol Biol* 1984, 179(1):125-142.
- 190. Jones DT, Taylor WR, Thornton JM: A model recognition approach to the prediction of all-helical membrane protein structure and topology. *Biochemistry* 1994, 33(10):3038-3049.
- 191. Krogh A, Larsson B, von Heijne G, Sonnhammer EL: Predicting transmembrane protein topology with a hidden Markov model: application to complete genomes. *J Mol Biol* 2001, 305(3):567-580.

- 192. Cserzö M, Wallin E, Simon I, von Heijne G, Elofsson A: Prediction of transmembrane alpha-helices in prokaryotic membrane proteins: the dense alignment surface method. *Protein Eng* 1997, 10(6):673-676.
- 193. Tusnády GE, Simon I: The HMMTOP transmembrane topology prediction server. *Bioinformatics* 2001, 17(9):849-850.
- 194. Viklund H, Elofsson A: OCTOPUS: improving topology prediction by two-track ANN-based preference scores and an extended topological grammar. *Bioinformatics* 2008, 24(15):1662-1668.
- 195. Käll L, Krogh A, Sonnhammer EL: A combined transmembrane topology and signal peptide prediction method. *J Mol Biol* 2004, 338(5):1027-1036.
- 196. Hirokawa T, Boon-Chieng S, Mitaku S: SOSUI: classification and secondary structure prediction system for membrane proteins. *Bioinformatics* 1998, 14(4):378-379.
- 197. Fisher LE, Engelman DM, Sturgis JN: Detergents modulate dimerization, but not helicity, of the glycophorin A transmembrane domain. *J Mol Biol* 1999, 293(3):639-651.
- 198. Melnyk RA, Partridge AW, Deber CM: Retention of native-like oligomerization states in transmembrane segment peptides: application to the Escherichia coli aspartate receptor. *Biochemistry* 2001, 40(37):11106-11113.
- 199. Tang P, Mandal PK, Xu Y: NMR structures of the second transmembrane domain of the human glycine receptor alpha(1) subunit: model of pore architecture and channel gating. *Biophys J* 2002, 83(1):252-262.
- 200. Tulumello DV, Deber CM: SDS micelles as a membrane-mimetic environment for transmembrane segments. *Biochemistry* 2009, 48(51):12096-12103.
- 201. Britz D, Mortensen J: COMPUTER-AIDED STAIRCASE-TENSAMMETRIC TITRATION FOR THE ACCURATE MEASUREMENT OF CRITICAL MICELLE CONCENTRATION MEASUREMENTS ON SODIUM DODECYL-SULFATE IN SODIUM-CHLORIDE SOLUTIONS. *Journal of Electroanalytical Chemistry* 1981, 127(1-3):231-240.
- 202. Böhm G, Muhr R, Jaenicke R: Quantitative analysis of protein far UV circular dichroism spectra by neural networks. *Protein Eng* 1992, 5(3):191-195.
- 203. Melnyk RA, Partridge AW, Deber CM: Transmembrane domain mediated self-assembly of major coat protein subunits from Ff bacteriophage. *J Mol Biol* 2002, 315(1):63-72.
- 204. Artemenko EO, Egorova NS, Arseniev AS, Feofanov AV: Transmembrane domain of EphA1 receptor forms dimers in membrane-like environment. *Biochim Biophys Acta* 2008, 1778(10):2361-2367.

- 205. Adair BD, Engelman DM: Glycophorin A helical transmembrane domains dimerize in phospholipid bilayers: a resonance energy transfer study. *Biochemistry* 1994, 33(18):5539-5544.
- 206. Li E, You M, Hristova K: Sodium dodecyl sulfate-polyacrylamide gel electrophoresis and forster resonance energy transfer suggest weak interactions between fibroblast growth factor receptor 3 (FGFR3) transmembrane domains in the absence of extracellular domains and ligands. *Biochemistry* 2005, 44(1):352-360.
- 207. Schick S, Chen L, Li E, Lin J, Köper I, Hristova K: Assembly of the m2 tetramer is strongly modulated by lipid chain length. *Biophys J* 2010, 99(6):1810-1817.
- 208. Lemmon MA, Flanagan JM, Hunt JF, Adair BD, Bormann BJ, Dempsey CE, Engelman DM: Glycophorin A dimerization is driven by specific interactions between transmembrane alpha-helices. *J Biol Chem* 1992, 267(11):7683-7689.
- 209. Ng DP, Deber CM: Modulation of the oligomerization of myelin proteolipid protein by transmembrane helix interaction motifs. *Biochemistry* 2010, 49(32):6896-6902.
- 210. Samanta U, Pal D, Chakrabarti P: Packing of aromatic rings against tryptophan residues in proteins. *Acta Crystallogr D Biol Crystallogr* 1999, 55(Pt 8):1421-1427.
- 211. Liu CY, Xu ZH, Kaufman RJ: Structure and intermolecular interactions of the luminal dimerization domain of human IRE1 alpha. *Journal of Biological Chemistry* 2003, 278(20):17680-17687.
- 212. Korennykh AV, Egea PF, Korostelev AA, Finer-Moore J, Zhang C, Shokat KM, Stroud RM, Walter P: The unfolded protein response signals through high-order assembly of Ire1. *Nature* 2009, 457(7230):687-693.
- 213. Yau WM, Wimley WC, Gawrisch K, White SH: The preference of tryptophan for membrane interfaces. *Biochemistry* 1998, 37(42):14713-14718.
- 214. van der Wel PC, Reed ND, Greathouse DV, Koeppe RE: Orientation and motion of tryptophan interfacial anchors in membrane-spanning peptides. *Biochemistry* 2007, 46(25):7514-7524.
- 215. Kelkar DA, Chattopadhyay A: The gramicidin ion channel: a model membrane protein. *Biochim Biophys Acta* 2007, 1768(9):2011-2025.
- 216. Ridder A, Skupjen P, Unterreitmeier S, Langosch D: Tryptophan supports interaction of transmembrane helices. *J Mol Biol* 2005, 354(4):894-902.
- 217. Sal-Man N, Gerber D, Bloch I, Shai Y: Specificity in transmembrane helix-helix interactions mediated by aromatic residues. *J Biol Chem* 2007, 282(27):19753-19761.

- 218. McClellan AL: Tables of Experimental Dipole Moments. San Francisco: W.H. Freeman; 1963.
- 219. Ruan W, Becker V, Klingmüller U, Langosch D: The interface between self-assembling erythropoietin receptor transmembrane segments corresponds to a membrane-spanning leucine zipper. *J Biol Chem* 2004, 279(5):3273-3279.
- 220. Ebie AZ, Fleming KG: Dimerization of the erythropoietin receptor transmembrane domain in micelles. *J Mol Biol* 2007, 366(2):517-524.
- 221. van Meer G, Voelker DR, Feigenson GW: Membrane lipids: where they are and how they behave. *Nat Rev Mol Cell Biol* 2008, 9(2):112-124.
- 222. Gardner BM, Pincus D, Gotthardt K, Gallagher CM, Walter P: Endoplasmic reticulum stress sensing in the unfolded protein response. *Cold Spring Harb Perspect Biol* 2013, 5(3):a013169.
- 223. Kimata Y, Kohno K: Endoplasmic reticulum stress-sensing mechanisms in yeast and mammalian cells. *Curr Opin Cell Biol* 2011, 23(2):135-142.
- 224. Johnson RM, Hecht K, Deber CM: Aromatic and cation-pi interactions enhance helix-helix association in a membrane environment. *Biochemistry* 2007, 46(32):9208-9214.
- 225. Smith SO, Smith CS, Bormann BJ: Strong hydrogen bonding interactions involving a buried glutamic acid in the transmembrane sequence of the neu/erbB-2 receptor. *Nat Struct Biol* 1996, 3(3):252-258.
- 226. Ron D, Walter P: Signal integration in the endoplasmic reticulum unfolded protein response. *Nat Rev Mol Cell Biol* 2007, 8(7):519-529.
- 227. Dong B, Niwa M, Walter P, Silverman RH: Basis for regulated RNA cleavage by functional analysis of RNase L and Ire1p. *RNA* 2001, 7(3):361-373.
- 228. Han D, Lerner AG, Vande Walle L, Upton JP, Xu W, Hagen A, Backes BJ, Oakes SA, Papa FR: IRE1alpha kinase activation modes control alternate endoribonuclease outputs to determine divergent cell fates. *Cell* 2009, 138(3):562-575.
- 229. Papa FR, Zhang C, Shokat K, Walter P: Bypassing a kinase activity with an ATP-competitive drug. *Science* 2003, 302(5650):1533-1537.
- 230. Wiseman RL, Zhang Y, Lee KP, Harding HP, Haynes CM, Price J, Sicheri F, Ron D: Flavonol activation defines an unanticipated ligand-binding site in the kinase-RNase domain of IRE1. *Mol Cell* 2010, 38(2):291-304.
- 231. Das SK, Chu WS, Mondal AK, Sharma NK, Kern PA, Rasouli N, Elbein SC: Effect of pioglitazone treatment on endoplasmic reticulum stress response in human adipose and in

- palmitate-induced stress in human liver and adipose cell lines. *Am J Physiol Endocrinol Metab* 2008, 295(2):E393-400.
- 232. Achard CS, Laybutt DR: Lipid-induced endoplasmic reticulum stress in liver cells results in two distinct outcomes: adaptation with enhanced insulin signaling or insulin resistance. *Endocrinology* 2012, 153(5):2164-2177.
- 233. Cui W, Ma J, Wang X, Yang W, Zhang J, Ji Q: Free fatty acid induces endoplasmic reticulum stress and apoptosis of β-cells by Ca2+/calpain-2 pathways. *PLoS One* 2013, 8(3):e59921.
- 234. Lee KP, Dey M, Neculai D, Cao C, Dever TE, Sicheri F: Structure of the dual enzyme Ire1 reveals the basis for catalysis and regulation in nonconventional RNA splicing. *Cell* 2008, 132(1):89-100.
- 235. Iwaki T, Figuera M, Ploplis VA, Castellino FJ: Rapid selection of Drosophila S2 cells with the puromycin resistance gene. *Biotechniques* 2003, 35(3):482-484, 486.
- 236. Volkmann K, Lucas JL, Vuga D, Wang X, Brumm D, Stiles C, Kriebel D, Der-Sarkissian A, Krishnan K, Schweitzer C *et al*: Potent and selective inhibitors of the inositol-requiring enzyme 1 endoribonuclease. *J Biol Chem* 2011, 286(14):12743-12755.
- 237. Wang L, Perera BG, Hari SB, Bhhatarai B, Backes BJ, Seeliger MA, Schürer SC, Oakes SA, Papa FR, Maly DJ: Divergent allosteric control of the IRE1α endoribonuclease using kinase inhibitors. *Nat Chem Biol* 2012, 8(12):982-989.
- 238. Korennykh AV, Egea PF, Korostelev AA, Finer-Moore J, Stroud RM, Zhang C, Shokat KM, Walter P: Cofactor-mediated conformational control in the bifunctional kinase/RNase Ire1. *BMC Biol* 2011, 9:48.
- 239. Korennykh A, Walter P: Structural basis of the unfolded protein response. *Annu Rev Cell Dev Biol* 2012, 28:251-277.
- 240. Axten JM, Medina JR, Feng Y, Shu A, Romeril SP, Grant SW, Li WH, Heerding DA, Minthorn E, Mencken T *et al*: Discovery of 7-methyl-5-(1-{[3-(trifluoromethyl)phenyl]acetyl}-2,3-dihydro-1H-indol-5-yl)-7H-pyrrolo[2,3-d]pyrimidin-4-amine (GSK2606414), a potent and selective first-in-class inhibitor of protein kinase R (PKR)-like endoplasmic reticulum kinase (PERK). *J Med Chem* 2012, 55(16):7193-7207.
- 241. Nagar B, Hantschel O, Seeliger M, Davies JM, Weis WI, Superti-Furga G, Kuriyan J: Organization of the SH3-SH2 unit in active and inactive forms of the c-Abl tyrosine kinase. *Mol Cell* 2006, 21(6):787-798.
- 242. Bossemeyer D, Engh RA, Kinzel V, Ponstingl H, Huber R: Phosphotransferase and substrate binding mechanism of the cAMP-dependent protein kinase catalytic subunit from porcine heart as deduced from the 2.0 A structure of the complex with Mn2+

- adenylyl imidodiphosphate and inhibitor peptide PKI(5-24). *EMBO J* 1993, 12(3):849-859.
- 243. Bastidas AC, Deal MS, Steichen JM, Keshwani MM, Guo Y, Taylor SS: Role of Nterminal myristylation in the structure and regulation of cAMP-dependent protein kinase. *J Mol Biol* 2012, 422(2):215-229.
- 244. Hantschel O, Nagar B, Guettler S, Kretzschmar J, Dorey K, Kuriyan J, Superti-Furga G: A myristoyl/phosphotyrosine switch regulates c-Abl. *Cell* 2003, 112(6):845-857.
- 245. Koegl M, Zlatkine P, Ley SC, Courtneidge SA, Magee AI: Palmitoylation of multiple Src-family kinases at a homologous N-terminal motif. *Biochem J* 1994, 303 (Pt 3):749-753.
- 246. Ren W, Jhala US, Du K: Proteomic analysis of protein palmitoylation in adipocytes. *Adipocyte* 2013, 2(1):17-28.
- 247. Leekumjorn S, Cho HJ, Wu Y, Wright NT, Sum AK, Chan C: The role of fatty acid unsaturation in minimizing biophysical changes on the structure and local effects of bilayer membranes. *Biochim Biophys Acta* 2009, 1788(7):1508-1516.
- 248. Schwenk RW, Holloway GP, Luiken JJ, Bonen A, Glatz JF: Fatty acid transport across the cell membrane: regulation by fatty acid transporters. *Prostaglandins Leukot Essent Fatty Acids* 2010, 82(4-6):149-154.
- 249. Hostetler HA, McIntosh AL, Atshaves BP, Storey SM, Payne HR, Kier AB, Schroeder F: L-FABP directly interacts with PPARalpha in cultured primary hepatocytes. *J Lipid Res* 2009, 50(8):1663-1675.